2010

Investigations into the origins of polyatomic ions in inductively coupled plasma-mass spectrometry

Sally Mcintyre
Iowa State University

Investigations into the origins of polyatomic ions in inductively coupled plasma-mass spectrometry

by

Sally M. McIntyre

A dissertation submitted to the graduate faculty

in partial fulfillment of the requirements for the degree of

DOCTOR OF PHILOSOPHY

Major: Analytical Chemistry

Program of Study Committee:

R.S. Houk, Major Professor

Joseph Burnett

Mark Gordon

Klaus Schmidt-Rohr

Emily Smith

Iowa State University

Ames, Iowa

2010

TABLE OF CONTENTS

CHAPTER 1. INTRODUCTION

ICP-MS

An inductively coupled plasma-mass spectrometer (ICP-MS) is an elemental analytical instrument capable of determining nearly all elements in the periodic table at limits of detection in the parts per quadrillion and with a linear analytical range over 8-10 orders of magnitude [1-2]. Three concentric quartz tubes make up the plasma torch. Argon gas is spiraled through the outer tube and generates the plasma powered by a looped load coil operating at 27.1 or 40.6 MHz. The argon flow of the middle channel is used to keep the plasma above the innermost tube through which solid or aqueous sample is carried in a third argon stream. A sample is progressively desolvated, atomized and ionized.

The torch is operated at atmospheric pressure. To reach the reduced pressures of mass spectrometers, ions are extracted through a series of two, approximately one millimeter wide, circular apertures set in water cooled metal cones. The space between the cones is evacuated to approximately one torr. The space behind the second cone is pumped down to, or near to, the pressure needed for the mass spectrometer (MS). The first cone, called the sampler, is placed directly in the plasma plume and its position is adjusted to the point where atomic ions are most abundant. The hot plasma gas expands through the sampler orifice and in this expansion is placed the second cone, called the skimmer. After the skimmer traditional MS designs are employed, i.e. quadrupoles, magnetic sectors, time-of-flight.

Extraction Process in ICP-MS

ICP-MS is the coupling of two devices with opposite requirements. A hot collision rich environment is needed in the plasma for atomization and ionization. A mass spectrometer needs a cooler environment with long path lengths so collisions do not deflect and remove ions trajectories. These two diametrically opposite zones are bridged with the interface region. Plasma is pulled from the ICP via a vacuum. The space behind a circular aperture is pumped down to ~1 torr or 0.1mbar. As the plasma species enter the aperture they retain their temperature and collisional behavior, but as they expand into the low pressure interface region they speed up until they surpass the local speed of sound. This occurs at a distance from the sampler tip of about half the sampler diameter. If the diameter of the sampler is 1 mm, the gas velocity hits Mach one at approximately 0.5 mm [3]. After this point the gas expands quickly and the mean free path increases. Velocity is gained at the expense of temperature, or gas kinetic energy. Thus, this region appears dark in photographs and is called the zone of silence [4]. The zone is shaped like an elliptical paraboloid with bright sides and end cap due to the cool slow background gas of the interface finally colliding with the hot plasma gas to convert enough speed back into temperature and consequent collisions transfer energy and produce emission. But now the collisions are undesirable because they can be an area for ion-electron recombinations, formation reactions and general scatter and loss of analyte ions [5]. New polyatomic ions are avoided as much as possible by placing the second cone inside the zone of silence, away from and before these shock zones. Sharp fine tips are used in skimmers to minimize their disturbance to the expanding gas but evidence still suggests some shock waves develop around and even in front of the skimmer tip [6]. This means collisional frequency would assume a bimodal distribution along the centerline of the

cones; first, the zone at the sampler tip where the plasma first enters the interface, then the zone of silence where collisions drop and finally an upsurge as atoms expand through shock waves at the skimmer tip into the second and higher vacuum stage.

The particles during the journey above appear to be in electrical 'quasineutrality', meaning roughly equal amounts of electrons and ions [5]. This is thanks to a small Debye length in the plasma (~10^{-3} mm) [5]. The Debye length is the distance in which ions in a plasma will be influenced by electric fields. The sampler aperture is orders of magnitude larger (~1 mm) and therefore the charged particles in the ICP can pass through uninhibitated by the conductive metal. The Debye length grows to ~10^{-2} mm by the skimmer [5], but this is still small enough to allow the electrons and ions to pass undisturbed into second vacuum stage. After the skimmer tip is another story.

The pressure behind the skimmer is sufficiently low that enough electrons have enough mobility to leave the ion beam emerging from the skimmer significantly positive [5]. The cations repel each other and the ion beam defocuses. Lightweight species are repelled farthest and fastest and so heavier masses are transmitted preferentially. Most, if not all, ICP-MS instruments have some degree of a mass bias. The entire distance from sampler to skimmer is traveled in ~3 μs.

The need to extract positive ions and repel negative ones requires putting a voltage difference between the cones and ion optics. This is not so much a problem however as a voltage difference between the cones and the plasma. In the early days of ICP-MS the RF powered load coil was connected to the power source at one end and grounded at the other. The resulting potential gradient would capacitively couple with the plasma. If the plasma gained too much potential an electrical discharge would occur between the plasma and the

sampler cone. This discharge would widen the kinetic energy spread of the ions degrading resolutions. Methods to reduce the plasma potential were quickly developed. The method used in this dissertation is a guard or shield electrode. A grounded sheath of Pt is wrapped around the torch so that it is positioned between the load coil and the plasma. ICP's with this type of shield electrode are referred to as shielded.

Polyatomic Ions

General Problem

Although the high temperature of the ICP (~5500 K) gives extensive atomization, large concentrations of Ar, O, H and N move dissociation reactions back toward polyatomic ions. This rather annoying fact has been a constant since the ICP-MS was developed in the 1980's [7]. The most common polyatomic ions involve atoms from the plasma, the solvent, and entrained air. Diatomics dominate (Ar_2^+, ArH^+, ArO^+, MO^+, NO^+, OH^+, O_2^+) although H_2O^+ and H_3O^+ are abundant as well.

Though mostly low in mass, these diatomic ions interfere with certain important isotopes. For example, $^{40}Ar^1H^+$ and $^{38}Ar^1H^+$ overlap with $^{39}K^+$ and $^{41}K^+$ (93.3% and 6.7% abundance), $^{15}N^{16}O^+$ and $^{14}N^{17}O^+$ with the monoisotopic $^{31}P^+$, $^{16}O^{16}O^+$ with the major isotope of $^{32}S^+$ (95% abundance), $^{40}Ar^{16}O^+$ with $^{56}Fe^+$ and $^{40}Ar^{40}Ar^+$ and $^{36}Ar^{40}Ar^+$ with $^{80}Se^+$ and $^{78}Se^+$. These examples can be separated with a sector-field instrument but not with the more prevalent quadrupoles. Also, metal oxides (MO^+) and metal hydrides (MH^+) starting near mass-to-charge 90 require resolutions exceeding that of the current magnetic sector instruments [2].

Behavior of Polyatomic Ions

At first it was thought that polyatomics might serve as internal standards during analyses [8]. Unfortunately it became apparent that polyatomics behaved differently than analyte ions and sometimes differently than other polyatomics. For instance, while analyte ions give a Gaussian signal profile across the ICP, Ar^+ and argon containing polyatomics have a bimodal profile with a minimum where analyte ions are maximized [9]. Along the length of the ICP, analyte and polyatomic ions tend to peak at different points [9].

Dealing with Polyatomic Ions in ICP-MS

Several successful techniques have been developed to ameliorate polyatomic ions. Cool plasma refers to operating the ICP at lower powers (600-800 W) and higher argon gas flow rates. This reduces the ionizing energy of the plasma dramatically reducing the presence of high ionization energy species such as Ar^+, and O^+ and their compounds like ArX^+ and CO^+. Unfortunately, analyte ions with high ionization energies are also greatly reduced. Still this is a common technique for measuring Ca^+, K^+ and Fe^+.

Collision cells have become nearly ubiquitous for newer quadrupole instruments. In collision cells another gas is added to a multipole through which the ion beam passes. For example, NH_3 gas added to a collision cell will react with ArO^+ to produce Ar, O and NH_3^+. The charged ammonia molecules can then be removed to prevent further, unwanted, reactions [10-11]. Alternatively, the gas can be added to the ion beam at the cone tips through special cones with hollow sides, with similar results [12].

Solvent removal can reduce polyatomic ions with solvent constituent atoms while maintaining, or even enhancing, analyte levels [11]. The sample spray from the nebulizer is

passed through a cooled and/or heated apparatus before reaching the plasma. A heated porous membrane is also used in some configurations to prevent solvent nucleation [13].

Several polyatomic ions can be resolved away from isobaric analyte ions with the use of double focusing mass spectrometers. Paired magnetic and electric sectors give resolutions up to ~10,000 although at the sacrifice of signal.

Although usually used for isobaric analyte signals, mathematical corrections could be applied to polyatomic ions as well [14]. For instance, the signal at m/z 52 ($^{38}Ar^{14}N^{+}$) could be used to correct for $^{40}Ar^{14}N^{+}$ at m/z 54. In another method, ion ratios could be measured in a blank sample so that monitoring the non-interfering ion in the sample would give the interference's levels [14].

Thermodynamic Equilibrium and Temperatures

Chemists are used to working with systems that can be described with one temperature. However, temperature is a measure of energy and there can be different energies in a system. The ICP is such a system and it cannot be described with one temperature. This goes beyond the obvious temperature gradients that appear as different levels of brightness. If attention is focused on a small area of the plasma and different types of data are collected, the resulting temperatures can span a fair range [15].

Ions are extracted from the ICP at just such an area. Tuning an ICP-MS for maximum signal places the sampler at a certain point. This point will have similar characteristics from day to day, electron number density, optical emission line intensities, and temperature. The temperature values measured, however, vary with the method and species used.

The energy that exists as kinetic motion can be found in terms of a gas kinetic temperature, T_{gas}. T_{gas} can be measured using ion kinetic energies, Doppler widths of emission lines, Thomson and Rayleigh scattering and gas velocities [15-18]. Similarly, energy available for ionization processes can be found in terms of ionization temperature, T_{ion}. T_{ion} can be found by optical or mass spectrometric measurements of neutral atoms, single and doubly charged ions finding the temperature in the corresponding Saha equation [5]. These two temperatures describe most of the work in this dissertation, but other temperatures have been measured in the ICP, including rotational temperature, T_{rot}, from molecular band emissions [15], and excitation temperature T_{exc} from optical measurements and Bolzmann plots [19].

At the sampling point, ionization temperatures (~7000 K) tend to be one to two thousand Kelvin higher than gas kinetic temperatures (~5500 K) while rotational temperatures measured from OH lines tend to be substantially lower (~3500 K) [15]. Excitation temperatures tend be similar to gas kinetic temperatures [20-23]. Some have found a non-Boltzmann distribution of particles among energy states [20,24-25], but later studies saw Boltzmann distributions and their conditions are closer to those studied in this dissertation[21-23,26-27].

Dissertation Organization

This dissertation is organized into five chapters and two appendices. The first chapter is a general introduction to ICP-MS and polyatomic ion interferences. Chapters 2, 3, 4 and 5 are manuscripts of papers to be submitted to Spectrochimica Acta Part B. Chapter 2 describes the mathematical method used throughout the chapters and in Appendix A,

evaluating the effect of certain modifications and additions. Chapter 3 applies the mathematical method to a set of experimental data, using the results to draw conclusions on the behavior of specific polyatomic ions. Chapter 4 examines variations of the mathematical method applied to ArO^+, an ion requiring a different approach than the ions in chapter 3. Chapter 5 reports studies on the memory behavior of certain metal oxides. Appendix A is a paper published in Spectrochimica Acta Part B on which I appear as a secondary author. I contributed data analysis and minor editing assistance. Appendix B is a paper published in Analytical Chemistry on which I also appear as a secondary author. I contributed by replicating several of the experiments; this was necessary because the results were very surprising.

References

[1] Houk, R.S., ICP-MS Short Course I.
[2] Thermo-Finnegan ELEMENT2 software.
[3] D.J. Douglas, J.B. French, Gas dynamics of the inductively coupled plasma mass spectrometer interface, J. Anal. At. Spectrom. 3(1988) 743-747.
[4] K.E. Jarvis, A.L. Gray, R.S. Houk, Handbook of Inductively Coupled Plasma Mass Spectrometry, Blackie, Glasgow, 1992.
[5] H. Niu, R.S. Houk, Fundamental aspects of ion extraction in inductively coupled plasma-mass spectrometry, Spectrochim. Acta Part B 51 (1996) 779-815.
[6] M. Liezers, 1.2 Sampling Interface Design and Function and 1.3 Ion Extraction and Focusing, in ICP Mass Spectrometry Handbook, Ed. S.M. Nelms, Blackwell Publishing, Oxford UK, 2005.
[7] Houk, R.S., Fassel, V.A., Flesch, G.D., Svec, H.J., Gray, A.L., and Taylor, C.E. Inductively coupled argon plasma as an ion source for mass spectrometric determination of trace elements, Anal. Chem., 52 (1980) 2283-2289.

[8] Chen, X. and R.S. Houk, Polyatomic Ions as Internal Standards for Matrix Corrections in Inductively Coupled Plasma Mass Spectrometry, J. Anal. At. Spect., 10 (1995) 837-841.
[9] Holliday, A.E., and D. Beauchemin, Review: Spatial profiling of analyte signal intensities in inductively coupled plasma mass spectrometry, Spectrochim. Acta B 59 (2004) 291-311.
[10] S.D. Tanner, V.I. Baranov, D.R. Bandura, Review: Reaction cells and collision cells for ICP-MS: a tutorial review, Spectrochim. Acta B 57 (2002) 1361-1452.
[11] R. Thomas, Practical Guide to ICP-MS, Marcel Dekker, Inc., New York, 2004
[12] Varian, Inc., Palo Alto, CA, USA
[13] J.L. Todoli, F. Vanhaecke, Liquid Sample Introduction and Electrothermal Vaporisation for ICP-MS: Fundamentals and Applications, in ICP Mass Spectrometry Handbook, Ed. S.M. Nelms, Blakwell Publishing, Oxford, UK, 2005.
[14] J.W. Ferguson, Chapter 1. Introduction, Ph.D. Dissertation, Iowa State University, 2006.
[15] R.S. Houk, N. Praphairaksit, Dissociation of polyatomic ions in inductively coupled plasma, Spectrochim. Acta B 56 (2001) 1069-1096.
[16] A. Montaser, H. Zhang, Mass spectrometry with mixed-gas and helium ICPs, in Inductively Coupled Plasma Mass Spectrometry ed. A. Montaser, Wiley-VCH, New York, 1998.
[17] D.J. Douglas, S.D. Tanner, Fundamental considerations in ICPMS, in Inductively Coupled Plasma Mass Spectrometry ed. A. Montaser, Wiley-VCH, New York, 1998.
[18] J.B. Olsen, J.H. Macedone, P.B. Farnsworth, Source fas kinetic temperatures in an ICP-MS determined by measurements of the gas velocities in the first vacuum stage, J. Anal. At. Spectrom. 21 (2006) 856-860.
[19] E.L. Bydder, G.P. Miller, A relaxation method for determining state of equilibrium and temperature ratio T_e/T_g in an argon ICPT, Spectrochim. Acta B 43 (1988) 819-829.
[20] G. Kruening, F.J.M.J. Maessen, Effects of the solvent plasma load of various solvents on the excitation conditions in medium power inductively coupled plasma, Spectrochim. Acta B 44 (1989) 367-384.
[21 K. Wagatsuma, Y. Danzaki, T. Nakahara, Comparative Study on the Excitation Mechanism of Chromium Emission Lines in the Argon Radio-Frequency Inductively-

Coupled Plasma, Nitrogen Microwave Induced Plasma, and Argon or Nitrogen Glow Discharge Plasmas, Spectr. Letters 36 (2003) 99-115.

[22] S. Sengoku, K. Wagatsuma, Comparative Studies of Spectrochemical Characteristics between Axial and Radial Observations in Inductively Coupled Plasma Optical Emission Spectrometry, Anal. Sciences 22 (2006) 245-248.

[23] Z. Cui, K. Kodama, H. Oyama, K. Kitagawa, Two-dimensional observation of excited atoms and ions and excitation temperature in inductively coupled plasma using newly developed four channel spectrovideo camera, J. Vis. 13 (2010) 89-96.

[24] P.B. Farnsworth, The Inductively Coupled Plasma as a Source for the Measurement of Fundamental Spectroscopic Constants, Physica Scripta. T47 (1993) 36-41.

[25] M. Grotti, C. Lagomarsino, J.M. Mermet, Effect of operating conditions on excitation temperature and electron number density in axially-viewed ICP-OES with introduction of vapours or aerosols, J. Anal. At. Spectrom. 21 (2006) 963-969.

[26] Y. Danzaki, K. Wagatsuma, Effect of acid concentrations on the excitation temperature for vanadium ionic lines in inductively coupled plasma-optical emission spectrometry, Analytica Chimica Acta 447 (2001) 171-177.

[27] P. Andre, J. Ondet, R. Pellet, A. Lefort, The calculation of monatomic spectral lines' intensities and composition in plasma out of thermal equilibrium; evaluation of thermal disequilibrium in ICP torches, J. Phys. D: Appl. Phys. 30 (1997) 2043-2055.

CHAPTER 2. MEASUREMENT OF DISSOCIATION TEMPERATURES FOR POLYATOMIC IONS IN INDUCTIVELY COUPLED PLASMA-MASS SPECTROMETRY: VALIDATION AND VARIATIONS OF A METHOD

A paper to be submitted to Spectrochimica Acta Part B

Sally M. McIntyre, Jill Wisnewski Ferguson, R.S. Houk

Abstract

The general method of comparing measured ion ratios to calculated ion ratios to determine a gas kinetic temperature, T_{gas}, is reviewed. Various mathematical refinements to the calculated partition functions are examined for their effect on the determined T_{gas}. It is found that, (a) excited electronic states should be included for ArO^+, and neutral NO, and O_2; (b) a 10% error in solvent load, sample gas flow rate, vibrational constant, rotational constant or measured ion ratio produces only a 1-3% error in T_{gas}; (c) a 10% error in dissociation energy creates nearly a 10% error in T_{gas}; (d) high temperature corrections to the partition functions produce minimal change and can generally be neglected; (e) sufficient collisions occur in the supersonic expansion to account for additional polyatomic ions created after the plasma.

1. Introduction

Inductively coupled plasma-mass spectrometry (ICP-MS) is one of the major elemental analysis techniques used today. An ICP-MS instrument works by atomizing and ionizing a liquid or gas sample. Unfortunately, even at 5000 to 6000 K, not all of the sample is con-

verted to single atoms [1-2]. Statistical thermodynamics shows that a small fraction of polyatomic ions will survive the plasma, even those with very weak bonds like ArO^+ and Ar_2^+ (0.312 and 1.2 eV) [3-4].

Polyatomic ions that interfere with elemental signals at the same nominal mass-to-charge (m/z) values lead to incorrect analyses and poorer limits of detection. Particular problems arise from polyatomic ions containing Ar, O, H and N due to the great abundance of those elements in the plasma, sample and/or solvent. Many studies have investigated the effect of various plasma and instrument conditions on polyatomic signals [5]. Methods such as collision cells [6-7], high resolution instruments [8], cool plasmas [9-10], and solvent removal [11-12], have been developed to attenuate their effects. While these techniques have been largely successful, a better fundamental understanding of the origin and behavior of polyatomic ions could lead to the construction of instruments that intrinsically minimize the formation of these interferences. Existing techniques would be even more effective resulting in lower limits of detection, higher throughput and lower costs.

In 1988 Douglas and French applied a hemispherical sink model to the flow of plasma particles through the sampler cone of an ICP-MS. They calculated that an analyte atom would collide with argon atoms at most 250 times during the flow from Mach 0.7 (0.1 mm downstream from the sampler tip) to the skimmer tip [13]. Collisions between analyte atoms and atoms of oxygen and hydrogen from the sample solvent would be two to three orders of magnitude less frequent. They concluded that the production of metal oxide ions (MO^+) after the Mach 0.7 position would be essentially nonexistent.

In 1994, Nonose et al. compared measured polyatomic ion signals to theoretical number densities calculated from spectroscopic data [4]. This allowed them to divide the polya-

tomics studied into two groups. ArX^+ species appeared to reach dissociation equilibrium in the interface. NO^+, O_2^+ and MO^+ species were observed at levels characteristic of the plasma.

In 1996 Cleland and Meeks used a similar technique to determine the most probably formation mechanism of Ar_2^+. They found a T_{gas} at which experimental ion ratios equaled calculated ion ratios. Of the mechanisms investigated, they found the collision of neutral and charged argon atoms to give the argon dimer to have the most realistic T_{gas} of 2400 K [14].

In 2001, Houk and Praphairaskit used this same idea and reported the T_{gas} at which experimental ion ratios equaled ion ratios calculated at various T_{gas} values [3]. They postulated that the T_{gas} value measured in this way would be indicative of the area of the instrument where final dissociation equilibrium was established. They argued that, at the very least, comparison between polyatomic ions would be instructive. In 2006 Ferguson et al. expanded this work to investigate the effect of operating conditions on T_{gas}, and to apply the method to some additional polyatomic ions not considered previously, e.g. $C_xH_yO^+$ [15-17].

In 2002, Evans, et al. used this same technique along with two variations of Boltzmann plots [18]. Although the Evans' group used only a few of the polyatomics listed in Nonose et al., and Houk and Praphairaksit, similar results were found for the ions that did overlap.

2. Theory[3,19-22]

2.1 Origin of Polyatomic Ion from T_{gas}

The method used in Nonose et al., Houk and Praphairaskit, Evans et al. and Ferguson et al. postulates a dissociation reaction for the polyatomic ion. Assume a generic polyatomic

ion, AB^+, with a dissociation energy, D_o, and where A may be one or more atoms and B is either Ar, O or H,

$$AB^+ \rightleftharpoons A^+ + B, \Delta E = D_o \quad (1)$$

The equilibrium constant, K_d, for this reaction can be found in two ways, by measuring equilibrium number densities, *n*, concentrations and by calculation with partition functions, Z, at a given temperature.

$$\frac{n_{A^+} n_B}{n_{AB^+}} = K_d = \frac{Z_{A^+} Z_B}{Z_{AB^+}} e^{-D_o / kT} \quad (2)$$

The T_{gas} that gives best agreement between the two sides is considered to be indicative of the region where the polyatomic ion is made. The sampling point of the plasma, the position that gives highest atomic ion signal, is consistently at a gas kinetic temperature of 5000 to 6000 K. If the measured T_{gas} values fall within that range, AB^+ is made in the plasma and neither created nor destroyed in the interface. If $T_{gas} < 5000$ K there is an excess of AB^+; if $T_{gas} >$ 6000 K, less AB^+ is being measured compared to that expected from the plasma. To avoid misnaming and confusion K_d is called the dissociation constant.

2.2 Mass Bias Corrections and Number Densities of Neutral Species

When using the measured ion ratio a correction should be done to account for mass bias in the instrument. We use an instrument response curve based on Ingle et al. [23,15]. To calculate neutral B number density entrained air is neglected leaving the major constituents of the plasma as argon, oxygen and hydrogen from the plasma and aqueous sample solution. These three elements have low ionization efficiencies in the plasma, 0.04%, 0.1% and

0.1% respectively, so they are present almost totally as neutrals [1]. The total number density in the plasma is calculated from the Ideal Gas Law.

$$n_{tot} = n_{Ar} + n_O + n_H = \frac{P}{RT_{gas}} \tag{3}$$

Neutral oxygen and hydrogen atoms are assumed to come from the nearly complete dissociation of water. If the amount of water loaded into the ICP torch per unit time is measured and the sample carrier gas flow rate is known, n_o can be calculated by the following,

$$n_O = \frac{\mathrm{N_A L T_{room}}}{\mathrm{F M_{H_2O} T_{gas} 1000}} \tag{4}$$

Where N_A is Avogadro's number, L is the measured solvent load (g min^{-1}), T_{room} is the room temperature (298 K), F is the sample gas flow rate (l min^{-1}) and M is the molar mass of water (g mol^{-1}).

Once the number density of oxygen is known the density of the other neutrals can be found,

$$n_H = 2n_O \tag{5}$$

$$n_{Ar} = \frac{P}{RT_{gas}} - 3n_O \tag{6}$$

2.3 High Temperature Corrections to the Partition Functions

Partition functions come from the denominator of the Boltzmann equation,

$$\mathrm{Z} = \sum_{i=0}^{\infty} g_i e^{-\epsilon_i / k_B T} \tag{7}$$

where ϵ_i is the energy of the ith level, g_i is the degeneracy of ith level and k_B is the Boltzmann constant. Energy level equations are derived using the time-independent Schroedinger

equation and simple models. For a molecule, the energy levels are treated as the sum of the electronic, translational, vibrational and rotational energies. The total partition function then becomes a product.

$$Z = z_{elec} z_{trans} z_{vib} z_{rot} \tag{8}$$

Translational energy levels are addressed simply and accurately with the particle-in-a-box model and the resulting partition function works for both atoms and molecules.

Electronic partition functions for atoms and atomic ions have been conveniently computed in the form of polynomials for temperatures ranging from 1500 K to ~12,000 K [24-26]. For molecules the first excited electronic state is usually high enough in energy that it makes an insignificant contribution to the electronic partition function. Statistical thermodynamics texts recommend addition of electronic levels other than ground state only if highly accurate calculations are being done, there is an unusually low-lying excited state, or high temperatures are being used [19,22]. Because ϵ_0 can be set to zero, the molecular electronic partition function simplifies to the degeneracy of the ground state which is approximated by the multiplicity for sigma terms and two times the multiplicity for all other terms [19,22].

Vibrational and rotational energy levels come from the harmonic oscillator and rigid rotor models. More accurate models would be the Morse oscillator and the vibrating rotor, but agreement between the first and second models is good for all but the most precise calculations, as long as the majority of molecules remain in low vibrational levels. As temperature increases and higher levels are populated the two sets of models will gradually diverge leading to larger errors in the overall partition function. Since the ICP is at high temperatures, such corrections should be investigated.

At high temperatures three corrections can be applied to the energy levels of the harmonic oscillator and rigid rotor [19,27].

1. Addition of centrifugal stretching constants (D_e,…) to account for the increased rotational energy increasing the centrifugal force and stretching the internuclear bond.

$$E_{rot} = BhcJ(J+1) - D_e hcJ^2(J+1)^2 + \ldots \tag{9}$$

E_{rot} is rotational energy, B is the rotational constant, h is Planck's constant, c is the speed of light and J is the rotational quantum number.

2. Addition of anharmonicity constants (x_e, y_e,…) to help correct deviation from Morse oscillator behavior:

$$E_{vib} = hc\omega\left(v+\frac{1}{2}\right) - x_e hc\omega\left(v+\frac{1}{2}\right)^2 + y_e hc\omega\left(v+\frac{1}{2}\right)^3 + \ldots \tag{10}$$

where v is the vibrational quantum number and ω is the vibrational constant.

3. Addition of coupling constants (α, β,...) because rotation and vibration are not truly independent. In the Morse oscillator changing vibrational levels changes the mean internuclear distance, changing the moment of inertia and thus the rotational constant. B and D_e from equation 9 then become B_v and D_v where,

$$B_v = B - \alpha\left(v+\frac{1}{2}\right) + \ldots \tag{11}$$

$$D_v = D_e + \beta\left(v+\frac{1}{2}\right) + \ldots \tag{12}$$

Unless very precise calculations are needed, the expansions are truncated after the first correction terms, D_e, x_e and α.

2.4 Correction for Ionization Reactions

The previous work approached the polyatomic ion dissociation reaction as isolated from any additional equilibria considerations. In particular, the extent of ionization for neutral polyatomic and atomic ions was not incorporated because overall number densities are much larger than losses to ionization, formation and dissociation reactions. One way to test any impact of considering multiple reactions is to expand reaction 1 into three reactions using a thermodynamic cycle.

$$AB \rightleftharpoons A + B \qquad K_d\,(AB) = f(T_{gas}) \tag{13}$$

$$A \rightleftharpoons A^+ + e^- \qquad K_{ion}\,(A) = f(T_{ion}) \tag{14}$$

$$AB^+ + e^- \rightleftharpoons AB \qquad 1/K_{ion}\,(AB) = f(T_{ion}) \tag{15}$$

where T_{ion} = ionization temperature. The dissociation constant for reaction 1 can then be calculated by multiplying the constants of reactions 13-15. Note that 14 and 15 use ionization constants which are functions of T_{ion} which does not equal T_{gas} in the ICP [28]. Otherwise K_{ion} can be calculated in the same manner as K_d (equation 2) where neutral B is just replaced with an electron.

3. Experimental Section

Adjustments were done to the original calculations from 24 experimental runs outlined in another paper [29]. These trials spanned different cone materials (Ni, Pt, Al and mixes), plasma conditions (hot vs. cold) and X vs H skimmer cone geometries. All data analysis and calculations were done in Microsoft Excel 2003 or 2007.

All partition functions, neutral B number densities, and dissociation constants were calculated iteratively in 10 K increments. Ionization constants were calculated using the Saha

equation [1] and a T_{ion} of 7000 K for hot plasma conditions. This value is a compromise between older values of 7500 K [1] and 6529 K from a newer study by Bayon et al. [28]. For cold plasma conditions T_{ion} = 4750 K was used [30]. For the ionization efficiencies shown in Table 3, $n_e = 1x10^{15}$ cm^{-3} [1] was used.

Instrument response curves for hot plasma conditions take blank subtracted intensities divided by isotope abundance, ionization efficiency in the plasma [1], and concentration in solution and plot the response versus m/z. Under cold plasma conditions ionization efficiencies were recalculated but resulting response curves made no sense and a polynomial line could only be fit to an R^2 of 0.2748. When ionization efficiency was ignored or hot plasma efficiencies were used a polynomial could be fit to the result with an $R^2 = 0.9671$. Therefore, instrument response curves for cold plasma runs were calculated in the same manner as for hot plasma runs.

High temperature corrections for diatomic molecules were done by using the following equation [19] for the rotational and vibrational partition functions. Pitzer's appendix was also useful in understanding this derivation [27].

$$z'_{rv} = \frac{1}{\sigma y}\left(\frac{1}{1-e^{-t}}\right)\left(1+\frac{y}{3}+\frac{2\gamma}{y}+\frac{\delta}{e^{t}-1}+\frac{2x_e t}{\left(e^{t}-1\right)^2\left(1-2x_e\right)}\right) \tag{16}$$

where σ is the symmetry number of the diatomic molecule. Heteronuclear diatomic ions have σ = 1 and homonuclear diatomic ions have σ = 2. Symbols *y*, *t*, γ and δ are substitution constants as follows,

$$y = \frac{hc}{kT}\left(\mathrm{B}-\frac{1}{2}\alpha\right) \tag{17}$$

$$t = \frac{hc}{kT}\left(\omega - 2\omega x_e\right) \tag{18}$$

$$\gamma = \frac{\mathrm{D_e}}{\left(\mathrm{B} - \frac{1}{2}\alpha\right)} \tag{19}$$

$$\delta = \frac{\alpha}{\left(\mathrm{B} - \frac{1}{2}\alpha\right)} \tag{20}$$

As can be seen, only the first order corrections for centripedal stretching, D_e, anharmonicity, x_e, and vibrational stretching, α, are used. These constants are often reported with basic spectroscopic data [31] but can also be calculated as was done in this work.

$$x_e = \frac{hc\omega}{4D} \tag{21}$$

$$\mathrm{D_e} = \frac{4\mathrm{B}^3}{\omega^2} \tag{22}$$

$$\alpha = \frac{6\mathrm{B}^2}{\omega}\left[\left(\frac{x_e\omega}{\mathrm{B}}\right)^{1/2} - 1\right] \tag{23}$$

D is well depth or the dissociation energy plus the zero point energy.

Equation 16 is the result of truncating after the first or second terms of the Euler-Maclaurin expansions of the energy level summations. Preliminary work with MATLAB (MathWorks, Natick, Massachusetts) showed no effect when additional terms were added.

4. Results and Discussion

4.1 Electronic Partition Functions of Diatomic Molecules

Table 1 lists ground and excited electronic states for each of the diatomic ions studied in this paper (excluding CeO^+ and ScO^+), the energy difference between the ground and first excited electronic levels and any error in the electronic partition function that comes from not adding the first excited electronic state. The ground electronic state assumption at 5000 K gives a less than 5% difference for every diatomic ion except ArO^+. ArO^+ proved to be surprisingly difficult to evaluate for gas kinetic temperatures. Work with this polyatomic ion is discussed in another paper [36].

In equations 13 and 15 the partition function for the neutral diatomic molecule needs to be calculated. Table 2 lists the first two electronic states of some neutral diatomic molecules and their contributions to the electronic partition function. Two species have an important low lying electronic level, O_2 and NO. In fact, these two molecules are often given as cases when excited electronic states need to be included, even at room temperature [19,21]. Therefore calculations with these two neutral diatomics always included the first excited electronic states.

4.2 Effect of High Temperature Rotational-Vibrational Corrections to Partition Functions

The high temperatures of 5000 to 6000 K at the sampling point in the ICP are well above the warning line of 3000 to 4000 K given in some statistical thermodynamics texts [19]. Yet when equation 16 was used there were only minimal changes in T_{gas} compared to simpler calculation models [3]. Across the 23 trials T_{gas} measured from Ar_2^+, ArH^+, O_2^+, ScO^+ never changed more than 10 K. ArN^+ and OH^+ showed a 10 K increase once. CeO^+

and NO^+ gave the largest T_{gas} values in this work and therefore would be expected to need the temperature correction most. The largest changes in T_{gas} were seen in these two with increases by up to 40 K, although this would still not change the diagnoses of the origins of these ions [29].

Because the main goal of this work is to estimate ion origin and such minor changes in T_{gas} do not affect these diagnoses, high temperature corrections were therefore not used further in this work.

4.3 Addition of Ionization Energy for Neutral Diatomic Molecules

O_2^+, NO^+, OH^+, CeO^+ and ScO^+ were examined for the effect of including ionization equilibria. Table 3 lists the ionization energies and calculates the percent ionization of each species at T_{ion} = 7000 K and an electron density of $1x10^{15}$ cm^{-3} [40-41]. The results are given in Figures 1 and 2. Note that n_e was only used to calculate the values in Table 3. In equations 14 and 15 the electron number densities cancel.

In the hot plasma trials no species changed its essential behavior. CeO^+ and O_2^+ still gave characteristic plasma temperatures at the sampling point. NO^+ still gave a high temperature indicating less NO^+ than expected. OH^+ still gave a low temperature indicating more OH^+ than expected given plasma conditions alone.

For cool plasma conditions ScO^+ was used to give the estimated temperature range for the plasma at the sampling point because Ce^+ signal was insufficient. Inclusion of ionization energies led to similar changes as described above as shown in Figure 2. Average T_{gas} values changed slightly but overall diagnoses did not. The two possible exceptions are NO^+ and O_2^+. The average T_{gas} for NO^+ dropped by 240 K. The black box in Figure 2 shows an

approximate 1000 K difference with the center on the T_{gas} of ScO^+. NO^+ goes from just above this box to just below the top line of this box. This could move NO^+ from loss of polyatomic ion after extraction to levels expected in the plasma. However, it seems more likely that the possible temperature spread for the plasma would be smaller under cold conditions shrinking the box and keeping NO^+ at a diagnosis of loss-in-the-interface.

By the same consideration O_2^+ could change its diagnosis from plasma levels to excess polyatomic ion. However, the argument from NO^+ applied here would leave O_2^+ firmly in the later category for both calculation methods.

To summarize, inclusion of ionization reactions in the calculated K_d does change the T_{gas} but not to a degree outside the day to day variations and not to a point of changing the diagnosis of the probable origin of the ions.

4.4 Error Analysis

Error analysis in these calculations is not a matter of simple error propagation. Iteration is used precisely because there is no straightforward equation to find T_{gas} from the measured signal ratio and K_d. Therefore, to test the effect of change in one variable, value + 10% was entered into the spreadsheet and the new T_{gas} evaluated. In this way the effect of 10% errors in solvent load, sample gas flow rate, vibrational constant, rotational constant, dissociation energy and the ion ratio were investigated for one day's data. Results from this error analysis are presented in Table 4. The day under consideration used nickel cones, an H-geometry skimmer, and 'hot' plasma conditions.

As expected, the dissociation energy had the largest impact. A 10% change in D_o led to about 10% changes in temperature. Thus, reasonably accurate values for this quantity are

a priority. Changing solvent load, sample gas flow rate, vibrational constants, rotational constants and even ion ratios by 10% usually produced errors in the T_{gas} only about a tenth of that (-140 to 40 K change, 0.7-3.1% of T_{gas}). In general, such errors will not affect the diagnosis of ion origin.

4.5 Number of Collisions

It is a valid question to ask whether these observed variations to the equilibrium ion ratios are even possible from a kinetics perspective. For example, excess polyatomic ions can only be made if the constituents first collide. Douglas and French believed that there were insufficient collisions to create many polyatomic ions after the sampler cone [13]. They calculated that in the nozzle of the sampler cone analyte ions collide 120 times with argon atoms before the Mach 1 position (~0.5 mm downstream of the sampler tip). Use of number densities to scale down gives approximately 10 collisions with O atoms and 20 collisions with H atoms.

New work has been done using experimental data and more complex modeling to show that the plasma cools more extensively than Douglas and French calculated [42], mainly due to thermal contact of the plasma with the cooled metal sampler cone. This would increase the number of collisions. Nevertheless, French and Douglas can be treated as a conservative estimate and their model will be taken as the basis for the following discussion.

First the number of two body collisions was calculated.

$$A^+ + B \rightarrow AB^+ \tag{20}$$

Number densities for neutral Ar, O and H were calculated based on solvent load and the T_{gas} measured from the CeO^+/Ce^+ ratio on the same day. O^+ and Ar^+ number densities were

found by assuming 0.1 and 0.04% ionization of the O and Ar [1]. All other atomic and polyatomic ion number densities were found using mass bias adjusted ratios.

The number density of A^+ was then multiplied by 120, 10 or 20 depending on the identity of the neutral B species. This was the number of two-body collisions.

Using the calculated dissociation constant and the neutral B number density, the predicted number density of AB^+ at the CeO^+ T_{gas} was calculated. This predicted number density was subtracted from the number density of AB^+ calculated from the spectral signal. This difference is the amount of AB^+ that would need to be made after the plasma and was divided by the number of two-body collisions and multiplied by 100 to find the percentage of the A^+ and B collisions that would need to result in the creation of an AB^+ molecule. Those results are presented in Table 5.

The fraction of the collisions needed depends on the reaction under consideration. For example, Ar^+ and Ar collisions only needed to make Ar_2^+ 0.0002% of the time to account for the measured T_{gas} for Ar_2^+ while ~14% of the OH^+ and H collisions would need to make H_2O^+ to produce the temperatures measured.

Of course, the production of polyatomic ions is unlikely by two-body collisions. A three-body collision is most likely needed with the third species carrying off excess kinetic energy and allowing the other two species to bond. The rate of three-body collisions is 10^{-2}-10^{-3} times that of two-body collisions [43]. However, collisions with Ar are six times more likely than with H and 12 times more likely than with O. So, for polyatomic ions where the dissociation product is neutral O, the percentage of successful two-body collisions should be divided by 0.12-0.012. When neutral H is considered, the percentage should be divided by 0.06-0.006 and when neutral Ar is the dissociation product the percentage should be divided

by 0.01-0.001 to get the percentage of the three-body collisions needed to form the excess polyatomic ions seen.

Now the creation of excess polyatomic ions through collisions in the interface looks less realistic. However, the number of collisions was calculated for only the first 0.5 mm of the expansion. French and Douglas predicted an analyte species would collide with Ar *another* 120 times in the zone of silence of the supersonic expansion [13]. Also other reaction paths than the one used here are possible. In the case of H_2O^+ for instance, neutral OH and H may collide to make H_2O and then be ionized to H_2O^+ or H_3O^+ may collide with another species and disassociate into H_2O^+ and H. In short, production of excess polyatomic ions in the interface to the levels seen in the mass spectrum is not outside the realm of possibility.

On certain days, Ar_2^+, ArN^+, O_2^+ and NO^+ gave gas kinetic temperatures higher than that for CeO^+ indicating less polyatomic ion than expected from the plasma. If it assumed that all of the loss is through collision induced dissociations and that the two-body collisions are between the polyatomic ions and argon, only 1% of the collisions or less would be needed to explain the loss seen.

Acknowledgements

This research was supported by the National Science Foundation through the Institute for Physical Research and Technology at ISU. The ICP-MS instrument was obtained with funds provided by the U. S. Department of Energy, Office of Nuclear Nonproliferation (NA-22) and the Office of Basic Energy Sciences.

References

[1] H. Niu, R.S. Houk, Fundamental aspects of ion extraction in inductively coupled plasma-mass spectrometry, Spectrochim. Acta Part B 51 (1996) 779-815.

[2] D.J. Douglas, J.B. French, An improved interface for inductively coupled plasma mass spectrometry, Spectrochim. Acta B 41 (1986) 197-204.

[3] R.S. Houk, N. Praphairaksit, Dissociation of polyatomic ions in inductively coupled plasma, Spectrochim. Acta B 56 (2001) 1069-1096.

[4] N.S. Nonose, N. Matsuda, N. Fudagawa, M. Kubota, Some characteristics of polyatomic ion spectra in inductively coupled plasma-mass spectrometry, Spectrochim. Acta Part B 49 (1994) 955-974.

[5] A.E. Holliday, D. Beauchemin, Review: Spatial profiling of analyte signal intensities in inductively coupled plasma mass spectrometry, Spectrochim. Acta B 59 (2004) 291-311. And references therein.

[6] J.T. Rowan, R.S. Houk, Attenuation of polyatomic ion interferences in inductively coupled plasma mass spectrometry by gas-phase collisions, Appl. Spectrosc. 43 (1989) 976-980.

[7] S.D. Tanner, V.I. Baranov, D.R. Bandura, Reaction cells and collision cells for ICPMS:a tutorial review, Spectrochim. Acta B 57 (2002) 1361-1452.

[8] N. Bradshaw, E.F.H. Hall, N.E. Sanderson, Inductively coupled plasma as an ion source for high-resolution mass spectrometry, J. Anal. At. Spectrom. 8 (1989) 801-803.

[9] S.J. Jiang, R.S. Houk, M.A. Stevens, Alleviation of overlap interferences for determination of potassium isotope ratios by inductively coupled plasma mass spectrometry, Anal. Chem. 60 (1988) 1217-1221.

[10] S.D. Tanner, Characterization of ionization and matrix suppression in inductively coupled 'cold' plasma mass spectrometry, J. Anal. At. Spectrom. 10 (1995) 905-921.

[11] L.C. Alves, D.R. Wiederin, R.S. Houk, Reduction of polyatomic ion interferences in inductively coupled plasma mass spectrometry by cryogenic desolvation, Anal. Chem. 64 (1992) 1164-1169.

[12] M.G. Minnich, R.S. Houk, Comparison of cryogenic and membrane desolvation for attenuation of oxide, hydride and hydroxide ions and ions containing chlorine in inductively coupled plasma mass spectrometry, J. Anal. At. Spectrom. 13 (1998) 167-174.
[13] D.J. Douglas, J.B. French, Gas dynamics of the inductively coupled plasma mass spectrometer interface, J. Anal. At. Spectrom. 3 (1988) 743-747.
[14] T.J. Cleland, F.R. Meeks, Statistical mechanics of Ar_2^+ in an inductively coupled plasma, Spectrochim. Acta B 51 (1996) 1487-1490.
[15] J.W. Ferguson, R.S. Houk, High resolution studies of the origins of polyatomic ions in inductively coupled plasma-mass spectrometry, Part 1. Identification methods and effects of neutral gas density assumptions, extraction voltage, and cone material, Spectrochim. Acta Part B 61 (2006) 905-915.
[16] J.W. Ferguson, T.J. Dudley, K.C. Sears, S.M. McIntyre, M.S. Gordon, R.S. Houk, Polyatomic ions in inductively coupled plasma-mass spectrometry Part II: Origins of N_2H^+ and H_xCO^+ ions using experimental measurements combined with calculated energies and structures, Spectrochim. Acta B 64 (2009) 690-696.
[17] J.W. Ferguson, T.J. Dudley, M.S. Gordon, R.S. Houk, High resolution studies of the origins of polyatomic ions in ICP-MS Part III: $CrO_xH_y^+$ ions, Manuscript (2006).
[18] E.H. Evans, L. Ebon, L. Rowley, Comparative study of the determination of equilibrium dissociation temperature in inductively coupled plasma-mass spectrometry, Spectrochim. Acta Part B 57 (2002) 741-754.
[19] R.E. Sonntag and G.J. Van Wylen, Fundamentals of Statistical Thermodynamics, John Wiley and Sons, Inc., New York, 1966.
[20] J.H. Knox, Molecular Thermodynamics: An Introduction to Statistical Mechanics for Chemists, Chapter 6, Rev. Ed. John Wiley and Sons, Chichester, 1978.
[21] K.J. Laidler, J.H. Meiser, Physical Chemistry, Chapter 15, Houghton Mifflin Co., Boston, 1999.
[22] N.M. Laurendeau, Statistical Thermodynamics: Fundamentals and Applications, Chapter 9, Cambridge University Press, Cambridge, 2005.
[23] C.P. Ingle, B.L. Sharp, M.S.A. Horstwood, R.R. Parrish, D.J. Lewis, Instrument response functions, mass bias and matrix effects in isotope ratio measurements and semi-

quantitative analysis by single and multi-collector ICP-MS, J. Anal. At. Spect. 18 (2003) 219-229.

[24] L. De Galan, R. Smith, J.D. Winefordner, The electronic partition function of atoms and ions between 1500^{o}K and 7000^{o}K, Spectrochim. Acta B 23 (1968) 521-525.

[25] S. Tamaki, T. Kuroda, The electronic partition functions of atoms and ions between 7000 and 12 000 K, Spectrochim. Acta B 42 (1987) 1105-1111.

[26] B. Faggetter, G. Heisz, M.W. Blades, Research Note: The electronic partition functions of lanthanide atoms and ions between 1500 and 8000 K, Spectrochim. Acta B 42 (1987) 1235-1236.

[27] K.S. Pitzer, Quantum Chemistry. Prentice-Hall, Inc. New York, 1953.

[28] M.M. Bayón, J.I.G. Alonso, A.S. Medel, Enhanced semiquantitative multi-analysis of trace elements in environmental samples using inductively coupled plasma mass spectrometry, J. Anal. At. Spect., 13 (1998) 277-282.

[29] S. M. McIntyre, J.W. Ferguson, R.S. Houk, Polyatomic ions in inductively coupled plasma-mass spectrometry: Effects of cone material, skimmer cone geometry and cold plasma conditions on calculated versus measured ion ratios, manuscript (2010).

[30] D.M. McClenathan, W.C. Wetzel, S.E. Lorge, G.M. Hieftje, Effect of the plasma operating frequency on the figures of merit of an inductively coupled plasma time-of-flight mass spectrometer, J.Anal. At. Spectrom., 21 (2006) 160-167.

[31] K.P. Huber, G. Herzberg, Molecular Spectra and Molecular Structure IV. Constants of Diatomic Molecules, Van Nostrand Reinhold, New York, 1979.

[32] W.R. Wadt, The electronic states of Ar^{+}_{2}, Kr^{+}_{2}, Xe^{+}_{2}. I. Potential curves with and without spin-orbit coupling, J. Chem. Phys., 68 (1978) 402-414.

[33] L. Broström, M. Larsson, S. Mannervik, D. Donnek, The visible photoabsorption spectrum and potential curves of ArN^{+}, J. Chem. Phys., 94 (1991) 2734-2740.

[34] A.V. Stolyarov, M.S. Child, Phys. Chem. Chem. Phys., 7 (2005) 2259-2265.

[35] H.Frenking, W. Koch, D. Cremer, J. Gauss, J.F.Liebman, Neon and Argon Bonding in First-Row Cations NeX^{+} and ArX^{+} (X = Li-Ne), J. Phys. Chem., 93, (1989) 3410-3418.

[36] S. M. McIntyre, J.W. Ferguson, R.S. Houk, Determination of dissociation temperature for ArO^{+} in inductively coupled plasma-mass spectrometry, manuscript (2010).

[37] Periodic Table of the Elements, VWR Scientific Products Sargent Welch (1996) Buffalo Grove, IL.

[38] R.J. Ackermann, E.G. Rauh, R.J. Thorn, The thermodynamics of ionization of gaseous oxides; the first ionization potentials of the lanthanide metals and monoxides, J. Chem. Phys., 65 (1976) 1027-1031.

[39] D.E. Clemmer, J.L. Elkind, N. Aristov, P.B. Armentrout, Reaction of Sc^+, Ti^+, and V^+ with CO. MC^+ and MO^+ bond energies, J. Chem. Phys. 95 (1991) 3387-3393.

[40] R.S. Houk, Y. Zhai, Comparison of mass spectrometric and optical measurements of temperature and electron density in the inductively coupled mass spectrometric sampling, Spectrochim. Acta B 56 (2001) 1055-1067.

[41] D.J. Douglas, S.D. Tanner, Chapter 8 "Fundamental considerations in ICPMS", in Inductively Coupled Plasma Mass Spectrometry, Ed. A. Montaser, Wiley-VCH, New York, 1998.

[42] R.L Spencer, N. Taylor, P.B. Farnsworth, Comparison of calculated and experimental flow velocities upstream from the sampling cone of an inductively coupled plasma mass spectrometer, Spectrochim. Acta B 64 (2009) 921-924.

[43] H. Pauly, Atom, Molecule, and Cluster Beams: Basic theory, production, and detection of thermal energy beams, Springer, 2000.

Tables

Table 1. Effect of including first excited state on the electronic partition function of certain charged diatomic molecules.

	Ground State		First Excited Electronic State						
Ion	Term Symbol	$g_0(z_{elec})$	Term Symbol	g_1	Energy (cm^{-1})	$g_1e^{(-E1/kT)}$	z_{elec}	%Difference in z_{elec}	Source
O_2^+	$^2\Pi$	4	$^4\Pi$	8	32,964	0.00060723	4.00060723	0.0152	31
NO^+	$^1\Sigma$	1	$^3\Sigma$	3	52,190	0.00000090	1.00000090	0.00009	31
OH^+	$^3\Sigma$	3	$^1\Delta$	2	17,660	0.01241478	3.01241478	0.4	31
Ar_2^+	$^2\Sigma$	2	$^2\Pi$	4	12,986	0.09531766	2.09531766	4.8	32
ArN^+	$^3\Sigma$	3	$^3\Pi$	6	14,047	0.10534204	3.10534204	3.5	33
ArH^+	$^1\Sigma$	1	$^3\Pi$	6	49,163	0.00000430	1.00000430	0.0004	34
ArO^+	$^4\Sigma$	4	$^2\Pi$	4	3,490	1.46515850	5.46515850	36.6	35

Table 2. Effect of including first excited state on the electronic partition function of certain neutral species.

Ion	Ground State Term Symbol	$g_0(z_{elec})$	First Excited Electronic State Term Symbol	g_1	Energy (cm^{-1})	$g_1e^{(-E1/kT)}$	z_{elec}	%error	Source
O_2	$^3\Sigma$	3	$^1\Delta$	2	7,918	0.20485707	3.20485707	6.8	31
NO	$^2\Pi$	4	$^2\Pi$	4	120	3.86442842	7.86442842	96.6	31
OH	$^2\Pi$	4	$^2\Sigma$	2	32,684	0.00016454	4.00016454	0.0	31
ScO	$^2\Sigma$	2	$^2\Delta$	4	15,030	0.05292773	2.05292773	2.6	31

Table 3. Ionization energies and ionization efficiencies for atoms and neutral polyatomic ions under hot plasma conditions. $\% = \frac{n_{A+}}{n_A + n_{A+}} \times 100$

Species	Ionization Energy (eV)	(at T_{ion}= 7000 K, T_{gas}=5000 K and n_e = 1x10^{15} cm^{-3}) % ionization	Reference
O_2	12.071	0.5	31
O	13.618	0.02	37
OH	12.9	0.1	31
NO	9.26436	5	31
N	14.534	0.02	37
CeO	4.9	100	38
Ce	5.47	100	37
ScO	6.6	100	39
Sc	6.54	100	37

Table 4. Error analysis of one run. Hot plasma mode, Ni cones, H-skimmer geometry.

		CeO^+	Ar_2^+	ArN^+	ArH^+	O_2^+	OH^+	NO^+	H_2O^+	H_3O^+
	Initial T	5390	5130	5520	4880	5390	4670	7470	4080	3780
Solvent Load	*Plus 10%*	5410	5100	5490	4910	5420	4710	7510	4100	3790
	Difference	20	-30	-30	30	30	40	40	20	10
	%Difference	0.4	-0.6	-0.5	0.6	0.6	0.9	0.5	0.5	0.3
Sample Gas Flow Rate	*Plus 10%*	5360	5160	5540	4850	5350	4640	7430	4050	3770
	Difference	-30	30	20	-30	-40	-30	-40	-30	-10
	%Difference	-0.6	0.6	0.4	-0.6	-0.7	-0.6	-0.7	-0.6	-0.2
ω	*Plus 10%*	5370	4990	5410	4860	5360	4660	7440		
	Difference	-20	-140	-110	-20	-30	-10	-30		
	%Difference	-0.4	-2.7	-2.0	-0.4	-0.6	-0.2	-0.4		
B	*Plus 10%*	5360	4990	5410	4850	5350	4640	7430		
	Difference	-30	-140	-110	-30	-40	-30	-40		
	%Difference	-0.6	-2.7	-2.0	-0.6	-0.7	-0.6	-0.5		
D_0	*Plus 10%*	5870	5560	5990	5340	5900	5110	8180	4470	4090
	Difference	480	430	470	460	510	440	710	390	310
	%Difference	8.9	8.4	8.5	9.4	9.5	9.4	9.5	9.6	8.2
Ion Ratio	*Plus 10%*	5410	5290	5640	4910	5420	4710	7510	4100	3790
	Difference	20	160	120	30	30	40	40	20	10
	%Difference	0.4	3.1	2.2	0.6	0.6	0.9	0.5	0.5	0.3

Table 5. Summary of percent of 2 and 3-body collisions needed to make additional polyatomic as indicated by measured T_{gas}.

Collision Species	Polyatomic Ion	Average % of 2-body collisions needed to make polyatomic.	Average % of 3-body collisions needed to make Polyatomic	Number of trials
$Ar^+ + Ar$	Ar_2^+	0.00024	0.024-0.24	7
$H^+ + Ar$	ArH^+	0.57	57-570	20
$N^+ + Ar$	ArN^+	0.00034	0.034-0.34	12
$O^+ + O$	O_2^+	0.40	3.3-33	13
$O^+ + H$	OH^+	0.58	9.7-97	20
$OH^+ + H$	H_2O^+	13.7	230-2,300	20
$H_2O^+ + H$	H_3O^+	0.80	13-130	19

Figures

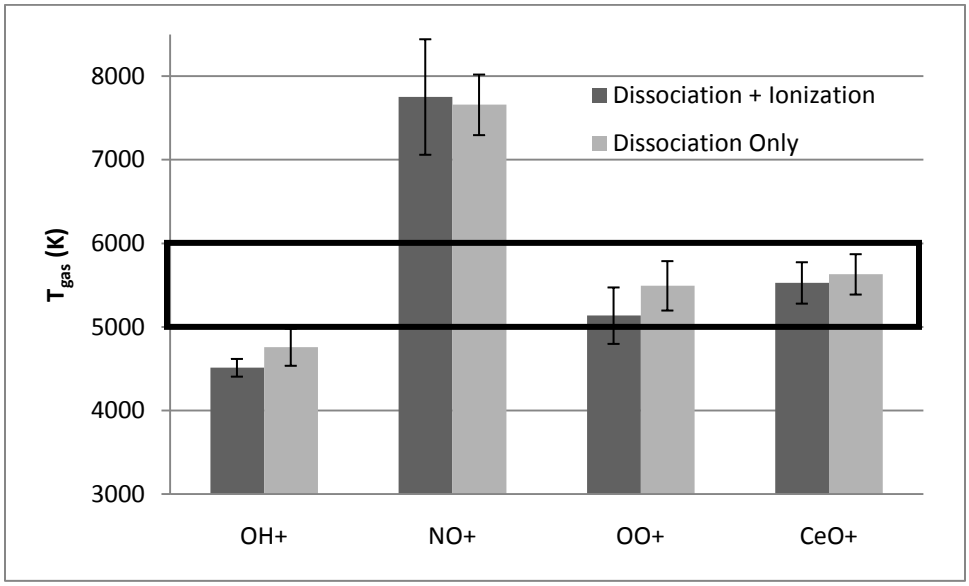

Figure 1. Gas kinetic temperature calculated setting Equations 2 and 3 equal to each other (Original) and calculated including ionization energy of the polyatomic molecule and charged dissociation product (Equations 8-10) (New) in a hot plasma. Box represents the typical range of plasma temperatures at the sampling point (5000-6000K). n = 20 and error bars correspond to standard deviation.

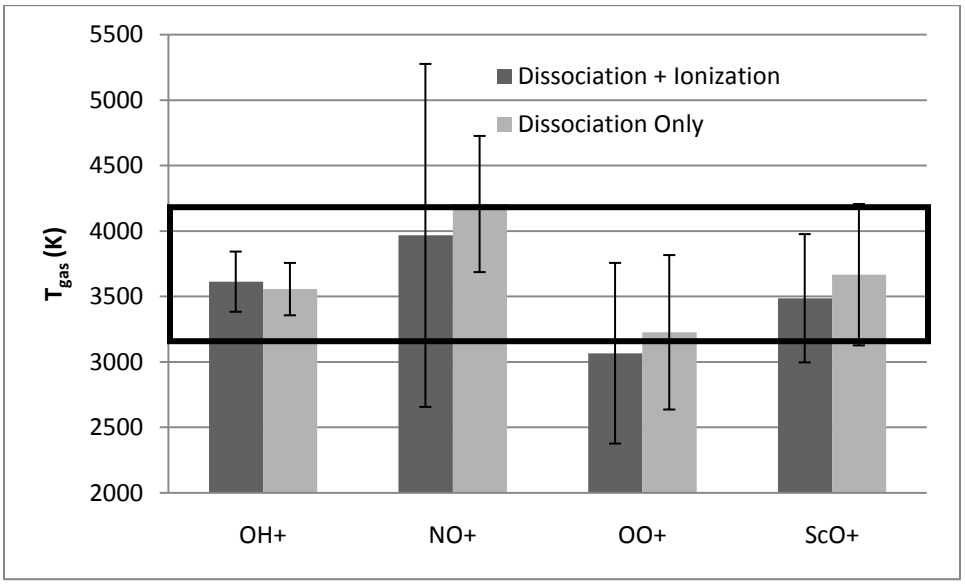

Figure 2. Gas kinetic temperature calculated setting Equations 2 and 3 equal to each other (Dissociation Only) and calculated including ionization energy of the polyatomic molecule and charged dissociation product (Equations 8-10) (Dissociation + Ionization) in a 'cold' plasma. Assuming the metal oxide gives a characteristic temperature of the plasma, the box represents a one thousand Kelvin range for the plasma temperature. Sixteen spectra on each of three days were averaged. Error bars correspond to range over the three days.

CHAPTER 3. GAS KINETIC TEMPERATURES OF POLYATOMIC IONS IN INDUCTIVELY COUPLED PLASMA-MASS SPECTROMETRY: EFFECTS OF CONE MATERIAL, SKIMMER CONE GEOMETRY AND COOL PLASMA CONDITIONS ON CALCULATED VERSUS MEASURED ION RATIOS

A paper to be submitted to Spectrochimica Acta Part B

Sally M. McIntyre, Jill Wisnewski Ferguson, R.S. Houk

Abstract

Gas kinetic temperatures (T_{gas}) are measured for eight common polyatomic species (NO^+, H_2O^+, H_3O^+, Ar_2^+, ArN^+, OH^+, ArH^+, O_2^+) as well as CeO^+ and ScO^+ by comparing measured ion ratios to ratios calculated with partition functions. Temperatures are reported for nickel, aluminum and platinum-tipped nickel cones and certain mixtures of sampler and skimmer cones. Temperatures are reported for standard H-skimmer geometry versus the newer X-skimmer geometry and for 'hot' and 'cool' plasmas. In general, for hot plasmas CeO^+, Ar_2^+, ArN^+, ArH^+, and O_2^+ gave temperatures characteristic of the plasma at the point of ion extraction (5000-6000 K), NO^+ gave a temperature above the plasma temperature (> 6000 K) and H_2O^+, H_3O^+ and OH^+ gave temperatures below the plasma temperature (< 5000 K). X-skimmers lowered T_{gas} values from Ar_2^+ and ArH^+ to below the plasma temperature except when the X-skimmer was paired with an aluminum sampler. Cool plasmas gave lower gas kinetic temperatures and less ion-to-ion variations in temperature overall, as ex-

pected. In the cool plasma Ar_2^+ and ArN^+ were again uniquely affected and gave temperature below that of the plasma.

1. Introduction

Polyatomic ions have been observed and investigated since the beginnings of inductively coupled plasma-mass spectrometry (ICP-MS) [1]. Combinations of Ar, O, H, and N are particularly prevalent due to their presence in the plasma and solvents. Polyatomic ions made from these elements overlap with major isotopes of several important elements including iron, calcium, potassium and selenium. Oxides and hydrides formed with analyte and matrix elements interfere with isotopes across the periodic table. Consequently, several methods and instrumentations have been developed to decrease the deleterious effect of polyatomic ions. For example, most commercial quadrupole ICP-MS instruments sold today include collision cells, or other ways to add a collision gas [2], to attenuate polyatomic ions.

Beyond their attenuation and elimination, the nature and origin of polyatomic ions have also been studied. It has been calculated that for the strongly bound metal oxides like CeO^+ (8.81 eV) [3-5] the metal oxide to metal (MO^+/M^+) signal ratios should be 1-2 % given the plasma temperature [6-7]. It has also been shown that dissociation and ionization reactions occur in the interface as well [8-9] offering another possible pathway for polyatomic ion generation or loss. The behavior of various polyatomics with plasma operating conditions has been a common subject [10].

In terms of determining generation or depletion behavior of polyatomic ions, this paper follows the method outlined in Nonose et al., Cleland and Meeks, Evans et al. and Houk

and Praphairaksit [11-16]. For polyatomic ions containing Ar, O or H, a dissociation reaction is proposed such that polyatomic ion AB^+ dissociates into A^+ and B where B is Ar, O or H and A^+ may be one or more atoms.

$$AB^+ \rightleftharpoons A^+ + B,\ \Delta E = D_o(A^+\text{-}B) \tag{1}$$

A dissociation constant, K_d, is found from experimental data (number densities, *n*) and calculated partition functions (Z),

$$\frac{n_{A^+} n_B}{n_{AB^+}} = K_d = \frac{Z_{A^+} Z_B}{Z_{AB^+}} e^{-D_o / k_B T_{gas}} \tag{2}$$

where D_o is the bond dissociation energy of AB^+ and k_B is the Boltzmann constant in the units of D_o. The T_{gas} that gives the best agreement between the two sides of equation 2 is considered to be indicative of the origin of the polyatomic ion. If T_{gas} is between 5000 and 6000 K the polyatomic ion is considered to come only from the plasma as this is the general temperature range of the part of the plasma that is extracted into the mass spectrometer [13]. If the T_{gas} is below 5000 K then it is considered that additional polyatomic ion is being made after the plasma, during the extraction through the interface where temperature falls as the expansion cools. If the T_{gas} is above 6000 K then it is considered that some of the polyatomic ion is removed during the extraction through the interface.

This paper compares T_{gas} values measured with different cone metals, X-geometry skimmer cones and cool plasma conditions. Cone material and structure have been shown to affect MO^+/M^+ ratios [17-19]. Skimmer cone geometry and cool plasma conditions can dramatically alter ArX^+ signal intensities [19-20].

2. Experimental Section

The instrument and basic experiment have been described elsewhere [14]. Basic operating conditions are reiterated in Table 1. For each daily run gas flows and ion optical voltages (occasionally torch position but not every run) were tuned to maximize $^{7}Li^{+}$, $^{115}In^{+}$ and $^{238}U^{+}$ signal. For this reason gas flows varied from day to day. A mass bias response curve [14,21] was measured using a 50 or 10 ppb solutions of Li, B, Na, Si, Sc, Fe, Co, Ga, Y, Rh, In, Lu, Tl, U in 1% nitric acid. Unfortunately, there was no way to test whether an atomic ion response curve is valid for polyatomic ions because at this time there is no known way of introducing standard amounts of polyatomic molecules into the ICP. This would be expescially problematic for additional polyatomic ions made in the interface if significant mass bias occurred there because the new polyatomic ions would not be exposed to the biasing effects for as long as the atomic ions. There is some evidence of mass bias occuring as far upstream as the plasma [22].

In hot plasma mode Ce^{+}, CeO^{+}, N^{+} ArN^{+}, NO^{+} and the elements in the response curve were measured in counting mode. The other species were measured in analog mode. All ratios were calculated using species measured in the same detection mode, i.e., CeO^{+} and Ce^{+} were both measured in counting mode to determine the ratio CeO^{+}/Ce^{+}, Ar_2^{+} and Ar^{+} in analog mode to determine the ratio Ar_2^{+}/Ar^{+} . All ions were measured at least 16 times for each run.

All solutions were made with deionized water (MilliporeQ, 18MΩ), and Ultrapure sub-boiled distilled nitric acid (J.T. Baker). Solvent load was found to be 0.04438 g min^{-1} (+/- 13.9% standard deviation). As reported in McIntyre et al. [15] a 10% difference in sol-

vent load yields less than a 1% change in T_{gas} so the standard deviation on the solvent load was not a concern.

The calculated dissociation constant equations are described elsewhere [13-15]. Statistical comparisons were done using a t-test at the 95% confidence interval [23].

Two skimmer geometries were used in these experiments: the standard, or older, H-skimmer and the newer X-skimmer. Both types were purchased from dealers and were specific to this commerical instrument. Magnified pictures of both types were taken in a LSX-500 (Cetac Technologies, Omaha, NE, USA) laser ablation cell of both an H and X geometry skimmer. A drawing detailing the observed differences is given in Figure 1. The outside of the cones are identical; the wall near the tip is narrower and the inner tip widens at a sharper angle in the X geometry.

Cool plasma mode was used on three days. To attain a cool plasma, $^{36}Ar^{16}O^{+}$, $^{115}In^{+}$ and $^{238}U^{16}O^{+}$ were monitored as the power was slowly reduced to 700 W and the sample gas flow rate was increased. The cool plasma mass bias response curves used some combination of ions from a 50 ppb solution of Li, Na, Mg, Fe, Co, Cu, Ga, and Rh in 1% HNO_3. In cold plasma mode there is little Ce^{+} signal, so Sc^{+} and ScO^{+} was measured with a 50 ppb solution of Sc in 1% HNO_3. Isotopes were chosen so that all ions could be measured in counting mode.

3. Results and Discussion

3.1 Cone Material

Aluminum, nickel and platinum-tipped-nickel cones were investigated (Table 2). The results of the statistical comparison are given in Table 3. One data point for ArN^+ in the aluminum cone sets could be rejected by the t_n test at the 95% confidence interval.

This study found few significant changes based on cone material. O_2^+ and OH^+ gave very consistent temperatures. In two comparisons where there was a statistical difference, there was still no change in the origin diagnosis for O_2^+ and OH^+ (NCD in Table 3). Interestingly, both comparisons involved a Ni vs a Pt skimmer. However, a Pt skimmer was only used two times, once with a Pt sampler and once with a Ni sampler. Further trials may show this to only be a coincidence, a suggestion supported by the fact that while both polyatomic ions yielded a higher temperature when moving from Ni sets to a Pt set, the T_{gas} of OH^+ was lower for a Pt skimmer/Ni sampler than for Ni skimmer/Ni sampler average.

Any other possible changes in origin diagnosis based on observed average gas T_{gas} values between different metal cones of the same geometry were not statistically different (NSD in Table 3) at the 95% confidence interval of a t-test. Interestingly, Ar_2^+ tends to return a higher T_{gas} when an aluminum sampler is used. The skimmer material does not affect this trend. This is also seen for ArN^+ but only when the skimmer is nickel and the difference in T_{gas} is also smaller.

Ferguson and Houk also found few diagnosis changes for these common polyatomic ions between nickel and aluminum cones [14]. If diagnosis changes are drawn sharply at 5000 and 6000 K then their results showed two possibilities, ArH^+ and O_2^+ shifting from 5050 to 4880 K and 5070 to 4590 K using Ni or Al cones respectively. The shift in the T_{gas}

for ArH^+ of 170 K is essentially within the standard deviation seen in this paper and less than the 250 K shift in T_{gas} for CeO^+. The 480 K shift for O_2^+ is more surprising given the low variation in T_{gas} for this polyatomic ion. Still, a range of 700 K was observed in three trials of Al cones for O_2^+ although in the twenty trials of this study it gave only one temperature below 5000 K and should probably be classified as coming from the plasma primarily.

Ferguson and Houk also saw a difference in the NO^+/N^+ ratio between Ni and Al cones and speculated that a smaller ratio for Ni cones was the result of NO^+ reacting with the hot Ni surface. This study on the other hand found essentially no difference between the two types of cones. In fact the highest gas kinetic temperature found for NO^+ was from an aluminum set.

3.2 Skimmer Cone Geometry

Distinct, statistically significant, origin diagnoses were observed for Ar_2^+ and ArN^+ between H and X skimmers. With the more blunt-tipped H-skimmer the ratio of these polyatomic ions to their atomic ion dissociation product was at levels expected from the plasma. With the thinner-tipped X-skimmer the gas kinetic temperatures indicated more polyatomic ion than expected from the plasma alone. An aluminum sampler mitigates the decrease in T_{gas} nearly offsetting any change due to the X-skimmer. This agrees with their behavior in the previous section where Al sampler cones gave higher temperatures than Ni or Pt samplers. ArH^+ also gives a lower T_{gas} when a nickel sampler and X-skimmer are used, but a similar T_{gas} to a standard Ni set when the sampler is aluminum. This is further evidence for the consistent behavior of ArX^+ species seen by Nonose et al. [11]. While the skimmer clearly plays a role in ArX^+ behavior, the sampler seems to play a larger one.

The other polyatomic ions remain unaffected by the new skimmer geometry. NO^+ and H_2O^+ are statistically different, but only one measurement was done for the Al sampler/Ni X-skimmer combination.

3.3 Cool Plasma

ScO^+ /Sc^+ replaced CeO^+ /Ce^+ when cool plasma conditions were used because sufficient Ce^+ could not be seen in the cool plasma spectrum. As expected, lower temperatures were seen for all polyatomics (Table 4). Cool plasma conditions are used to decrease the presence of Ar polyatomic ions and atomic Ar^+ itself so that isobaric analyte elements can be measured with lower resolution instruments. Given this it was expected that ArX^+ gas kinetic temperatures might rise above the metal oxide temperature to indicate the decreased presence of the diatomic ion. In fact, the opposite occurred, Ar_2^+ and ArN^+ move from averages representative of the plasma temperature to averages below the temperature from ScO^+. It would appear that while absolute ArX^+ signals decreased, Ar^+ and N^+ signals decreased by a larger factor yielding ratios weighted toward the polyatomic ions. In terms of equilibrium this makes sense. The lower temperature of the plasma shifts the dissociation reaction toward the left although why this should occur to a larger extent in Ar_2^+, ArN^+, O_2^+ and OH^+ than ArH^+ is unclear.

The large decrease in NO^+ temperature is consisent with the observations of others that NO^+ signal increased with cool operating conditions [20,24]. H_2O^+ changed origin diagnoses by moving from a temperature indicative of additional formation in the interface in hot plasmas to a temperature 140 K below the ScO^+ temperature in cool plasmas. Under hot plasma conditions H_3O^+ would be scraping the bottom of the assumed 500 K range around

the CeO^+ temperature used as the dividing lines for diagnoses. Because the total range of temperatures found in the cool plasma is narrower, the plasma temperature range would logically be narrower as well. An argument could be made for placing H_3O^+ in one of two origin regions.

Houk and Praphairaksit also compared plasmas with a home-made quadrupole instrument. Their second set of operating conditions produced a plasma described as 'warm' and power was lowered from 1.25 to 0.8 kW. This study lowered power to 0.7 kW and this is reflected in the lower temperatures seen. Gas kinetic temperatures for ArN^+, O_2^+, NO^+ and ScO^+ were ~1000 to 2000 K lower than seen in Houk and Praphairaksit. Ar_2^+, OH^+, H_2O^+, and H_3O^+ gave temperatures 203 to 767 K lower than Houk and Praphairaksit. Only one polyatomic ion, ArH^+ gave a temperature higher than the previous paper. The range in temperature differences are probably an artefact of the different partition functions' responses to changes in ratios and flow rates. The ArH^+ behavior is more puzzling and is part of the larger question of why the ArX^+ behaved differently between the two studies. Houk and Praphairaksit saw temperatures of 4050 K, 4220 K and 4190 K for Ar_2^+, ArN^+ and ArH^+ in a hot plasma (generation of more polyatomic ion after extraction) while this study found an averge of 5890 K, 5810 K and 4960 K (expected plasma levels) across all twenty trials. The difference may lay in the fact Houk and Praphairaksit used a nickel sampler but a stainless steel skimmer or in the fact that these cones had larger orifices than the Element1 (1.4 mm vs. ~1 mm). As noted in the previous sections, if cone geometry and material affect any polyatomic ions it would be these three.

Among the various polyatomic ions studied the temperature spread was 2690 K in cold plasma mode as compared to 4700 K in hot plasma. This may be significant or merely a

result of the lower overall temperature of the cool plasma. Note that the range is ~77% of the plasma temperature in the cool conditions and ~85% in the hot.

3.4 Response Curves

Ferguson and Houk found that the instrument had a greater mass bias when aluminum cones were used instead of nickel ones [14]. Ferguson and Houk attributed the behavior of aluminum to its larger thermal conductivity. These experiments found the same behavior for Al and Ni. Cones with a Ni base and a Pt tip were also used and the one set studied was found to give a response curve slightly shallower than the Ni average (Figure 2). Again, pure platinum has a thermal conductivity slightly lower than that of Ni at room temperature. Of course, the cones will be much warmer than room temperature when the plasma is running and thermal conductivities are a function of temperature. Ni, Pt and most Ni and Pt alloys have thermal conductivities within ~15 W m^{-1} K^{-1} of each other in the temperature range of 273 K to 973 K [25].

One X-skimmer gave a steeper response curve than the traditional H-skimmer while another X-skimmer's response curve was more shallow (Figure 3). It would be logical to assume the thinner tip of the X-skimmer should conduct heat to the lower body of the skimmer slower than the thicker H-skimmer tip. This decreased thermal conductivity should correspond to a sharper response curve as seen with aluminum cones and the second X-skimmer. Perhaps response curves are more variable than metal thermal conductivities alone can explain. The vastly different response curves do *not* translate into greatly different gas kinetic temperatures. The three X-skimmer/Ni sampler trials had some of the lowest standard deviations.

Acknowledgements

This research was supported by the National Science Foundation through the Institute for Physical Research and Technology at ISU. The Element1 ICP-MS was obtained with funds provided by the U. S. Department of Energy, Office of Nuclear Nonproliferation (NA-22) and the Office of Basic Energy Sciences.

The authors would also like to thank D.C. Perdian for making the CAD drawings of the skimmer tips.

References

[1] R.S. Houk, V.A. Fassel, G.D. Flesch, H.J. Svec, A.L. Gray, C.E. Taylor, Inductively coupled argon plasma as an ion source for mass spectrometric determination of trace elements, Anal. Chem. 52 (1980) 2283-2289.

[2] Y. Abdelnour, J. Murphy, The analysis of whole blood samples by Collision Reaction Interface Inductively Coupled Plasma Mass Spectrometry: Varian 820-MS, Varian ICP-MS Application Note Number 28. Accessed through www.varianinc.com on 05/24/10.

[3] IE Ce (5.47) + D_o CeO (8.18 eV) – IE CeO (4.9). IE Ce from reference 4, IE CeO and D_o from reference 5.

[4] Periodic Table of the Elements, VWR Scientific Products Sargent Welch (1996) Buffalo Grove, IL.

[5] R.J. Ackermann, E.G. Rauh, R.J. Thorn, The thermodynamics of ionization of gaseous oxides; the first ionization potentials of the lanthanide metals and monoxides, J. Chem. Phys., 65 (1976) 1027-1031.

[6] D.J. Douglas, J.B. French, An improved interface for inductively coupled plasma mass spectrometry, Spectrochim. Acta B 41 (1986) 197-204.

[7] H. Niu, R.S. Houk, Fundamental aspects of ion extraction in inductively coupled plasma-mass spectrometry, Spectrochim. Acta Part B 51 (1996) 779-815.
[8] H. Togashi, A. Hashizume, Y. Niwa, Molecular ionization in the interface of an inductively coupled plasma mass spectrometer, Spectrochim. Acta B 47 (1992) 561-568.
[9] J.H. Macedone, P.B. Farnsworth, Changes in plasma composition during the expansion into the first vacuum stage of an inductively coupled plasma mass spectrometer, Spectrochim. Acta B 61 (2006) 1030-1038.
[10] A.E. Holliday, D. Beauchemin, Spatial profiling of analyte signal intensities in inductively coupled plasma mass spectrometry, Spectromchim. Acta Part B 59 (2004) 291-311. And references therein.
[11] N.S. Nonose, N. Matsuda, N. Fudagawa, M. Kubota, Some characteristics of polyatomic ion spectra in inductively coupled plasma-mass spectrometry, Spectrochim. Acta Part B 49 (1994) 955-974.
[12] T.J. Cleland, F.R. Meeks, Statistical mechanics of Ar_2^+ in an inductively coupled plasma, Spectrochim. Acta B 51 (1996) 1487-1490.
[13] R.S. Houk, N. Praphairaksit, Dissociation of polyatomic ions in inductively coupled plasma, Spectrochim. Acta Part B 56 (2001) 1069-1096.
[14] J.W. Ferguson, R.S. Houk, High resolution studies of the origins of polyatomic ions in inductively coupled plasma-mass spectrometry, Part 1. Identification methods and effects of neutral gas density assumptions, extraction voltage, and cone material, Spectrochim. Acta Part B 61 (2006) 905-915.
[15] S. M. McIntyre, J.W. Ferguson, R.S. Houk, Measurement of dissociation temperatures for polyatomic ions in ICP-MS: Validation and variations of a method, Manuscript (2010).
[16] E.H. Evans, L. Ebon, L. Rowley, Comparative study of the determination of equilibrium dissociation temperature in inductively coupled plasma-mass spectrometry, Spectrochim. Acta Part B 57 (2002) 741-754.
[17] C. Latkoczy, D. Guenther, Enhanced sensitivity in inductively coupled plasma sector field mass spectrometry for direct solid analysis using laser ablation (LA-ICP-SFMS), J. Anal. At. Spectrom. 17 (2002) 1264-1270.

[18] K. Newman, P.A. Freedman, J. Williams, N.S. Belshaw, A.N. Halliday, High sensitivity skimmers and non-linear mass dependent fractionatio in ICP-MS, J. Anal. At. Spetrom. 24 (2009) 742-751.

[19] K.E. Jarvis, P. Mason, T. Platzner, J.G. Williams, Critical assessment of the effects of skimmer cone geometry on spectroscopic and non-spectroscopic interference in inductively coupled plasma mass spectrometry, J. Anal. At. Spectrom. 13 (1998) 689-696.

[20] S.J. Jiang, R.S. Houk, M.A. Stevens, Alleviation of overlap interferences for determination of potassium isotope ratios by inductively coupled plasma mass spectrometry, Anal. Chem. 60 (1988) 1217-1221.

[21] C.P. Ingle, B.L. Sharp, M.S.A. Horstwood, R.R. Parrish, D.J. Lewis, Instrument response functions, mass bias and matrix effects in isotope ratio measurements and semi-quantitative analysis by single and multi-collector ICP-MS, J. Anal. At. Spectrom. 18 (2003) 219-229.

[22] H. Andren, I. Rodushkin, A. Stenber, D. Malinovsky, D.C. Baxter, Sources of mass bias and isotope ratio variation in multi-collector ICP-MS: optimization of instrumental parameters based on experimental observations, J. Anal. At. Spectrom. 19 (2004) 1217-1224.

[23] D.C. Harris, Quantitative Chemical Analysis, 5th Ed. W.H. Freeman and Company, New York, 1999.

[24] S.D. Tanner, Characterization of Ionization and Matrix Suppression in Inductively Coupled 'Cold' Plasma Mass Spectrometry, J. Anal. At. Spectrom. 10 (1995) 905-921.

[25] CRC Handbook of Chemistry and Physics, 90th Ed. 2009-2010, accessed online at http://www.hbcpnetbase.com/ in May 2010.

Tables

Table 1. Instrument conditions for 'hot' and 'cool' plasmas.

	Hot	**Cool**
Power	1200 W	700 W
Cool Gas	13-16.08 l min^{-1}	16.08-16.18 l min^{-1}
Auxiliary Gas	0.7-0.8 l min^{-1}	0.8-0.95 l min^{-1}
Sample Gas	0.994-1.147 l min^{-1}	0.991-1.201 l min^{-1}
Tuning	maximize Li^+, Co^+, In^+	minimize ArO^+ maximize Li^+, In^+, U^+

Table 2. Summary of measured T_{gas} results for various cone materials and geometries. n is the number of days.

						Ni Sampler	
	Ni Sets	n=4	**Al Sets**	n=3	**Pt Set**[a]	**Ni X-skimmer**	n=3
Polyatomic Ion ratio	Average T_{gas} (K)	Standard deviation	Average T_{gas} (K)	Standard deviation	T_{gas} (K)	Average T_{gas} (K)	Standard deviation
CeO^+/Ce^+	5680	267	5363	206	5660	5590	193
Ar_2^+/Ar^+	5825	1040	6987	1174	5800	3580	200
ArN^+/N^+	5453	613	5910[b]	552	5230	4453	159
ArH^+/Ar^+	4968	162	4967	101	5060	4743	51
O_2^+/O^+	5485	67	5500	354	5670	5417	81
OH^+/O^+	4715	39	4953	569	4860	4690	56
NO^+/N^+	7695	288	7847	792	7490	7253	117
H_2O^+/OH^+	4228	517	3550	201	3860	4260	10
H_3O^+/H_2O^+	3718	210	3780	113	3870	3820	17

	Ni Sampler		**Ni Sampler**	**Al Sampler**		**Al Sampler**
	Al skimmer	n=3	**Pt Skimmer**[a]	**Ni Skimmer**[a]	n=3	**Ni X-Skimmer**[a]
Polyatomic Ion ratio	Average T_{gas} (K)	Standard deviation	T_{gas} (K)	Average T_{gas} (K)	Standard deviation	T_{gas} (K)
CeO^+/Ce^+	5690	195	5960	5477	119	6010
Ar_2^+/Ar^+	5787	1289	6030	7237	1106	5170
ArN^+/N^+	5410	373	5650	6430	313	4870
ArH^+/Ar^+	5103	98	4970	4890	62	4910
O_2^+/O^+	5087	481	5760	5680	142	5550
OH^+/O^+	4727	146	4630	4733	115	4610
NO^+/N^+	7783	189	7900	7603	212	7640
H_2O^+/OH^+	3613	259	3900	3713	168	3950
H_3O^+/H_2O^+	3863	38	3860	3763	49	3790

[a] n = 1

[b] n = 2

Table 3. Summary of statistical comparisons. NSD: No Statistical Difference but average T_{gas} changes origin. NCD: statistically different but No Change in Diagnosis. Blank: T_{gas} between the two sets considered are not statically different and show no change in diagnosis.

Polyatomic Ion	Sets				Ni Sampler		Al Sampler		
Ratio	Ni vs Al	Ni vs Pt	Al vs Pt	Ni H vs X Sk	Ni vs Al sk	Ni vs Pt sk	Al vs Ni sk	Al vs Xsk	Al/Ni vs Xsk
CeO^+/Ce^+								5360-6010	5480-6010
Ar_2^+/Ar^+	NSD5830-6990		NSD6990-5800	5830-3580					
ArN^+/N^+				5450-4450			NSD5910-6430		6430-4870
ArH^+/Ar^+					NSD4970-5100				
O_2^+/O^+		NCD				NCD			
OH^+/O^+		NCD				NCD			
NO^+/N^+									
H_2O^+/OH^+									
H_3O^+/H_2O^+									
	Ni Skimmer	Al skimmer	Ni X-Skimmer						
Sampler change	Ni vs Al	Al vs Ni	Ni vs Al						
CeO^+/Ce^+									
Ar_2^+/Ar^+	NSD5830-7240	NSD6990-5790	3580-5170						
ArN^+/N^+	NSD5450-6430		NCD						
ArH^+/Ar^+		NSD4970-5100	NCD						
O_2^+/O^+									
OH^+/O^+									
NO^+/N^+			NCD						
H_2O^+/OH^+			NCD						
H_3O^+/H_2O^+									

Table 4. Cold plasma results. Average T_{gas} taken from three days. Each day measured one T_{gas} by averaging 16 spectra.

Cold Plasma Conditions		
	Ni sets	
Polyatomic Ion ratio	Average T_{gas} (K)	Standard deviation
Ar_2^+/Ar^+	2240	412
ArN^+/N^+	2300	157
ArH^+/Ar^+	4227	379
O_2^+/O^+	3227	295
OH^+/O^+	3557	104
NO^+/N^+	4207	261
H_2O^+/OH^+	3527	91
H_3O^+/H_2O^+	3163	178
ScO^+/Sc^+	3667	280

Figures

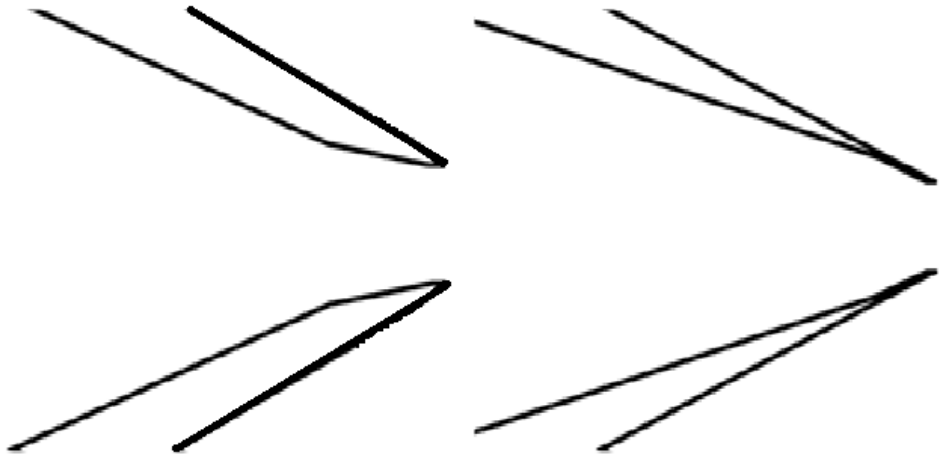

Figure 1. Drawing of observed differences between H-skimmer (left) and X-skimmer (right). Please note that the outside of the skimmers look identical.

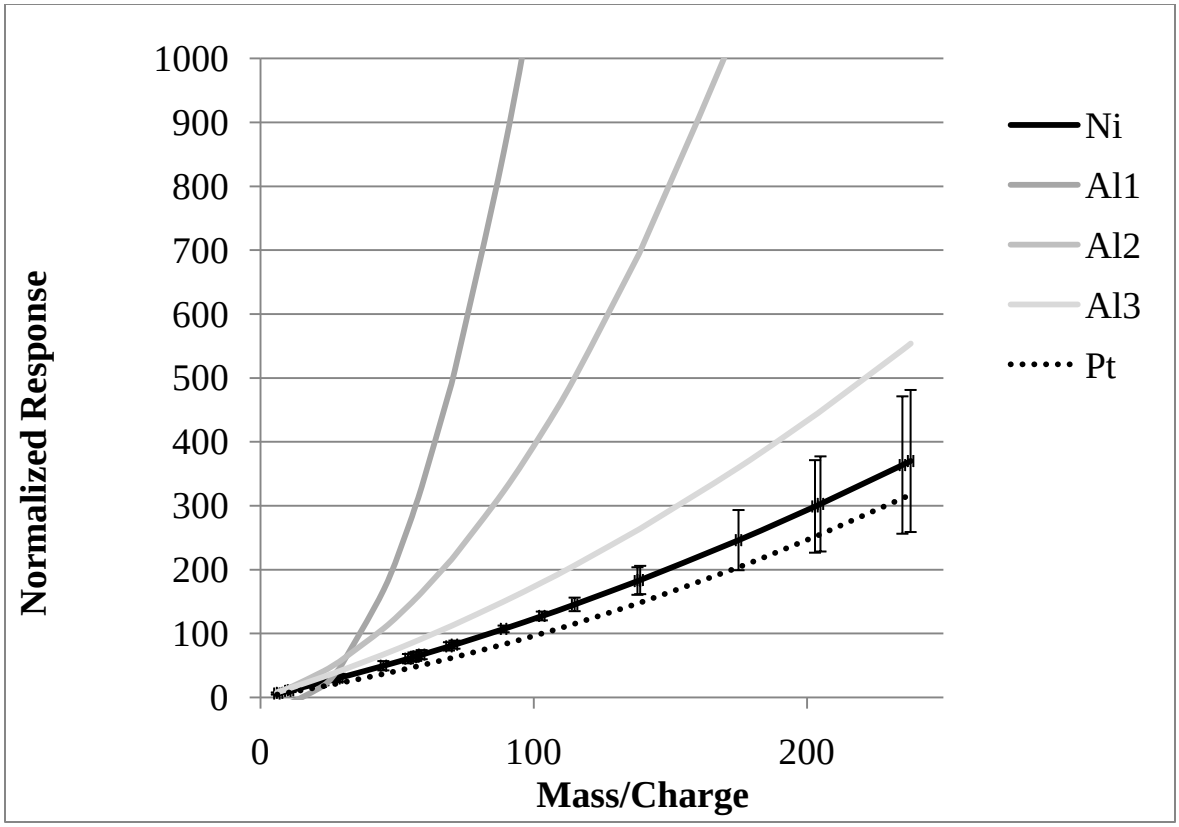

Figure 2. Instrument response curves. Ni line is average of 4 days with error bars corresponding to standard deviation. Only one Pt set was run so no error bars are given. For Al sets the individual runs were plotted instead of the average.

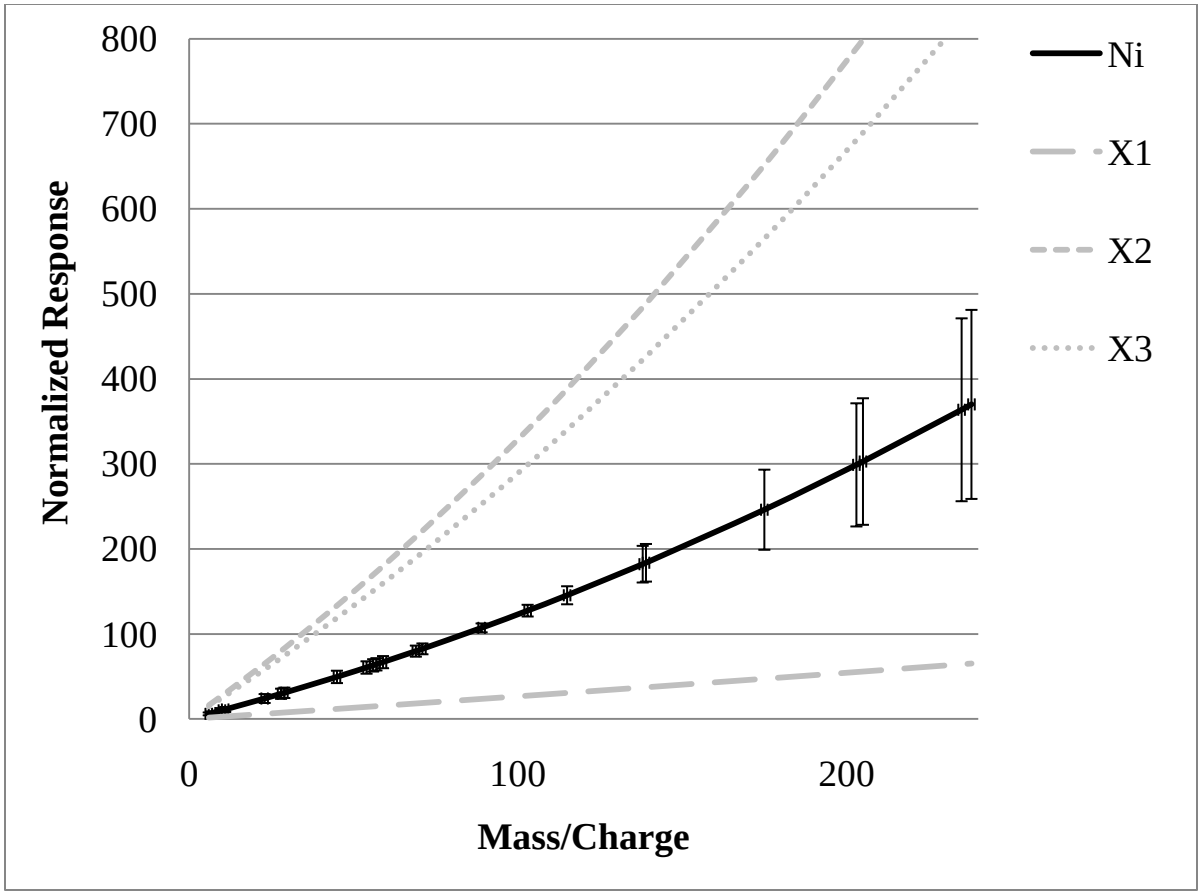

Figure 3. Normalized instrument response curves comparing H and X nickel skimmers. Ni line is average of 4 days with error bars corresponding to standard deviation. X1, X2 and X3 are individual runs. X2 and X3 are the same skimmer and different from X1.

CHAPTER 4. DETERMINATION OF DISSOCIATION TEMPERATURE FOR ArO^+ IN INDUCTIVELY COUPLED PLASMA-MASS SPECTROMETRY

A paper to be submitted to Spectrochimica Acta Part B

Sally M. McIntyre, Jill Wisnewski Ferguson, R.S. Houk

Abstract

The method of comparing experimental and calculated ion ratios to determine a gas kinetic temperature (T_{gas}) characteristic of the origin of a polyatomic ion in inductively coupled plasma-mass spectrometry (ICP-MS) was applied to ArO^+. Complications arise from the predicted presence of a low-lying excited $^2\Pi$ electronic state (~2000-4000 cm^{-1}). Omission of this excited state yields unreasonably high temperatures in excess of 10,000 K for nine out of nineteen trials. Inclusion of the excited electronic state in the partition function of ArO^+ causes temperatures to increase futher. The problem appears to be related to the prediction that ArO^+ in the $^2\Pi$ excited state dissociates into Ar^+ and O, different products than the $^4\Sigma$ ground state which dissociates into Ar and O^+. Adjustments to the calculations to account for these different products yield reasonable temperatures (< 10,000 K) that are similar to those seen for other polyatomic ion interferences.

1. Introduction

Polyatomic ion interferences are a major concern in ICP-MS. Previous studies have examined formation and dissociation reactions by calculating dissociation equilibrium con-

stants (K_d) using statistical thermodynamics and comparing them to the experimental data [1-9]. One theory holds that the gas kinetic temperature, T_{gas}, at which the two methods agree is indicative of the region in which polyatomic ions reach their final concentrations [3]. At the very least, similar temperatures can indicate groups of polyatomic ions that have similar behavior in ICP-MS. The diatomic ion ArO^+ is very common in the argon plasmas of ICP-MS [10] and was studied in three laboratories using the above method [1,3-9].

ArO^+ is of interest in other fields and spectroscopic constants for ArO^+ have been found from experimental data [11-12] and theoretical calculations [1,13-15]. In 1977 Ding et al. used elastic ion scattering to find the potential curve of ground state ArO^+ ($^4\Sigma$) so that it might be used as a reference [11]. In 1989 Frenking et al. calculated spectroscopic constants for ground and excited states of ArO^+ as part of a study of first row cations of neon and argon and with the purpose of understanding trends in noble gas chemistry [13]. In 1990 Flesch et al. found a dissociation energy for the ground state ArO^+ as part of their paper studying the cross-sections of reactions between $Ar^+(^2P_{3/2,1/2}) + O_2$ [12]. In 2003 Ascenzi et al. focused on cross sections for reactions between Ar^{2+} and O_2 [16]. From their computed heats of formation (at 0 K) a difference in energy between ArO^+ ($^4\Sigma$) and ArO^+ ($^2\Pi$) can be found. In 2008 Danailov et al. calculated ab initio potential energy curves for ArO^+ ($^4\Sigma$) and ArO^+ ($^2\Pi$) so that calculated transport properties of O^+ in Ar could be compared to experiment [14]. Also in 2008 Arnold et al. conducted theoretical studies of ArO^+ and $ArOH^+$ in order to better understand their experimental reactions with H_2 with the ultimate goal of improving the use of hydrogen gas to remove these two argon polyatomic ions from the ICP-MS [15]. The results pertinent to this work are summarized in Table 1.

Nonose et al. did their own *ab initio* calculations for ArO^+, ArH^+, ArN^+, and ArC^+ in 1994 so that they could compare calculated dissociation equilibria between the four ions [1]. In a quadrupole mass spectrometer with a shielded load coil they determined that extra ArO^+ was being formed in the interface. In 2001, Nonose and Kubota returned to ArO^+, this time with a shielded high resolution mass spectrometer, and found a range of temperatures (4800 to 6741 K) that depended on the acceleration voltage [17]. Houk and Praphairaksit used Nonose et al.'s 1994 values and determined ArO^+ was formed after the plasma (1810 K), but only when a shielded torch was used [3]. On a different instrument but also with a shielded torch, Ferguson and Houk found gas kinetic temperatures of 2930, 2880 and 1410 K [5]. Houk and Praphairaksit did an experiment on an unshielded torch and found a very different T_{gas} of 6350 K indicating plasma levels of ArO^+ only and perhaps even some loss [3]. In contradiction, Evans et al. found temperatures lower than 2800 K with their unshielded torch [4]. The Houk and Praphairaksit unshielded temperture of 6350 K would seem to be an outlier but it shall be seen this not uncommon given the method used.

However, none of these papers have included the fact that computational methods have revealed a low-lying excited electronic state ($^2\Pi$) only ~4000 cm^{-1} above the ground state [13,15-16]. At plasma temperatures larger than 5000 K this excited state changes the electronic partition function of ArO^+ by over 30%. Its existence must be accounted for in some way. This study is an attempt to find the best manner in which to do so.

2. Experimental Section

All data were collected on a magnetic sector ICP-MS (Element1, ThermoFinnigan, now Thermo Electron Corporation) as described elsewhere [5,9]. Various polyatomic ions were measured in medium resolution ($m/\Delta m \approx 4000$) over two years. On each day the forward power was 1200 W, the cool gas flow rate was usually around 16 l min^{-1}, the auxilary gas flow rate around 0.8 l min^{-1} and the sample gas flow rate between 0.994 and 1.147 l min^{-1}. On each day the sample gas flow rate and ion lens voltages were tuned for maximum signal of $^{7}Li^{+}$, $^{115}In^{+}$ and $^{238}U^{+}$. A 10 or 50 ppb solution of Li, B, Na, Sc, Fe, Co, Ga, Y, Rh, Lu, Tl, and U in 1% HNO_3 (diluted from sub-boiled Ultrapure concentrated J.T. Baker acid using 18 MΩ Millipore deionized water) was used to construct a mass response curve [5,8,18]. A 50 ppb solution of Ce in 1% HNO_3 was then analyzed to measure $^{140}Ce^{+}$, $^{142}Ce^{+}$, $^{140}Ce^{16}O^{+}$ and $^{142}Ce^{16}O^{+}$. While the blank 1% HNO_3 was aspirated, ions at m/z 15, 17, 18, 19, 20, 21, 30, 31, 36, 37, 38, 39, 54, 56, 78, and 80 were measured 16 times. Signals for Ar^{+}, O^{+}, and ArO^{+} were measured in analog mode.

Using Microsoft Excel 2003 or 2007, peaks were integrated from baseline to baseline and the average found. Signals for the mass response curve elements were blank subtracted; in general these blank corrections were small. Ion ratios were adjusted for mass bias using the second order polynomial of best fit for the mass response points normalized to the lowest data point.

Neutral atom number densities and dissociation constants were calculated iteratively at 10 K temperature intervals. The temperature which gave the minimum difference between the calculated dissociation constant and the experimental ratio multiplied by neutral atom density was reported as T_{gas}. Atomic electronic partition function equations were taken from

De Galan et al. [19], except when the indicated T_{gas} was above 7000 K (8750 K for O^+) then the equations from Tamaki and Kuroda were used [20].

Thirteen different mathematical methods for the calculated dissociation constant are reported here. Each method is labeled with a Greek letter. The results and methods used are summarized in Tables 2 and 3 and Figure 1. Each method is described in more detail with their Results. When chemical reactions are discussed, the associated dissociation constants (K_d) and bond energies (D_o) are labeled with a subscripted number equal to the identifying number for the chemical reaction as listed in the text.

3. Results and Discussion

Mass bias corrected signal ratios are listed in Table 3. Note that the ArO^+/O^+ and ArO^+/Ar^+ ratios vary substantially from day to day. Methods Alpha and Beta assume only the ground $^4\Sigma$ electronic state of ArO^+ is populated but use different dissociation energies. Methods Gamma and Delta include the $^2\Pi$ state in the electronic partition function of ArO^+ but use different energy differences, $\Delta\epsilon$, between the two levels.

$$z_{elec}^{ArO+} = g_0 + g_1 * e^{-\Delta\epsilon/k_B T} \quad (1)$$

Statistical weights (g_i) are found from the term symbols using the rules in Sonntag and Van Wylen and Laurendeau [21-22], i.e. g = multiplicity when the term symbol is a sigma and g = 2*multiplicity when the term symbol is anything else. Boltzmann's constant, k_B, is in the same units as the energy difference.

Method Epsilon includes the electronic, vibrational and rotation partition functions of the $^2\Pi$ level:

$$Z_{ArO^+} = z_{trans}\left[z_{vib,0}z_{rot,0}g_0 e^{-\epsilon_0/k_BT} + z_{vib,1}z_{rot,1}g_1 e^{-\epsilon_1/k_BT}\right] \quad (2)$$

where $z_{vib,i}$ is the vibrational partition function, $z_{rot,i}$ is the rotational paritition function, g_i is the electronic degeneracy and ϵ_i is the energy for the ith electronic level. The energy of the ground electronic state is placed at zero.

Method Zeta uses only the ground electronic state but includes high temperature corrections to the internal partition function using equations found in Sonntag and Van Wylen [21].

All the methods described so far assume the only products are Ar and O^+. The experimental temperatures are in excess of 20,000 K are seen for some trials. Such temperatures are unrealistically high for the ICP. Furthermore, the polynomials used for atomic partition functions are only valid up to ~12,000 K for Ar and ~19,000 K for O^+ [20].

It is possible that these high temperatures indicate extensive removal of ArO^+ molecules between the plasma and mass spectrometer due to the low binding energy of the ground state. However, this seems unlikely considering the large ArO^+ signal. ArO^+ signals were usually on the order of Ar_2^+ and Ar_2^+ would be expected to be more prevalent due to its higher bond energy (1.2 eV) [23]. For these reasons further improvements were desired and methods Alpha-Zeta were dismissed as inaccurate.

In the above methods ArO^+ dissociates to Ar and O^+ so the signal ratio ArO^+/O^+ is measured. Frenking et al. found that $ArO^+(^2\Pi)$ preferentially dissociates to Ar^+ and O [13]. Methods Eta, Theta and Iota attempt to include this detail by having all ArO^+ dissociate to Ar^+ and O. The dissociation energy for the ground state to these products was found using a thermodynamic cycle.

$$ArO^+ \rightleftharpoons Ar + O^+, \quad D_{o,3} = 0.312 \text{ eV} \quad (3)$$

$$Ar \rightleftharpoons Ar^+ + e^-, \quad IE_4 = 15.76 \text{ eV} \tag{4}$$

$$\underline{O^+ + e^- \rightleftharpoons O, \quad -IE_5 = -13.61 \text{ eV}} \tag{5}$$

$$ArO^+ \rightleftharpoons Ar^+ + O, \quad D_{o,6} = 2.46 \text{ eV} \tag{6}$$

IE is ionization energy.

Method Eta considers only the ground electronic state. Theta includes the electronic, vibrational and rotational partition functions of $ArO^+(^2\Pi)$. Iota includes high temperature corrections for $ArO^+(^4\Sigma)$ and $ArO^+(^2\Pi)$.

Temperatures using methods Eta, Theta and Iota are far more reasonable although they still span the three diagnostic regions for origin determination. Various techniques have measured the gas kinetic temperature at the usual sampling of the ICP to be around 5000 to 6000 K [24-25]. Therefore if 5000 K $\lesssim T_{gas} \lesssim$ 6000 K, ArO^+ is assumed to be at levels consistent with plasma conditions and that these levels remain unchanged until the detector. If, however, $T_{gas} \lesssim$ 5000 K then more ArO^+ may be created during the extraction process. Although French and Douglas calculated this to be a well-behaved supersonic expansion, optical and Langmuir probe studies have indicated the possibility of turbulent shock waves, particularly at or near the skimmer tip [26-28]. These shock waves are cooler, smaller plasmas where collisions could create more polyatomic ions. On the other hand, collision induced dissociation could also occur to preferentially remove ArO^+ and generate a $T_{gas} \gtrsim 6000$ K . High gas kinetic temperatures might also simply mean equilibrium is not fully established.

None of the methods so far discussed have allowed for the fact that the two electronic levels have different dissociation energies *and different products*. Method Kappa attempts to incorporate this fact as follows,

$$ArO^+(^4\Sigma) \rightleftharpoons Ar + O^+, \quad K_{d,7} \tag{7}$$

$$ArO^+(^2\Pi) \rightleftharpoons Ar^+ + O, \quad K_{d,8} \tag{8}$$

$$ArO^+(^4\Sigma) \rightleftharpoons ArO^+(^2\Pi), \quad K_{exc,9} \tag{9}$$

If these three reactions are added together,

$$2ArO^+(^4\Sigma) \rightleftharpoons Ar + O^+ + Ar^+ + O, \quad K_{d,10} = K_{d,7}K_{d,8}K_{exc,9} \tag{10}$$

The experimental side would be

$$K_{d,11} = n_{Ar}n_O\left(\frac{n_{O^+}}{n_{ArO^+(\,^4\Sigma)}}\right)\left(\frac{n_{Ar^+}}{n_{ArO^+(\,^4\Sigma)}}\right) \tag{11}$$

Note however, that n_{ArO^+} is only for ions in the ground state $^4\Sigma$.

$$n_{ArO^+,tot.} = n_{ArO^+(\,^4\Sigma)} + n_{ArO^+(\,^2\Pi)} \tag{12}$$

$$K_{exc,9} = \frac{n_{ArO^+(\,^2\Pi)}}{n_{ArO^+(\,^4\Sigma)}} \tag{13}$$

$$n_{ArO^+(\,^4\Sigma)} = \frac{n_{ArO^+,tot.}}{(1 + K_{exc,9})} \tag{14}$$

Use of method Kappa yields reasonable temperatures but they still span a large range that covers all three origin regions. Five trials give temperatures lower than 5000 K, five trials give temperatures between 5000 K and 6000 K and the rest are above 6000 K.

The concern with method Kappa is that the two electronic states of ArO^+ have very different bond lengths. Figure 2 is plotted using the Morse oscillator equation and the constants in Frenking et al [13,21]. All methods so far have assumed a Boltzmann distribution of ArO^+ between the two electronic levels. This would mean more molecules in the ground $^4\Sigma$ state than the in the excited $^2\Pi$ state even though the ground state is less stable. Method

Lambda attempts to avoid this assumption by finding the relative distribution between the two levels in another way.

From Frenking et al. three dissociation reactions can be written.

$$ArO^+(^2\Pi) \rightleftharpoons Ar(^1S) + O^+(^2D), \quad \frac{n_{Ar(^1S)}n_{O^+(^2D)}}{n_{ArO^+(^2\Pi)}} = K_{d,15} = \frac{Z_{Ar(^1S)}Z_{O^+(^2D)}}{Z_{ArO^+(^2\Pi)}} e^{-D_{o,15}/k_BT} \tag{15}$$

$$ArO^+(^2\Pi) \rightleftharpoons Ar^+(^2P) + O(^3P), \quad \frac{n_{Ar^+(^2P)}n_{O(^3P)}}{n_{ArO^+(^2\Pi)}} = K_{d,16} = \frac{Z_{Ar^+(^2P)}Z_{O(^3P)}}{Z_{ArO^+(^2\Pi)}} e^{-D_{o,16}/k_BT} \tag{16}$$

$$ArO^+(^4\Sigma) \rightleftharpoons Ar(^1S) + O^+(^4S), \quad \frac{n_{Ar(^1S)}n_{O^+(^4S)}}{n_{ArO^+(^4\Sigma)}} = K_{d,17} = \frac{Z_{Ar(^1S)}Z_{O^+(^4S)}}{Z_{ArO^+(^4\Sigma)}} e^{-D_{o,17}/k_BT} \tag{17}$$

The ratio of ArO^+ in the excited electronic state over the ground electronic state can be found by using reactions 15 and 17.

$$\frac{n_{ArO^+(^2\Pi)}}{n_{ArO^+(^4\Sigma)}} = \frac{K_{d,17}}{K_{d,15}} \frac{n_{O^+(^2D)}}{n_{O^+(^4S)}} \tag{18}$$

Since the ratio of O^+ partition functions and the ratio of O^+ number densities are equal equation 18 simplifies to,

$$\frac{n_{ArO^+(^2\Pi)}}{n_{ArO^+(^4\Sigma)}} = \frac{Z_{ArO^+(^2\Pi)}}{Z_{ArO^+(^4\Sigma)}} e^{-D_{o,17}+D_{o,15}/k_BT} \tag{19}$$

To find the number density for atoms in specific levels the electronic partition function for the level was divided by the total atomic electronic partition function and multiplied by the ion signal or calculated neutral number density. Unfortuanely, it must still be assumed that ArO^+ is all in the ground state and the first calculated excited state. Then reaction 16 can be used to find T_{gas}.

Method Lambda indicates that most ArO^+ is in the $^2\Pi$ state relative to $^4\Sigma$ and that the ratio of $^2\Pi$ to $^4\Sigma$ decreases as temperature increases. This seems counterintuitive but may make sense from an equilibrium perspective. Even at the low temperature of 2000 K, very little ground state ArO^+ will exist simply because equilibrium lies far to the right because of the low dissociation energy. Excited O^+ atoms that collide with neutral argon see a much deeper energy well. As temperature increases $K_{d,15}$ increases more than $K_{d,17}$.

Method Mu uses the same calculations as Lambda but substitutes ground state values from Danailov et al. [14]. Both Mu and Lambda give consistent temperatures in the range 2000 to 4000 K indicating creation of additional ArO^+ after extraction from the plasma. These temperatures agree with the previous work [1,3-5]. It should be noted that the other argon containing polyatomic ion ratios, ArN^+/N^+, ArH^+/Ar^+, Ar_2^+/Ar^+, give average gas kinetic temperatures in the high 4000's to low 6000's, more consistent with the results of methods Eta through Iota. In addition, the small ranges in T_{gas} from methods Lambda and Mu may not seem reasonable given the large range in measured ArO^+/O^+ signal ratios (three orders of magnitude) but similar large ratio range/small temperature ranges are seen in other polyatomics [9]. For example O_2^+/O^+ can vary over three orders of magnitude for a temperature that differs by only 1270 K.

Method Nu addresses the fact that Arnold et al. calculated the dissociation of $ArO^+(^2\Pi)$ to the same products as $ArO^+(^4\Sigma)$, therefore finding a smaller dissociation energy for the excited state [Arnold].

$$ArO^+(^4\Sigma) \rightleftharpoons Ar(^1S) + O^+(^4S), \quad \frac{n_{Ar(^1S)} n_{O^+(^4S)}}{n_{ArO^+(^4\Sigma)}} = K_{d,20} = \frac{Z_{Ar(^1S)} Z_{O^+(^4S)}}{Z_{ArO^+(^4\Sigma)}} e^{-D_{o,20}/k_B T} \tag{20}$$

$$ArO^+(^2\Pi) \rightleftharpoons Ar(^1S) + O^+(^4S), \quad \frac{n_{Ar^+(^2P)} n_{O^+(^4S)}}{n_{ArO^+(^2\Pi)}} = K_{21} = \frac{Z_{Ar(^1S)} Z_{O^+(^4S)}}{Z_{ArO^+(^2\Pi)}} e^{-D_{o,21}/k_B T} \quad (21)$$

The total ArO^+ signal was again assumed to be the sum of $ArO^+(^4\Sigma)$ and $ArO^+(^2\Pi)$. A third reaction is needed so the excitation of ArO^+ from the ground state to the excited state was used (Equation 9). All the same objections to this reaction apply; unsurprisingly, similar T_{gas} values to methods Gamma through Zeta result.

Method Nu is considered inferior to methods Kappa, Lambda and Mu because Arnold et al. appeared to be more concerned with the ground state and implied that $ArO^+(^2\Pi)$ was simply 0.293 eV lower in energy than the ground state products, not that $ArO^+(^2\Pi)$ necessarily dissociated to these same products. Frenking et al. and Danilov et al. agreed that the excited state is more stable than the ground state.

Acknowledgements

This research was supported by the National Science Foundation through the Institute for Physical Research and Technology at ISU. The ICP-MS instrument was obtained with funds provided by the U. S. Department of Energy, Office of Nuclear Nonproliferation (NA-22) and the Office of Basic Energy Sciences.

References

[1] N.S. Nonose, N. Matsuda, N. Fudagawa, M. Kubota, Some characteristics of polyatomic ion spectra in inductively coupled plasma-mass spectrometry, Spectrochim. Acta Part B 49 (1994) 955-974.

[2] T.J. Clelend, F.R. Meeks, Statistical mechanics of Ar_2^+ in an inductively coupled plasma, Spectrochim. Acta B 51 (1996) 1487-1490.

[3] R.S. Houk, N. Praphairaksit, Dissociation of polyatomic ions in inductively coupled plasma, Spectrochim. Acta B 56 (2001) 1069-1096.

[4] E.H. Evans, L. Ebon, L. Rowley, Comparative study of the determination of equilibrium dissociation temperature in inductively coupled plasma-mass spectrometry, Spectrochim. Acta Part B 57 (2002) 741-754.

[5] J.W. Ferguson, R.S. Houk, High resolution studies of the origins of polyatomic ions in inductively coupled plasma-mass spectrometry, Part 1. Identification methods and effects of neutral gas density assumptions, extraction voltage, and cone material, Spectrochim. Acta Part B 61 (2006) 905-915.

[6] J.W. Ferguson, T.J. Dudley, K.C. Sears, S.M. McIntyre, M.S. Gordon, R.S. Houk, Polyatomic ions in inductively coupled plasma-mass spectrometry Part II: Origins of N_2H^+ and H_xCO^+ ions using experimental measurements combined with calculated energies and structures, Spectrochim. Acta B 64 (2009) 690-696.

[7] J.W. Ferguson, T.J. Dudley, M.S. Gordon, R.S. Houk, High resolution studies of the origins of polyatomic ions in ICP-MS Part III: $CrO_xH_y^+$ ions, manuscript (2006).

[8] S. M. McIntyre, J.W. Ferguson, R.S. Houk, Measurement of dissociation temperatures for polyatomic ions in ICP-MS: Validation and variations of a method, manuscript (2010).

[9] S. M. McIntyre, J.W. Ferguson, R.S. Houk, Polyatomic ions in inductively coupled plasma-mass spectrometry: Effects of cone material, skimmer cone geometry and cold plasma conditions on calculated versus measured ion ratios, manuscript (2010).

[10] R.S. Houk, V.A. Fassel, G.D. Flesch, H.J. Svec, A.L. Gray, C.E. Taylor, Inductively coupled argon plasma as an ion source for mass spectrometric determination of trace elements, Anal. Chem. 52 (1980) 2283-2289.

[11] A. Ding, J. Karlau, J. Weise, The potential of Ar--O^+ ($^4\Sigma^-$), Chem. Phys. Letters 45 (1977) 92-95.

[12] G.D. Flesch, S. Nourbakhsh, C.Y. Ng, Absolute state-selected and staate-to-state total cross sections for the reaction Ar^+ ($^2P_{3/2,1/2}$) + O_2, J. Chem. Phys. 92 (1990) 3590-3604.

[13] H.Frenking, W. Koch, D. Cremer, J. Gauss, J.F.Liebman, Neon and Argon Bonding in First-Row Cations NeX^+ and ArX^+ (X = Li-Ne), J. Phys. Chem., 93, (1989) 3410-3418.

[14] D.M. Danailov, L.A. Viehland, R. Johnsen, T.G. Wright, A.S. Dickinson, Transport of O^+ through argon gas, J. Chem. Phys. 128 (2008) 134302.

[15] T. Arnold, J.N. Harvey, D.J. Weiss, An experimental and theoretical investigation into the use of H_2 for the simultaneous removal of ArO^+ and $ArOH^+$ isobaric interferences during Fe isotope ratio analysis with collision cell based Multi-collector Inductively Coupled Plasma Mass Spectrometry, Spectrochim. Acta B 63 (2008) 666-672.

[16] D. Ascenzi, P. Franceschi, P. Tosi, D. Bassi, M. Kaczorowska, J.N. Harvey, Bond-forming reactions of dications: Production of ArO^+ and ArO^{2+} in the reaction of Ar^{2+} with O_2, J. Chem. Phys., 118 (2003) 2159-2163.

[17] N. Nonose, M. Kubota, Non-spectral and spectral interferences in inductively coupled plasma high-resolution mass spectrometry Part I. Optical characteristics of micro-plasmas observed just behind the sampler and the skimmer in inductively coupled plasma high resolution mass spectrometry, J. Anal. At. Spectrom. 16 (2001) 551-559.

[18] C.P. Ingle, B.L. Sharp, M.S.A. Horstwood, R.R. Parrish, D.J. Lewis, Instrument response functions, mass bias and matrix effects in isotope ratio measurements and semi-quantitative analysis by single and multi-collector ICP-MS, J. Anal. At. Spect. 18 (2003) 219-229.

[19] L. De Gelan, R. Smith, J.D. Winefordner, The electronic partition function of atoms and ions between 1500^{o}K and 7000^{o}K, Spectrochim. Acta B 23 (1968) 521-525.

[20] S. Tamaki, T. Kuroda, The electronic partition functions of atoms and ions between 7000 and 12 000 K, Spectrochim. Acta B 42 (1987) 1105-1111.

[21] R.E. Sonntag and G.J. Van Wylen, Fundamentals of Statistical Thermodynamics, John Wiley and Sons, Inc., New York, 1966.

[22] N.M. Laurendeau, Statistical Thermodynamics: Fundamentals and Applications, Chapter 9, Cambridge University Press, Cambridge, 2005.

[23] W.R. Wadt, The electronic states of Ar^+_2, Kr^+_2, Xe^+_2. I. Potential curves with and without spin-orbit coupling, J. Chem. Phys., 68 (1978) 402-414.

[24] J.B. Olsen, J.H. Macedone, P.B. Farnsworth, Source gas kinetic temperatures in an ICP-MS determined by measurements of the gas velocities in the first vacuum stage, J. Anal. At. Spectrom. 21 (2006) 856-860.

[25] R.L Spencer, N. Taylor, P.B. Farnsworth, Comparison of calculated and experimental flow velocities upstream from the sampling cone of an inductively coupled plasma mass spectrometer, Spectrochim. Acta B 64 (2009) 921-924.

[26] K.E. Jarvis, A.L. Gray, R.S. Houk, Handbook of Inductively Coupled Plasma Mass Spectrometry, Blackie, Glasgow, 1992.

[27] H. Niu, R.S. Houk, Fundamental aspects of ion extraction in inductively coupled plasma-mass spectrometry, Spectrochim. Acta Part B 51 (1996) 779-815.

[28] B.S. Duersch, P.B. Farnsworth, Characterization of the ion beam inside the skimmer cone of an inductively coupled plasma mass spectrometer by laser excited atomic and ionic fluorescence, Spectrochim. Acta B 54 (1999) 545-555.

Tables

Table 1. Summary of spectroscopic constants for ArO^+ found in the literature.

			Ground State			Excited State			Dissociation Products					
			$ArO^+(^4\Sigma) \leftrightarrows Ar(^1S) + O^+(^4S)$			$ArO^+(^2\Pi)$			$Ar(^1S) + O^+(^4S)$		$Ar(^1S) + O^+(^2D)$		$Ar^+(^2P) + O(^3P)$	
Year	Reference	Method	De, Do (eV)	r (Å)	ω (cm^{-1})	ΔE (cm^{-1})	r (Å)	ω (cm^{-1})	De, Do (eV)		De, Do (eV)		De, Do (eV)	
1977	Ding, et al.	Calculated from elastic ion scattering data.	0.68, NA	2.02										
1989	Frenking, et al.	Ab initio theoretical calculations.	0.434, 0.416	2.292	258	3489	1.665	909			3.27, 3.21		2.19, 2.13	
1990	Hesch, et al.	Cross-section measurements.	NA, 0.7											
1994	Nonose, et al.	Ab initio theoretical calculations.	NA, 0.312	2.29	289.197									
2003	Ascenzi, et al.	Computed heats of formation.				3629								
2008	Danailov,et al.	Ab initio theoretical calculations.	0.62, 0.60	2.22	336.67	~2000								
2008	Arnold, et al.	Ab initio theoretical calculations.	NA, 0.593	2.26		2420	1.64		NA, 0.2934					

Table 2. Summary of numbers used in each mathematical method.

Mathematical Method	Dissociation Products	Ground Do (eV)	ω_0	B_0	z_{elec1}?	ΔE (cm^{-1})	z_{v1}, z_{r1}?	ω_1	B_1	Excited Do (eV)	High Temperature Corrections?
A	$Ar + O^+$	0.312	289.197	0.2804	N						N
B	$Ar + O^+$	0.416	289.197	0.2804	N						N
Γ	$Ar + O^+$	0.312	289.197	0.2804	Y	3489	N				N
Δ	$Ar + O^+$	0.312	289.197	0.2804	Y	3629	N				N
E	$Ar + O^+$	0.312	289.197	0.2804	Y	3489	Y	909	0.532		N
Z	$Ar + O^+$	0.312	289.197	0.2804	N						Y
H	$Ar^+ + O$	2.453	289.197	0.2804	N						N
Θ	$Ar^+ + O$	2.453	289.197	0.2804	Y	3489	Y	909	0.532		N
I	$Ar^+ + O$	2.453	289.197	0.2804	Y	3490	Y	909	0.532		Y
K	See Text	0.312	289.197	0.2804	Y	3489	Y	909	0.532	2.13	N
Λ	See Text	0.416	258	0.2807	Y	3489	Y	909	0.532	2.13 and 3.21	N
M	See Text	0.6008	336.67	0.2996	Y	3489		909	0.532	2.13 and 3.21	N
N	See Text	0.593	289.197	0.2804	Y	2420	Y	909	0.532	0.2934	N

Table 3. Summary of experiments run and the resulting T_{gas} results for each mathematical method.

			Measured signal Ratios[β]		Tgas Results (K) from Various Calculation Methods										
Date	Sampler	Skimmer	ArO+/O+	ArO+/Ar+	Alpha	Beta	Gamma	Delta	Epsilon	Zeta	Eta	Theta	Iota	Kappa	Lambda	Mu	Nu
1/11/2005	Ni	Ni	1.33E-04	1.45E-04	5570	6530	8260	8170	5930	33100	4830	4880	5630	5240	2750	2750	8470
1/11/2005	Al	Al	5.98E-04	1.41E-04	2180	2700	2280	2270	2200	2890	4990	5040	5870	4400	2820	2820	3580
8/24/2006	Ni 1730[α]	Ni X-15910	2.20E-04	1.03E-03	3870	4650	4800	4750	4010	15180	3660	3680	4010	3860	2180	2180	6090
8/31/2006	Al	Ni X-15910	1.36E-04	1.01E-04	5410	6360	7930	7820	5750	31770	5100	5150	6040	5420	2870	2870	8250
9/2/2006	Ni	Ni	4.02E-05	3.49E-05	15830	16760	24440	24380	17420	91930	6170	6260	7970	7940	3340	3350	19620
9/9/2006	Ni 1730	Ni X-15911	1.53E-04	1.15E-03	5030	5940	7090	7010	5310	28380	3610	3630	3950	3960	2160	2160	7730
9/20/2006	Ni 1712	Pt	3.49E-05	5.47E-05	17530	18420	26700	26630	19250	100880	5730	5800	7170	7560	3150	3150	21370
9/30/2006	Ni 1712	Al	3.23E-03	1.36E-04	1210	1540	1220	1220	1210	1320	5010	5070	5910	3690	2840	2840	2080
10/2/2006	Pt (a)	Pt	4.69E-05	8.59E-05	14020	14980	21950	21890	15440	82490	5230	5290	6240	6520	2930	2930	17740
10/2/2006	Pt (a)	Ni	3.37E-05	6.38E-05	18150	19040	27520	27460	19920	104220	5530	5600	6720	7350	3070	3070	22010
11/4/2006	Al	Ni	2.09E-05	8.51E-05	25160	25920	36460	36400	27370	144040	5310	5370	6380	7660	2970	2970	29180
2/1/2007	Ni 1712	Ni	7.09E-05	3.10E-04	9810	10820	15630	15550	10750	60020	4310	4340	4870	5090	2500	2500	13230
2/11/2007	Ni 1712	Ni	4.42E-05	2.43E-04	14600	15550	22760	22690	16070	85490	4490	4530	5130	5650	2590	2590	18340
3/8/2007	Ni 1730	Al (a)	4.99E-04	1.98E-04	2390	2950	2550	2540	2420	3420	4660	4700	5370	4280	2670	2670	3910
3/8/2007	Ni 1712	Al (b)	1.55E-04	1.33E-04	4870	5760	6740	6670	5130	26790	4950	5000	5810	5190	2810	2810	7500
3/9/2007	Al (a)	Al	3.73E-05	1.19E-04	16660	17580	25550	25490	18320	96310	5020	5070	5920	6480	2840	2840	20480
3/9/2007	Al (b)	Al	7.75E-05	8.43E-05	8940	9940	14170	14090	9760	55000	5310	5370	6380	6100	2970	2970	12250
3/16/2007	Al (a)	Ni (a)	1.57E-05	2.64E-05	30080	30790	42650	42600	32560	175290	6590	6700	8810	10200	3530	3530	34240
3/16/2007	Al (b)	Ni (b)	2.05E-05	3.79E-05	25440	26200	36810	36760	27660	145730	6140	6230	7930	8960	3340	3340	29470
	Cold Plasma Conditions																
12/19/2006	Ni	Ni	2.06E-03	1.04E-02	1410	1780	1420	1420	1410	1580	2860	2870	3030	2610	1770	1770	2390
2/3/2007	Ni	Ni	3.55E-02	8.54E-03	730	940	730	730	730	750	2930	2940	3110	2200	1800	1800	1280
2/11/2007	Ni 1712	Ni	9.84E-03	6.80E-03	930	1190	930	930	930	980	3040	3050	3240	2440	1860	1860	1620

α - Numbers indicate identifiable cones. Letters in parenthesis indicate the same or different cones for that day(s) but with no identifiable markings.

β - Ratios are adjusted for mass bias.

Figures

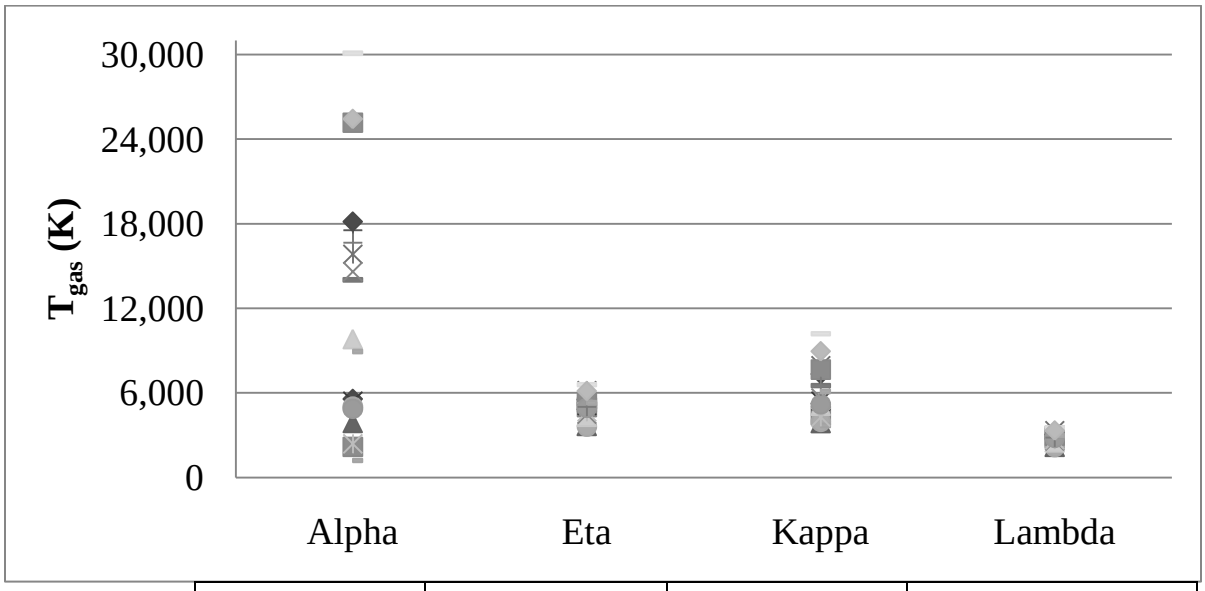

Alpha	Eta	Kappa	Lambda
ArO+(4Σ) ⇌ Ar + O+	$ArO^+(^4\Sigma) \rightleftharpoons Ar^+ + O$	$ArO^+(^4\Sigma) \rightleftharpoons Ar + O^+$	$ArO^+(^4\Sigma) \rightleftharpoons Ar(^1S) + O^+(^4S)$
	$ArO^+(^4\Sigma) \rightleftharpoons ArO^+(^2\Pi)$	$ArO^+(^4\Sigma) \rightleftharpoons ArO^+(^2\Pi)$	$ArO^+(^2\Pi) \rightleftharpoons Ar^+(^2P) + O(^3P)$
		$ArO^+(^2\Pi) \rightleftharpoons Ar^+ + O$	$ArO^+(^2\Pi) \rightleftharpoons Ar(^1S) + O^+(^2D)$

Figure 1. Graphical representation of T_{gas} values from the major methods of Table 3.

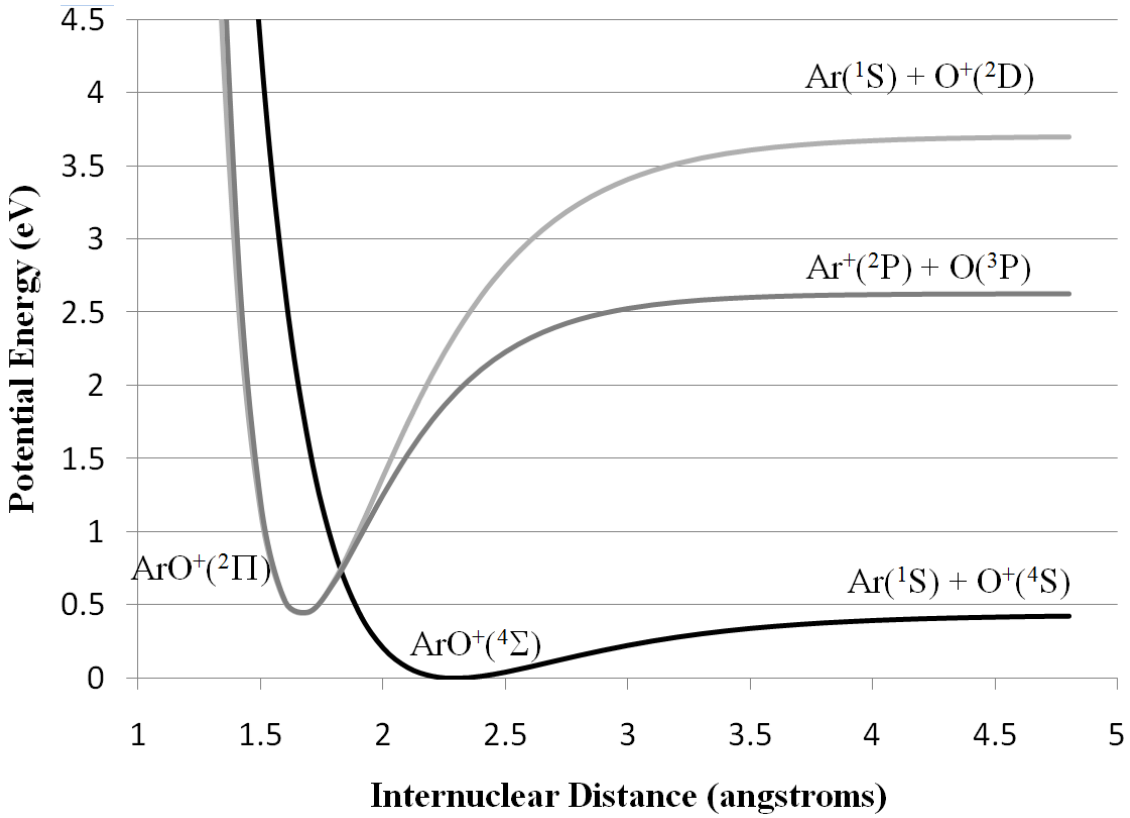

Figure 2. ArO^+ potential energies graphed using Morse oscillator equation [21]. Well depths, bond lengths and vibrational frequencies taken from Frenking et al. [13].

CHAPTER 5. METAL OXIDE MEMORY EFFECTS IN INDUCTIVELY COUPLED PLASMA-MASS SPECTROMETRY

A paper to be submitted to Spectrochimica Acta Part B

Sally M. McIntyre and R.S. Houk

Abstract

Ce^+ and CeO^+ signals were monitored during the 1% nitric acid rinse-out of a ~3 ppm solution of cerium on a ThermoFinnigan Element1. While both signals faded, CeO^+ memory unexpectedly leveled out at a greater level than Ce^+ memory. This oxide memory grew more prominent as higher concentrations and longer aspirating times were used. Sr, Ba, Y, Zr, Ga, and Ti showed large oxide memories as well, although none were as striking as cerium. Coating and cleaning experiments showed that the metal oxide memory was localized on the skimmer. The effect was not seen on a HP4500 quadrupole ICP-MS.

1. Introduction

While generally considered a good thing in daily life, long-term memory is very much unwanted in analytical instruments. Long rinse-out times degrade limits of detection. Time required to clean the instrument decreases throughput and costs companies and research groups manpower and money. Elements like B, Hg, I, and Br are infamous in ICP-MS for lingering in tubing and spray chambers and forming gaseous compounds that diffuse into the plasma slowly over time [1]. However, nearly any element can cause memory effects in

ICP-MS if the concentration is high enough. Chemicals lingering in the introduction system are not the only source either, memory has been seen coming from the cones and extraction lens [2-3]. The last requires breaking vacuum on the mass spectrometer to fully clean.

Memory effects are not restricted to isobaric elements. Memory from B and Hg comes in the form of hydrides and certain amounts of MO^+, MH^+, and MAr^+ will form in the plasma and interface [1,4]. These polyatomic ions tend to stay at a small fraction of the M^+ memory [3]. This paper reports a MO^+ memory higher in intensity than the corresponding M^+ signal. Though a MO^+/M^+ ratio greater than one was seen only with Ce, other elements gave a memory MO^+/M^+ ratio larger than their MO^+/M^+ ratio when the element comes from nebulized solutions.

2. Experimental Section

Most experiments were done on a Thermo-Finnigan Element1 double focusing ICP-MS. A Hewlett-Packard 4500 quadrupole ICP-MS was used for comparison purposes. All nitric acid (HNO_3) solutions were diluted from Ultrapure J.T. Baker concentrated acid using deionized water (18 MΩ MilliporeQ). Sampler and skimmer cones were made from nickel and the Element1 skimmer was H-geometry unless otherwise stated. Data were analyzed using Microsoft Excel 2003 and 2007.

The Element1 was tuned to maximize $^{7}Li^+$, $^{115}In^+$ and $^{238}U^+$signals using a 1 or 10 ppb tune solution also containing 1 or 10 ppb B, Na, Si, Sc, Fe, Co, Ga, Y, Rh, Lu, and Tl. Power was left at 1200 W. Coolant and auxiliary gas flows were left mostly alone. Most effort was focused on torch position, sample gas flow and the ion lenses. Autotune was run on the

Hewlett Packard instrument to maximize $^{7}Li^{+}$, $^{115}In^{+}$ and $^{238}U^{+}$ signal and minimize Ce^{2+}/Ce^{+} and CeO^{+}/Ce^{+} ratios by adjusting sample gas flow and torch position. Tune parameters were not changed throughout the rest of the experiment.

The basic experiment was as follows. A ~5 ppm solution of the specific metal was nebulized for five minutes. The sample was then switched to deionized water or 1% HNO_3 in deionized water. As quickly as possible after the switch data collection was started on the instrument.

Cleaning cones was a two step process. In the first step the cones were either sonicated for ~1 hour in aqueous 1% HNO_3 or soaked ~24 hours in 0.1 % HNO_3. The cones were then rinsed with deionized water. In the second step, the cones were swabbed with deionized water using a cotton applicator. The wet front and back surfaces were polished with 500-grit sandpaper and wiped clean with Kimwipes. Nitrile gloves were used to remove the cones from the acid and hold them during the water rinse off. Sometimes gloves were worn during the polishing step but not when the cones were transferred on and off the instrument. The metals sudied are not usually associated with skin contamination although Ti may come from lotions [5].

Gas kinetic temperatures were calculated using the method outlined in Houk and Praphairaksit [6-7]. The temperatures were calculated in slightly different ways and found to have minimal differences. The temperatures reported here used a thermodynamic cycle employing the dissociation of the neutral oxide, the ionization of the neutral oxide and the ionization of the metal atom [7]. Because the MO^{+} appears to originate at the skimmer, the number density used for neutral oxygen was calculated at the skimmer tip (9.2 mm from sampler tip in the Element1) using the equations in Douglas and French [4]. To determine

T_{ion} a ~5 ppm solution of Ba was nebulized for five minutes. After Ba^{2+}/Ba^{+} memory was measured, the signal ratio was corrected with the instrument response curve and set equal to the Saha equation [8]. Electron density in the plasma has been measured at $1x10^{15}$ cm^{-3}. The electron density at the skimmer tip was calculated in the same manner as neutral oxygen density. The result was T_{ion} = 5180 K.

Mass bias corrections were done using an instrument response curve generated from a 10 ppb solution of Li, B, Na, Si, Sc, Fe, Co, Ga, Y, Rh, In, Lu, Tl, U in 1 % HNO_3 [9-10]. With no way to verify and no suitable alternative, it was assumed that the response curve measured in this way would apply to ions made from skimmer deposits.

Laser ablation was done to spatially characterize deposits with a Q-switched quadrupled (266 nm) Nd:YAG laser (LSX 500, CETAC Technologies, Omaha, NE, USA). Each spot was ablated at 100% power, 20 shots at 10 Hz, 9 mJ energy and 5 ns pulse width. The skimmer was laid on its side so that the cone slope was flat and perpendicular to the laser axis. Six raster lines of 3-4 spots were done starting at the base of the cone and ending with a single shot at the tip. The laser was refocused between each raster line. For the inside spots the skimmer was rested straight up and down, with the tip pointing to the floor, in the foam ring that was used to package the cone. The laser was refocused for each spot. The first spot inside the cone was mid-way down the slope. Near the tip the cone was set at an angle to reach the very end of the tip. Analysis was done with the same Element1 ICP-MS. The time dependent signal was integrated from baseline to baseline.

3. Results and Discussion

3.1 Ce^+ and CeO^+ Memory

In order to observe the behavior of M^+ and MO^+ signals and MO^+/M^+ signal ratio during the rinse out of a concentrated solution, a 100 ppm Ce solution was aspirated for five minutes. A five minute analog run was started just after the nebulizer was switched to deionized water (Figure 1a). The signals for Ce^+ and CeO^+ quickly leveled out, but not at baseline levels and with the CeO^+ signal well above the Ce^+ signal. The more extensive memory for CeO^+ indicates the signal was not from the sample introduction system. The CeO^+/Ce^+ ratio when the ions come from the ICP is usually 1 to 2% as the trend indicates at the very beginning of the rinse out. At approxiamately 110, 180 and 280 s there are spikes in the Ce^+ and CeO^+ signals where the CeO^+/Ce^+ ratio drops 100 fold. We believe these to be extra Ce^+ and CeO^+ from residual drops of Ce solution in the sample introduction system that were carried into the plasma. This is supported by the fact that these spikes disappear when the sample gas is turned to zero and the spray chamber is removed from the back of the torch.

3.2 Effect of Concentration

To determine the approximate concentration where this long-lived memory effect develops, clean cones were placed on the instrument and 50 ppb, 190 ppb, and 3 ppm Ce solutions were nebulized for five minutes each with ten minute rinse-outs in between (Figure 1b-d). After the 50 ppb solution was run the signal quickly returned to baseline. After the 190 ppb solution was run, the signal quickly drops down to near baseline, however a slight CeO^+ signal can still be seen (Figure 1c). After the 3 ppm solution was run the CeO^+ memory effect

can be clearly seen. Even with build-up from the previous solutions, the 3 ppm solution did not produce a memory as large as the 100 ppm solution.

Thus we can conclude that a CeO^+ memory signal effect will appear after at least five minutes of running a 190 ppb solution and the effect will worsen as the concentration of the Ce is increased.

3.3 Localization of Phenomenon.

To determine the source of this extra CeO^+ memory two sets of Ni cones were cleaned. The 3 ppm Ce solution was then nebulized for five minutes on one set. After a five minute rinse-out the plasma was turned off, the sampler was exchanged for a second, clean one and the plasma was reignited. After approxiamately 15 minutes Ce^+ and CeO^+ were measured while nebulizing only the blank solution. The process was repeated again this time with a clean skimmer and the original 'dirty' sampler. In the third repeat both cones were replaced with the second, clean, set. The results are shown in Figure 2. The instrument was tuned only once, before the cones were coated. The same operating conditions were used in all four measurements.

CeO^+ memory signal dropped somewhat when only the sampler was replaced (Figure 2b) but dropped to the clean set's baseline when only the skimmer was replaced (Figure 2c). Therefore, we conclude that the memory originates mainly from the skimmer cone. The loss in signal when the sampler is replaced may simply be the consequence of turning the instrument off and on, and not retuning or waiting as long for the instrument to stabilize before taking data runs.

The sharp spikes in Ce^+ signal during rinse out disappear when the sample gas is turned off (Figure 3), which we take as additional evidence that they are caused by residual aerosol droplets containing Ce leaving the spray chamber and being atomized and ionized in the plasma as usual. If the spikes come from droplets of Ce finally leaving the spray chamber, the droplets cannot reach the plasma if the sample gas is turned off. On the other hand, the peaks decrease in frequency as time goes on and the runs without sample gas were done after five minute runs with sample gas. The runs without sample gas may simply sample a period where peaks would not appear anyway.

Localization of the source of this memory to the skimmer cone is in agreement with Zahran et al. who also ran a blank aqueous 1% HNO_3 solution while monitoring M^+ and MO^+ [3]. However, they examined metals coming from the cones themselves either because the metal made up the composition of the cone or the metal was deposited on the cones via chemical means in solution. In addition, Zahren et al. used an unshielded torch with high positive voltage placed on the cones, both of which probably contributed to a 'pinch', or secondary discharge, from the plasma to the cones. Nonetheless, they found sampler material did not affect ion signals in the mass spectra to anywhere near the extent skimmer material did.

3.4 Length of Run

In the interests of learning how long a 3 ppm solution of Ce would need to be run through the instrument to see the memory effect, one, two, three and four minute runs were done in succession with 5-10 minutes of rinse-out in between (Figure 4). Between the two and three minute runs another one minute run was performed to investigate build-up effect.

CeO^+ memory first becomes clearly visible after the two minute run (Figure 4b) and becomes more prominent with the three and four minute runs. The one minute run after the two minute run (Figure 4c) shows behavior closer to the two minute run (Figure 4b) rather than the one minute run (Figure 4a) implying the effect is at least somewhat cumulative.

3.5 Other Elements

Similar effects could be seen for the elements Sr, Ru, Eu, Lu, Zr, Ti, Ge, Ba, and Y although the MO^+/M^+ ratio never exceeded unity except for Y ($YO^+/Y^+ = 1.09$). For each element a clean skimmer reduced memory to baseline levels while a clean sampler decreased memory slightly, but did not eliminate it. MO^+ signal did increase in the rinse out plots over baseline levels and in all cases, except ruthenium, the oxide to metal ratio increased. While most elements do not display such dramatic results as CeO^+, the memory effect of a concentrated solution of these elements cannot be corrected for mathematically with a solution based ratio.

3.6 Composition of Cones

To determine if cone material might have any effect, two aluminum sets were compared to two nickel sets. Cerium and strontium was measured on both types of cones and behavior was found to be identical. Cone material seems to have little effect on this phenomenon.

3.7 Geometry of Skimmer Cone

The above studies were done with H-geometry skimmers as these are the most commonly used ones in our lab. To determine if skimmer geometry had an effect, two nickel X-skimmers were tested. The first X-skimmer had been used several times before with 10-50 ppb solutions of various metals in 1% nitric acid and had been soaked in 0.1% nitric acid overnight but not polished. The second X-skimmer was new and had never been used before. Behavior was identical to that seen on the older H geometry skimmers. Skimmer geometry and the method of cleaning the cones does not appear to affect memory behavior either.

3.8 Calculation of Temperatures

Gas kinetic temperatures for certain metal oxide to metal ion ratios were calculated using the Houk/Praphairaksit method [6-7,10]. The number density of oxygen was reduced to the level expected at the skimmer tip by using the equations found in Douglas and French [4],

$$n_{O,skimmer} = 0.161\ D^2_{sampler}/x^2_{skimmer} = 0.00161\ n_{O,plasma} \quad (1)$$

where D is diameter and x is the distance from the sampler. Results are shown in Table 2.

At first temperatures were found for Ce and Sr during the Ni vs. Al cone test. There was a nearly 1000 K difference in the calculated temperatures and this suggested that perhaps the CeO^+ and SrO^+ memory signals were coming from different spatial regions, or perhaps as a result of mass bias. Tests with Y and Ba dispelled this hypothesis. Then it was thought perhaps the order of coating had an effect as both Y and Ce had been coated before Ba and Sr. But when Ba was applied first its temperature did not change. This seems to leave some

sort of chemical property as the determinant of temperature region. Table 2 lists the calculated temperatures and various physical properties for Ce, Sr, Ba, Y, Zr, Ge, Ti, Lu, Eu and Ru. The best correlation (excluding Ru) was found to be between the T_{gas} and elemental boiling point (Figure 5). This is a completely empirical correlation. No causation is implied. The exclusion of Ru is not completely arbitrary. Early work had Ge as an outlier as well but it was found that GeO^+ has a low lying excited electronic level [18]. Including this excited electronic level yielded the present results. We believe a similar case may be true for RuO^+ but we have not found literature concerning excited electronic levels of RuO^+ as of yet.

3.9 Other Instruments

The experiment was repeated on a Hewlett-Packard 4500 quadrupole ICP-MS. Even though the experiment was repeated with longer nebulization times and more concentrated solutions, a cerium oxide memory greater than the cerium memory was never seen (Figure 6). Unfortunately, there are many differences between the two instruments. Though difficult to measure, the HP4500 appears to have a larger cone separation and it definitely has a smaller skimmer orifice diameter (~0.4 mm on the HP4500 vs. ~0.8 mm on the Element1). Quadrupoles have much lower extraction voltages than sector instruments like the Element1 and the HP was run with an unshielded torch while the load coil of the Element1 was shielded.

3.10 Laser Ablation Studies of Skimmer Cone

An expendable set of aluminum cones (H geometry skimmer) was placed on the Element1. Ce and Ba solutions were nebulized for five minutes separately with at least a five

minute rinse with 1% HNO_3 in between and after the Ba. The instrument was shut off and the cones switched to a Ni set so the instrument could be used for laser ablation ICP-MS. The Al skimmer was ablated in 21 spots on the outside slope (Figure 7a) and in 10 spots on the inside (Figure 7b). Before the Al cones were exposed to the Ce and Ba, a blank ablation was taken on the outside base of the cone half-way between the edge and the start of the cone slope. Results are shown in Figure 7. To a rough approximation it appears that Ce is concentrated slightly farther from the tip than is Ba.

The use of points on the outside of the skimmer is not to suggest material is boiling off and somehow making its way into the ion beam. Instead the correlation between deposition inside and outside of the cone was investigated to see if the outside could be sampled alone in the future because of the greater ease of access. The outside points could also be investigated for correlation with shock regions seen in photographic studies [1] and/or the ring patterns often seen on dirty skimmers.

Acknowledgements

This research was supported by the National Science Foundation through the Institute for Physical Research and Technology at ISU. The magnetic sector ICP-MS was obtained with funds provided by the U. S. Department of Energy, Office of Nuclear Nonproliferation (NA-22) and the Office of Basic Energy Sciences. The quadrupole ICP-MS was donated to Iowa State University by Agilent.

References

[1] K.E. Jarvis, A.L. Gray, R.S. Houk, Handbook of Inductively Coupled Plasma Mass Spectrometry, Blackie, Glasgow, 1992.

[2] I. Rodushkin, E. Engstroem, D.C. Baxter, Review: Sources of contamination and remedial strategies in the multi-elemental trace analysis laboratory, Anal. Bioanal. Chem. 396 (2010) 365-377.

[3] N.F. Zahran, A.I. Helal, M.A. Amr, A. Abdel-Hafiez, M.T. Mohsen, Formation of polyatomic ions from the skimmer cone in the inductively coupled plasma mass spectrometry, Int. J. Mass Spectrom. 226 (2003) 271-278.

[4] D.J. Douglas, J.B. French, Gas dynamics of the inductively coupled plasma mass spectrometer interface, J. Anal. At. Spectrom. 3 (1988) 743-747.

[5] R. Richter, Clean Chemistry Techniques for the Modern Laboratory, Milestone Press, Monroe, CT, 2003.

[6] R.S. Houk, N. Praphairaksit, Dissociation of polyatomic ions in inductively coupled plasma, Spectrochim. Acta Part B 56 (2001) 1069-1096.

[7] S. M. McIntyre, J.W. Ferguson, R.S. Houk, Measurement of dissociation temperatures for polyatomic ions in ICP-MS: Validation and variations of a method, Manuscript (2010).

[8] H. Niu, R.S. Houk, Fundamental aspects of ion extraction in inductively coupled plasma-mass spectrometry, Spectrochim. Acta Part B 51 (1996) 779-815.

[9] C.P. Ingle, B.L. Sharp, M.S.A. Horstwood, R.R. Parrish, D.J. Lewis, Instrument response functions, mass bias and matrix effects in isotope ratio measurements and semi-quantitative analysis by single and mult-collector ICP-MS, J. Anal. At. Spectrom. 18 (2003) 219-229.

[10] J.W. Ferguson, R.S. Houk, High resolution studies of the origins of polyatomic ions in inductively coupled plasma-mass spectrometry, Part 1. Identification methods and effects of neutral gas density assumptions, extraction voltage, and cone material, Spectrochim. Acta Part B 61 (2006) 905-915.

[11] Periodic Table of the Elements, VWR Sargent Welch, Buffalo Grove, IL 1996.

[12] M. Dulick, E. Murad, R.F. Barrow, Thermochemical properties of the rare earth monoxides, J. Chem. Phys. 85 (1986) 385- 390.

[13] Z.J. Wu, W. Guan, J. Meng, Z.M. Su, Density Functional Studies of Diatomic LaO to LuO, J. Cluster Science 18 (2007) 444-458.

[14] K.P. Huber, G. Herzberg, Molecular Spectra and Molecular Structure IV. Constants of Diatomic Molecules, Van Nostrand Reinhold, New York, 1979.

[15] N.F. Dalleska, P.B. Armentrout, Guided ion beam studies of reactions of alkaline earth ions with O_2, Int. J. Mass Spectrom. Ion Processes 134 (1994) 203-212.

[16] P. Song, W. Guan, C. Yao, Z.M. Su, Z.J. Wu, J.D. Feng, L.K. Yan, Electronic structures of 4d transition metal monoxides by density functional theory, Theor. Chem. Acc. 117 (2007) 407-415.

[17] E. Murad, D.L. Hildenbrand, Dissociation energies of GdO, HoO, ErO, TmO, and LuO; correlation of results for the lanthanide monoxide series, J. Chem. Phys. 73 (1980) 4005-4011.

[18] C.M.Clouthier, F. Grein, MRCI studies on the electronic spectrum of GeO^+, Chem. Phys. 315 (2005) 35-40.

Tables

Table 1. Operating Conditions

	ThermoFinnigan ELEMENT 1	Hewlett-Packard 4500
Resolution (m/Δm)	~300	~300
Nebulizer	pneumatic type	Babbington type
Spray Chamber	Teflon Scott type double pass	Cooled quartz Scott type double pass
Cones	Nickel, unless otherwise stated	Nickel
Power (W)	1200	1200
Gas flow rates	Optimized to produce greatest signal across mass range	
Torch	Shielded	Unshielded

Table 2. Table of calculated temperatures for MO^+/M^+ alongside certain constants for the metal and metal oxide species. D_o is dissociation energy, IE is ionization energy, ΔH_{vap} is the enthalpy of vaporization for the atomic metal and B.P. is the boiling point of the atomic metal.

$^{\alpha}$ Using D_o MO and IE MO, $D_o\ MO^+ = D_o$ MO – IE MO + IE M.

	T_{gas} (K)	D_o MO (eV)	$D_o\ MO^+$ (eV)	IE MO	IE M [11]	ΔH_{vap} [11]	B.P. [11]
Eu	2440	4.92 [12]	4.097$^{\alpha}$	6.533 [13]	5.67	175.73	1800
Sr	2560	4.88 [14]	3.975$^{\alpha}$	6.6 [15]	5.695	136.9	1655
Ru	2590	5.3 [14]	2.567$^{\alpha}$	9.003 16]	7.37	567.77	4425
Ba	2750	5.79 [14]	4.13$^{\alpha}$	6.911 [14]	5.212	140.2	2078
Ge	3030	6.78 [14]	3.579$^{\alpha}$	11.1 [14]	7.899	334.3	3107
Lu	3420	6.99 [12]	5.421$^{\alpha}$	7.049 [13]	5.43	355	3668
Ti	3450	6.87 [14]	7.29$^{\alpha}$	6.4 [14]	6.82	425.2	3560
Ce	3530	8.18 [14]	8.81[6]	5.2 [6,11]	5.47	313.8	3715
Y	3570	7.29 [14]	7.67$^{\alpha}$	6.0 [17]	6.38	393.3	3611
Zr	4040	7.85 [14]	8.95$^{\alpha}$	6.1 [14]	6.84	590.5	4682

Figures

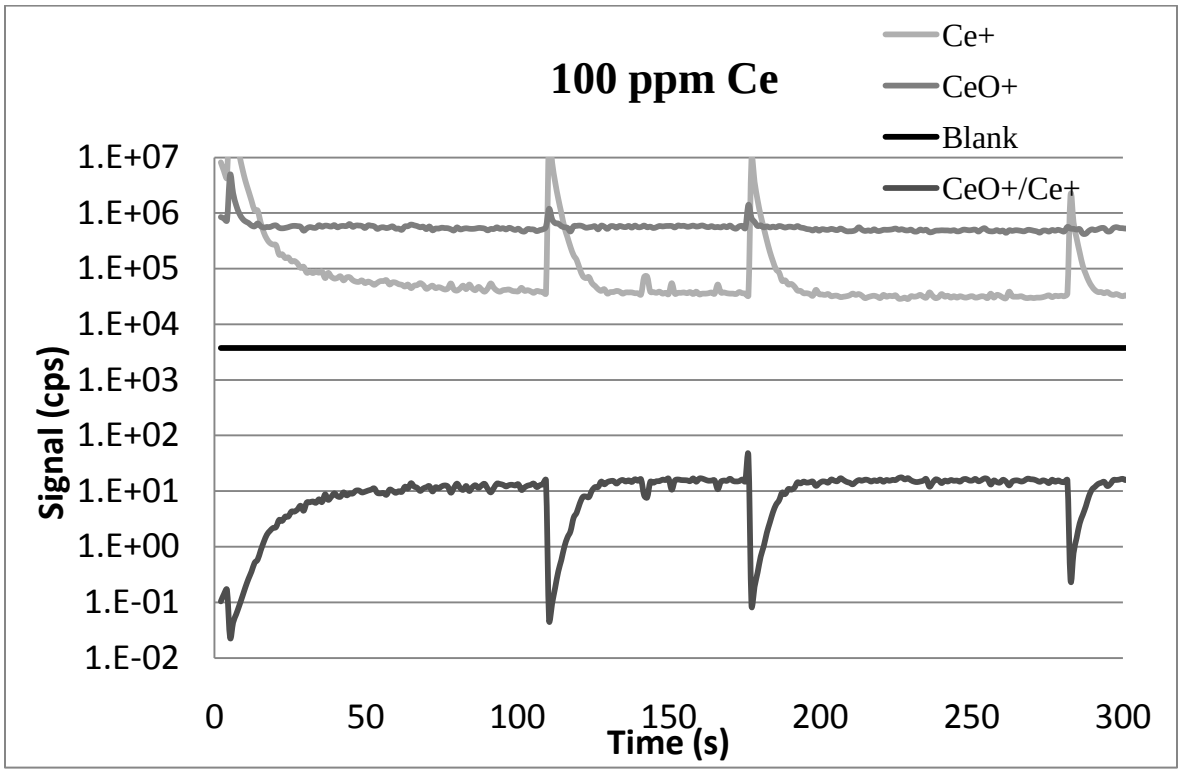

(a)

Figure 1

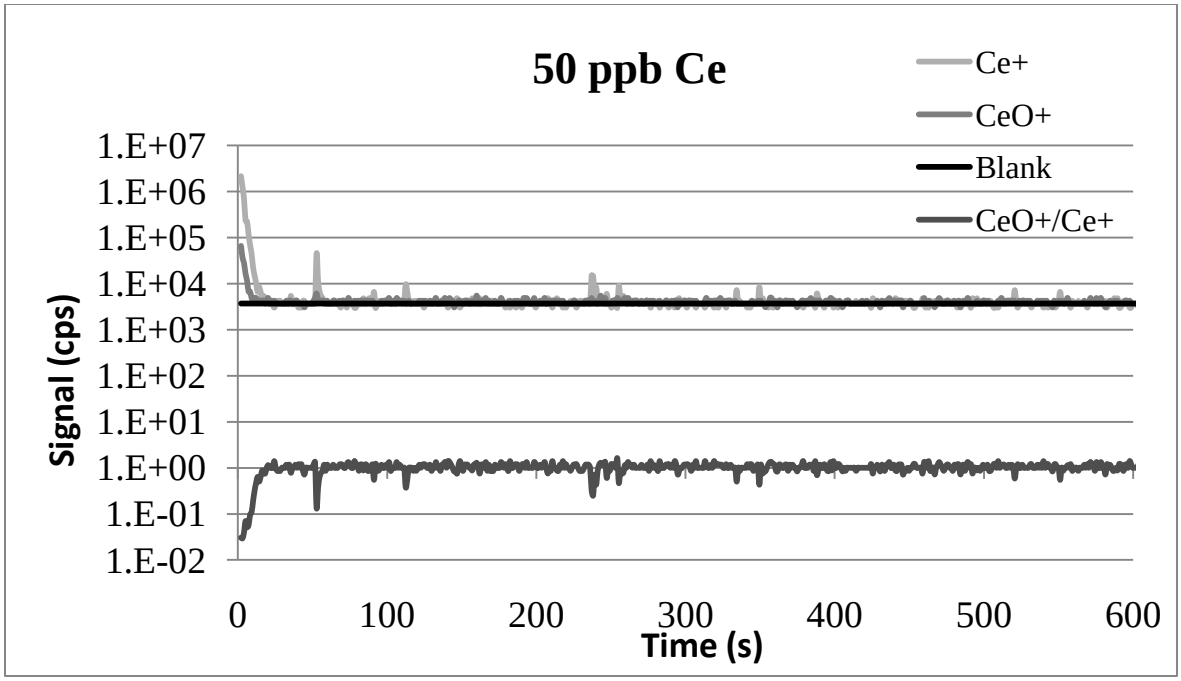

(b)

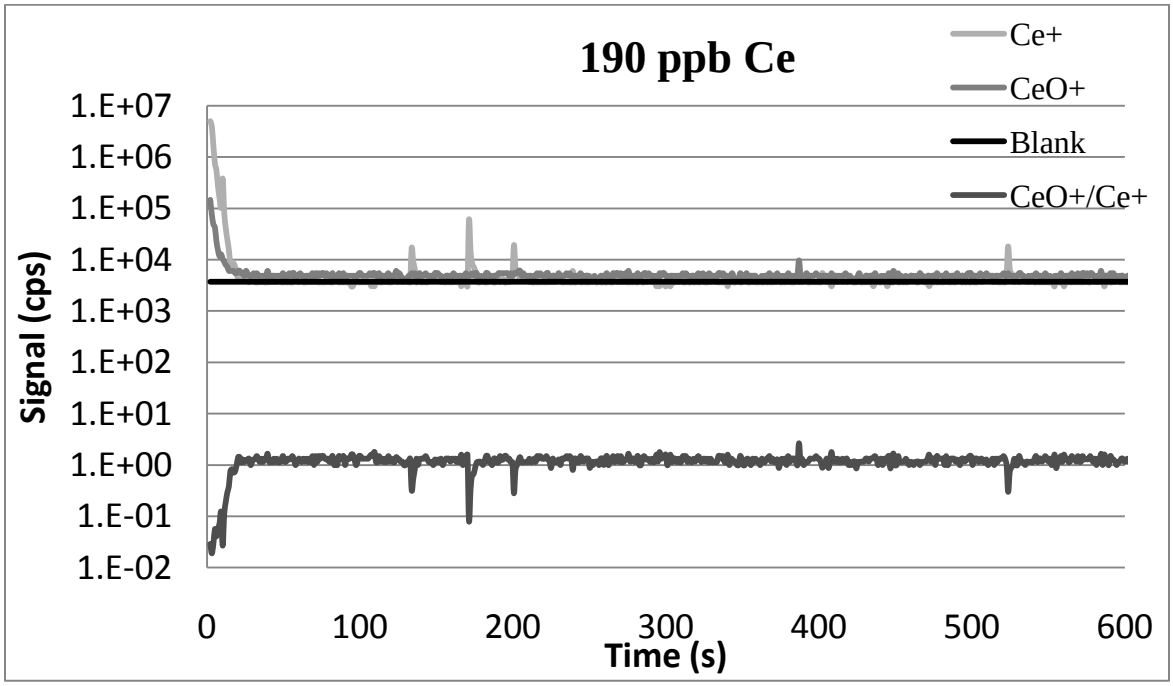

(c)

Figure 1

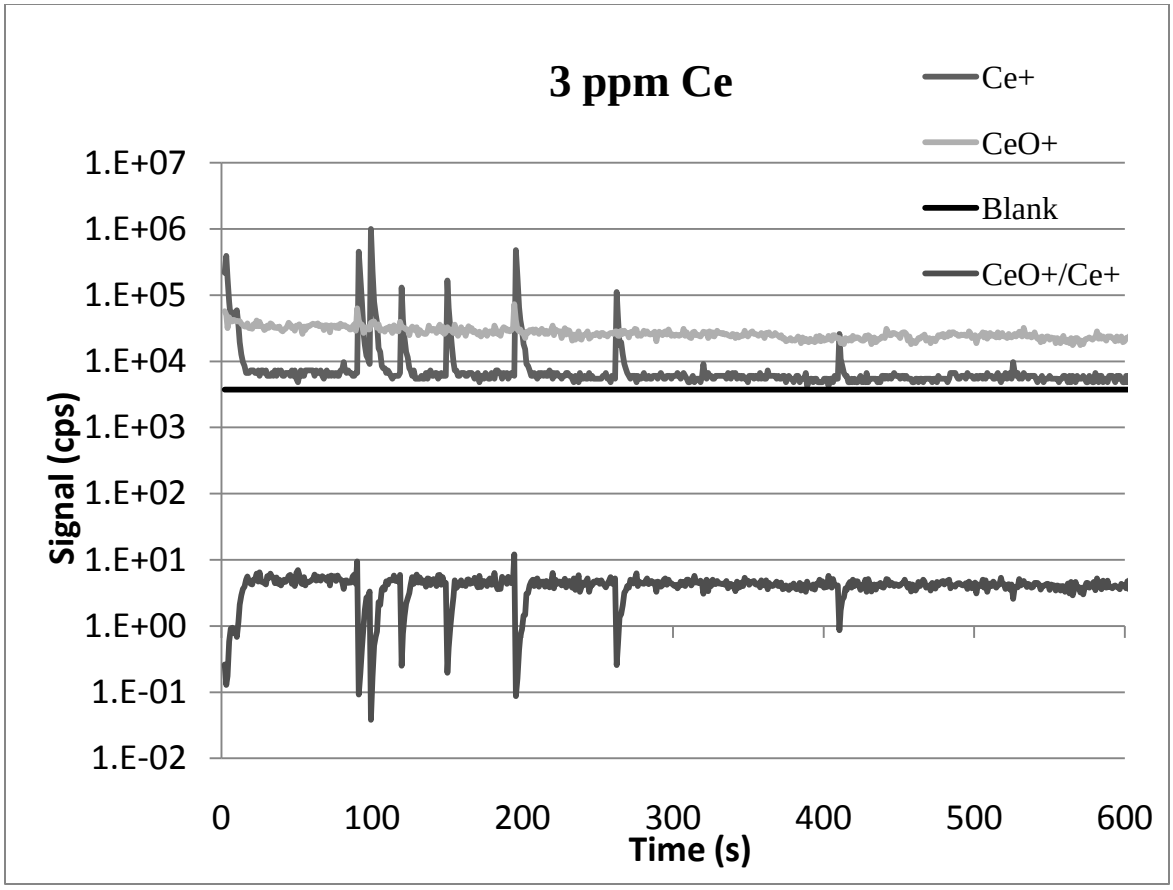

(d)

Figure 1(a-d): Rinse outs from Ce solutions of various concentrations. Notice the slight elevation in CeO^+ signal in the 185 ppb solution indicating beginnings of MO^+ memory effect.

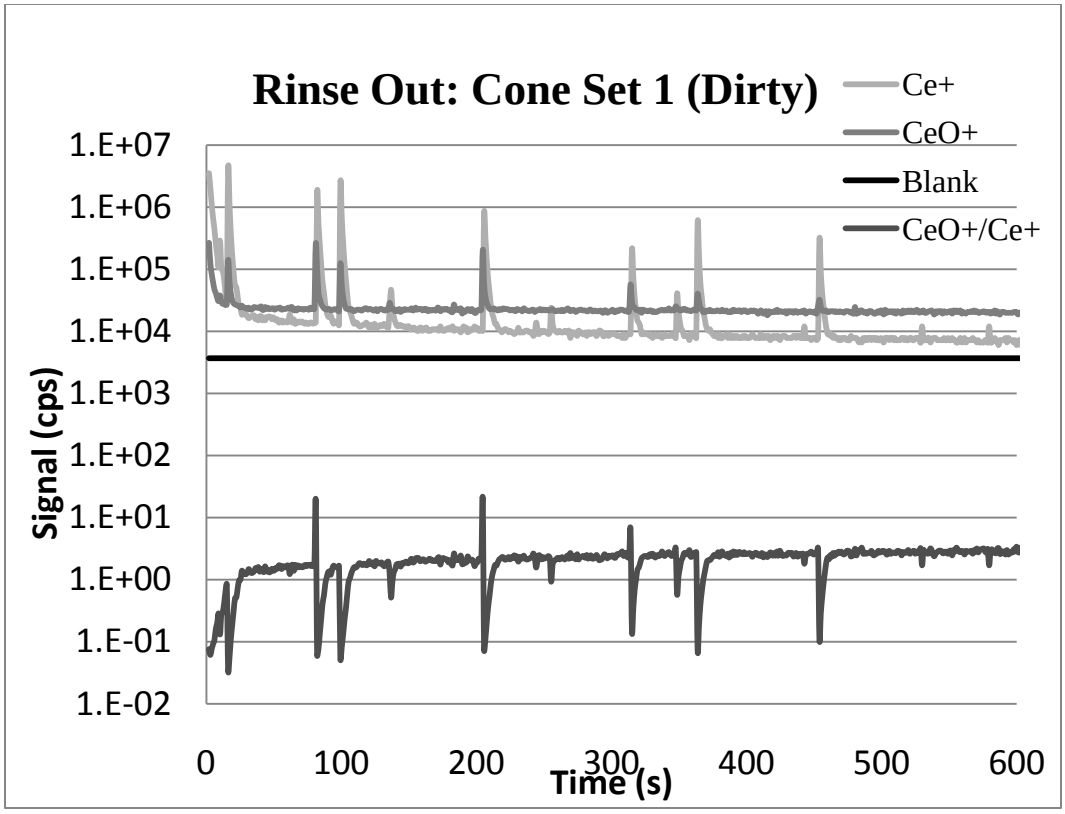

(a)

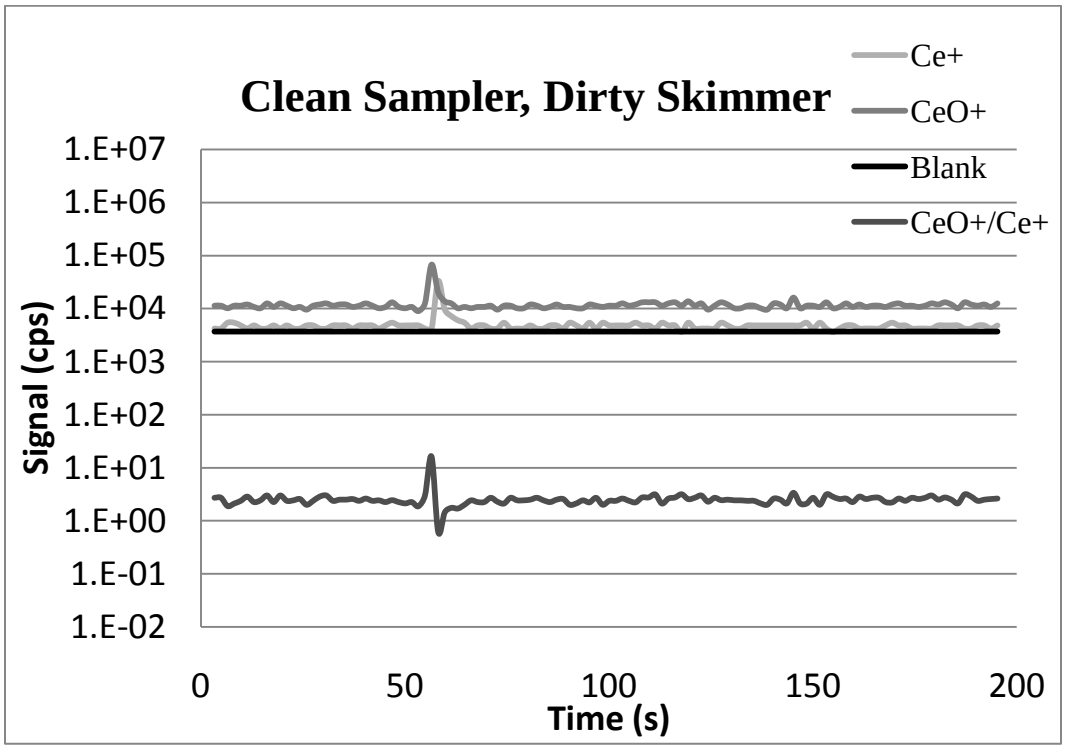

(b)

Figure 2

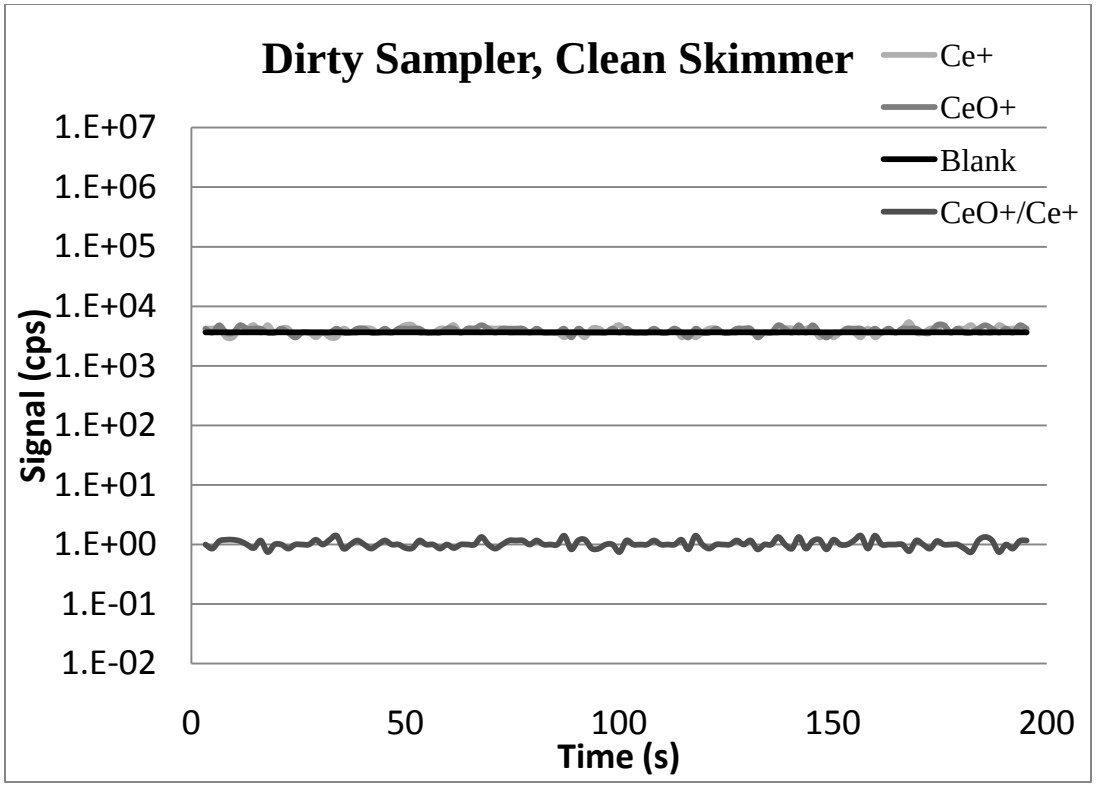

(c)

Figure 2a-c. Experiments to determine source of memory. Skimmer and sampler 1 were on the instrument when a 3ppm Ce solution was aspirated for 5 minutes. Skimmer and sampler 2 were a clean set.

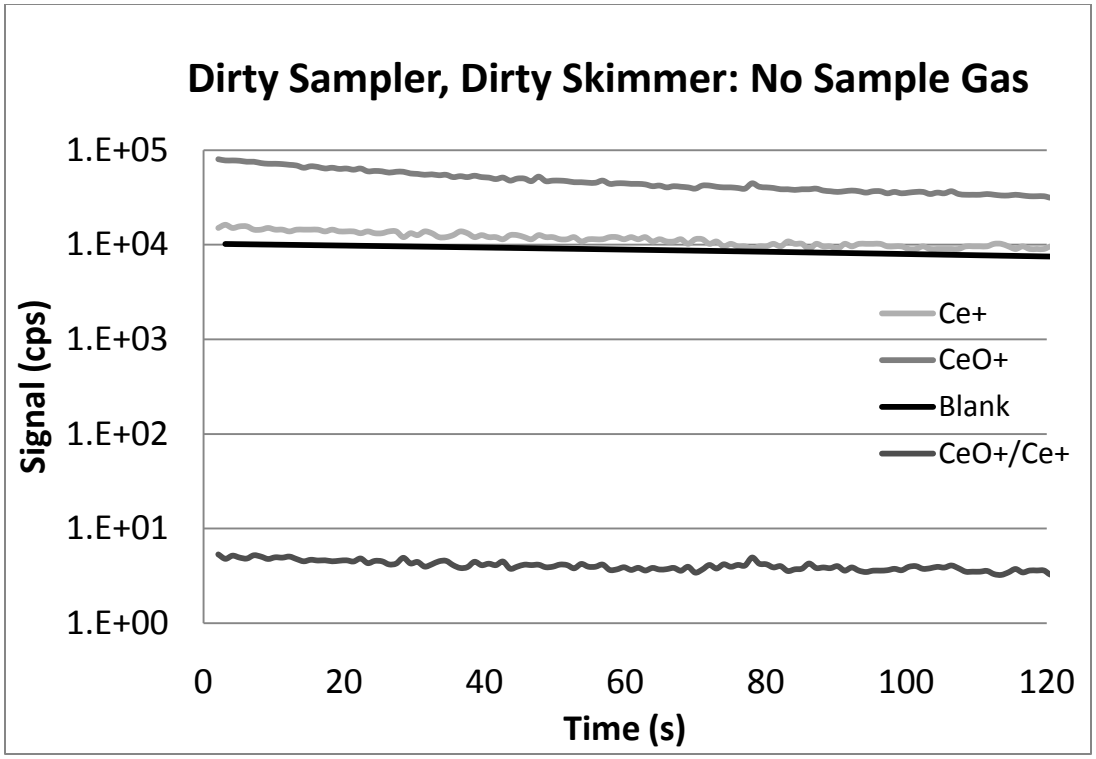

(a)

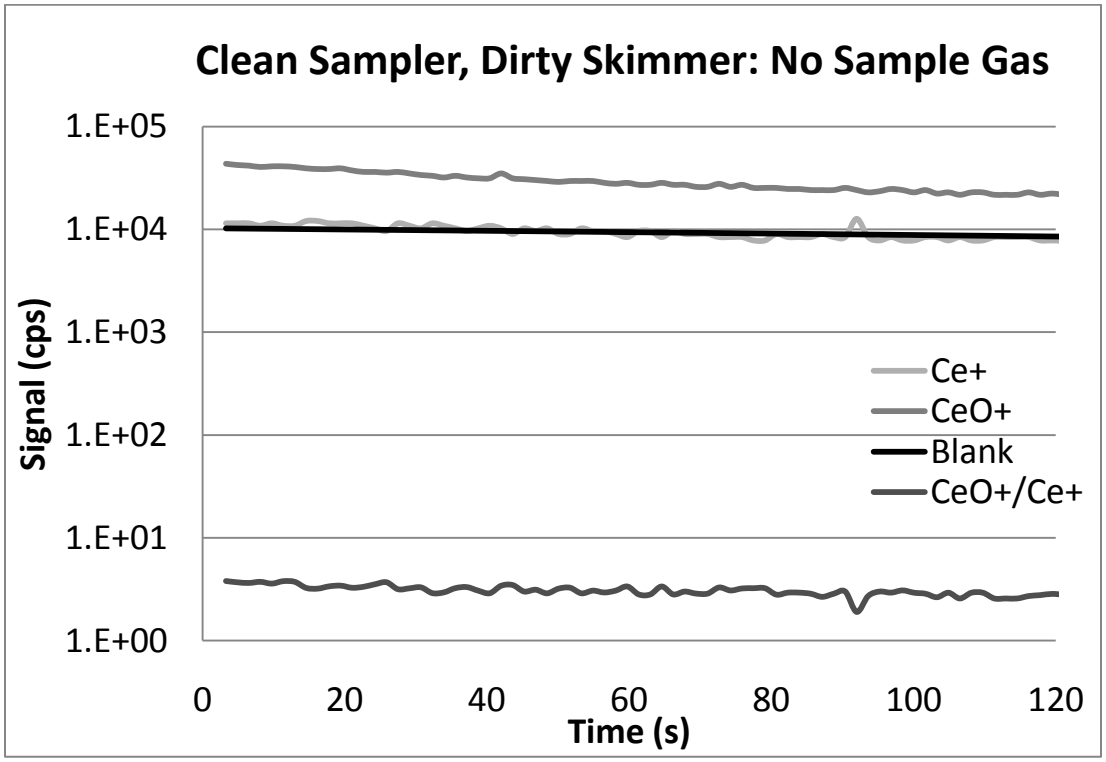

(b)

Figure 3

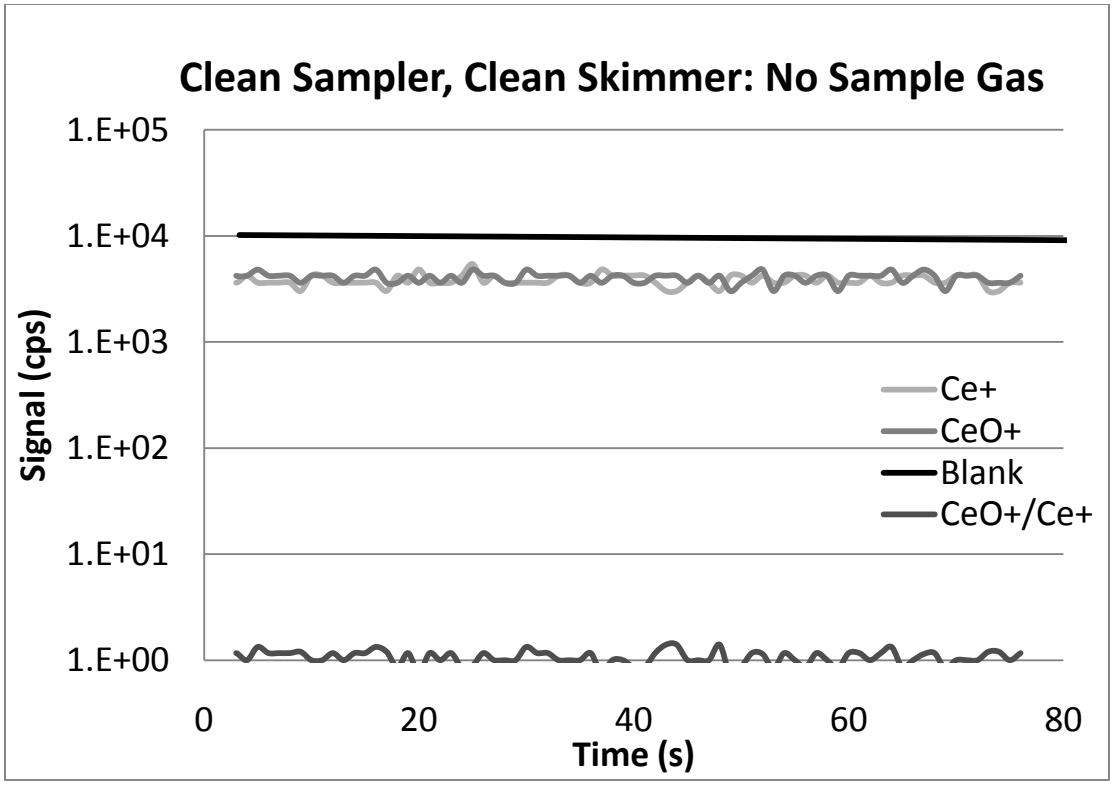

(c)

Figure 3a-c. Same experimental run as in Figure 2. Sampler and skimmer 1 were on the instrument when 3 ppm Ce solution was aspirated for 5 minutes. Sampler and skimmer 2 were a clean set. Sample gas turned to 0 l min^{-1}.

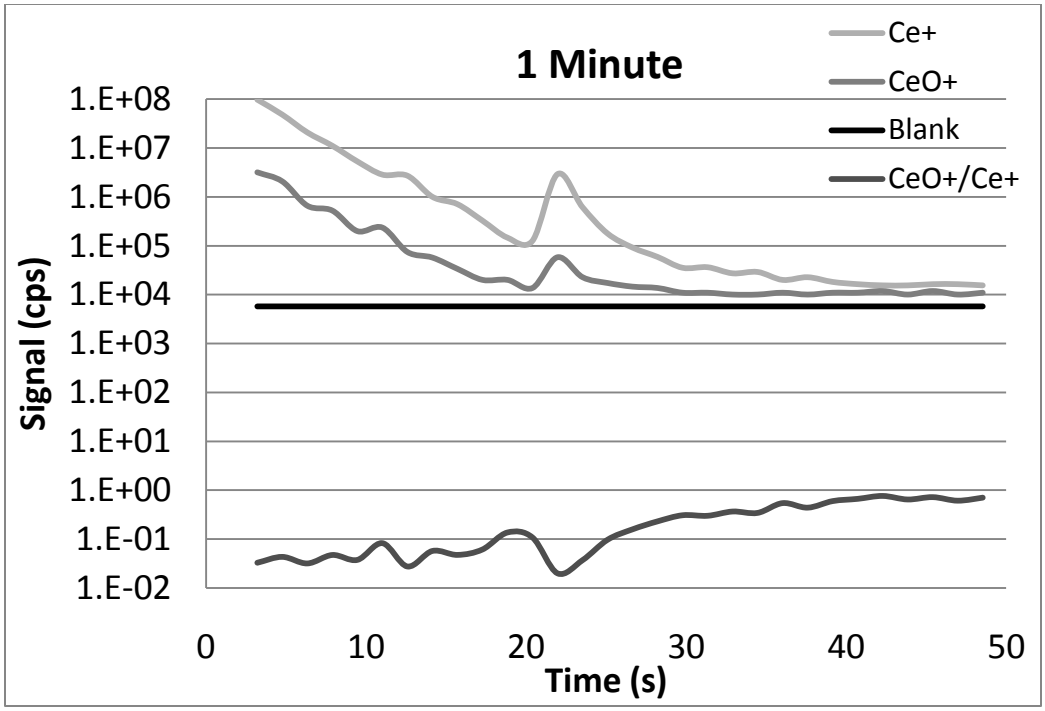

(a)

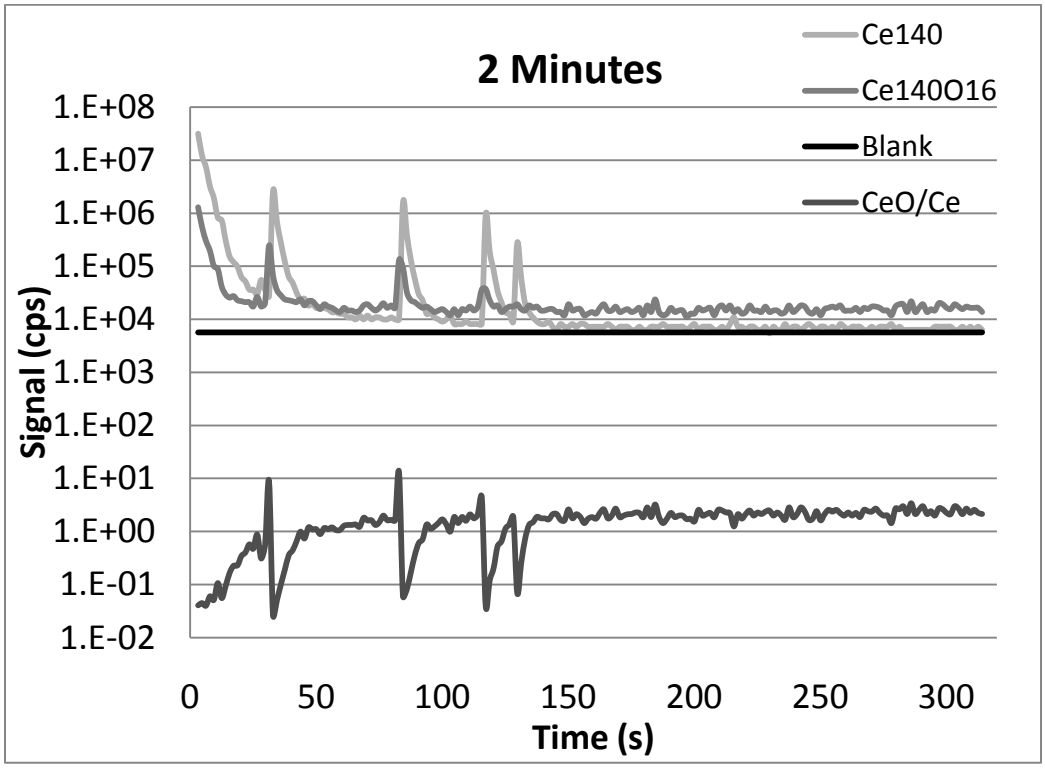

(b)

Figure 4

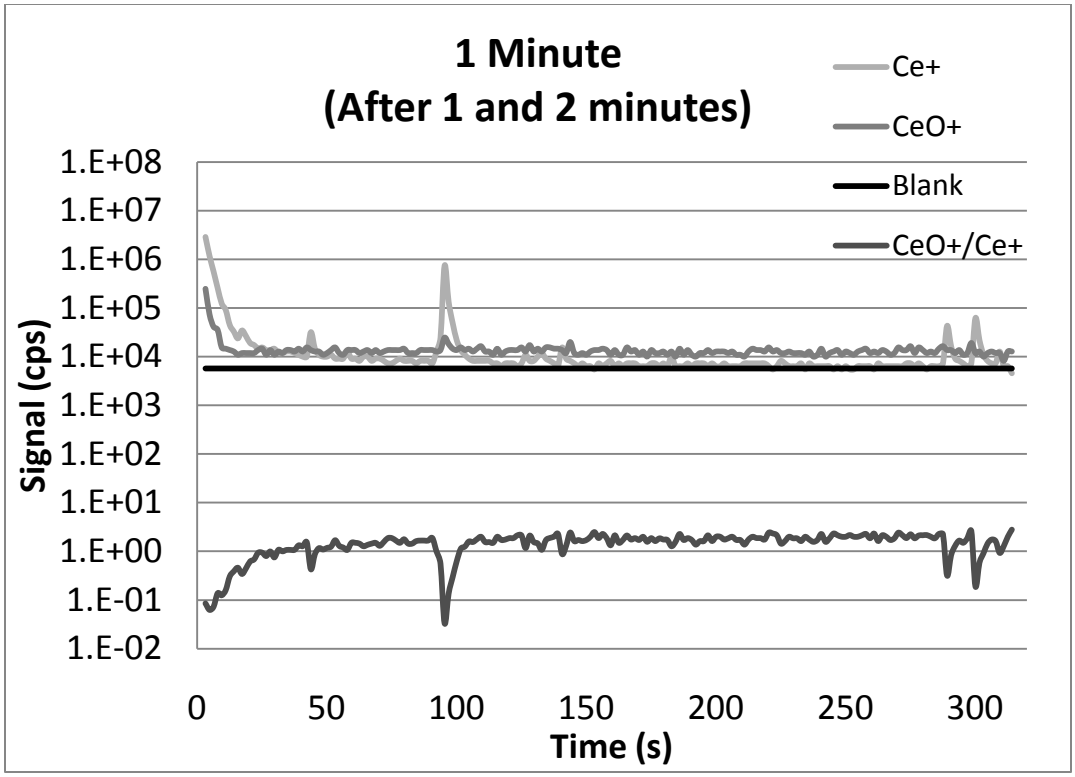

(c)

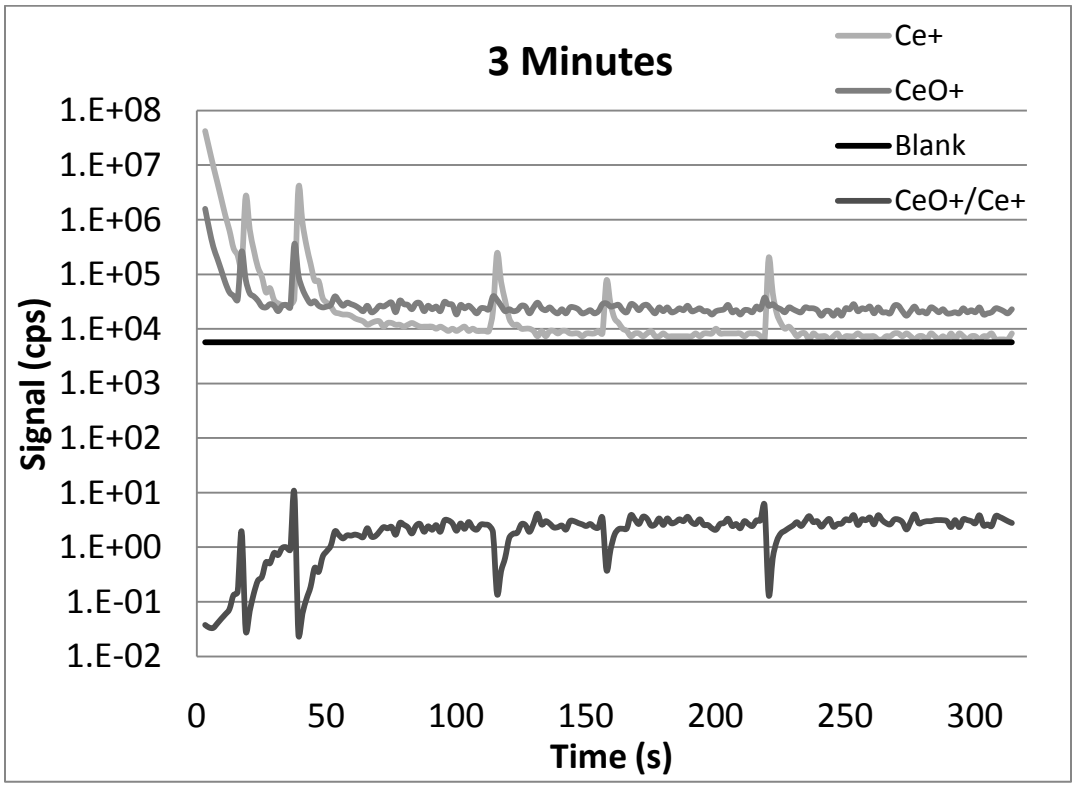

(d)

Figure 4

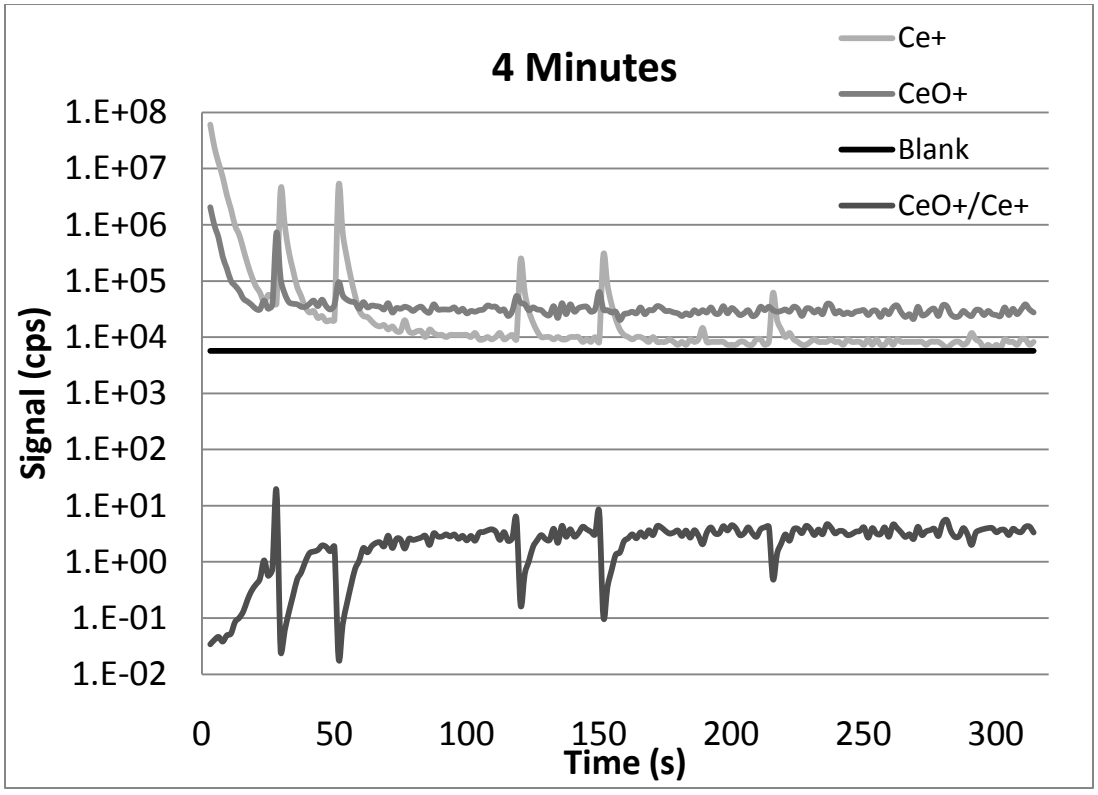

(e)

Figure 4a-e. Rinse-outs from various timed runs of a 3 ppm Ce solution.

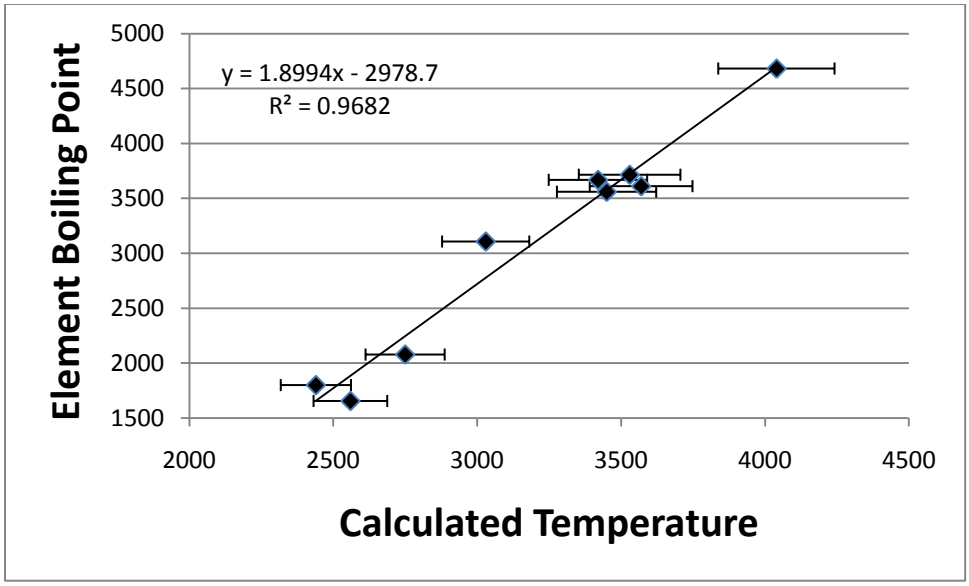

Figure 5. Boiling Point at 1 atm versus calculated temperature of MO^+/M^+ ratio. Excludes Ru. Error bars correspond to 5% error in calculated temperature.

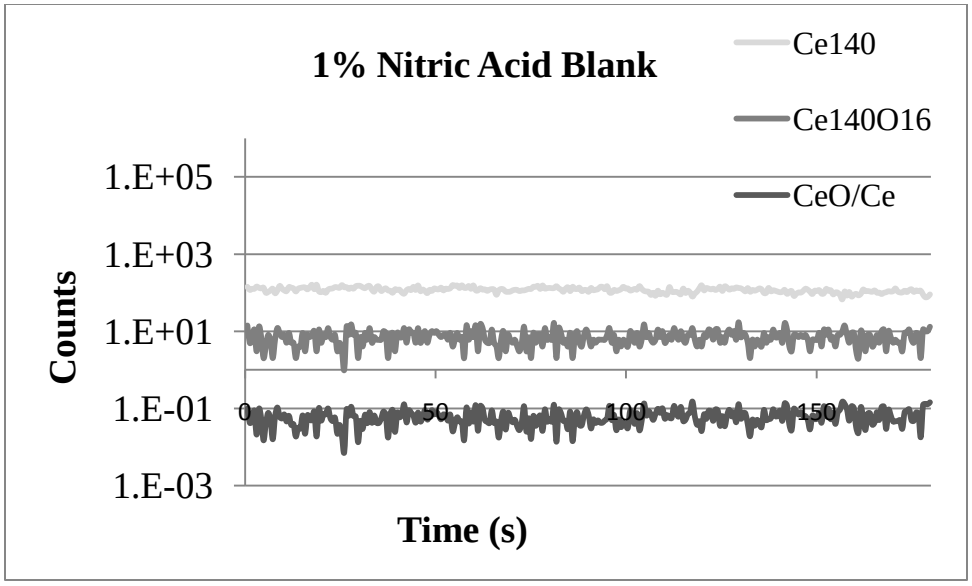

(a)

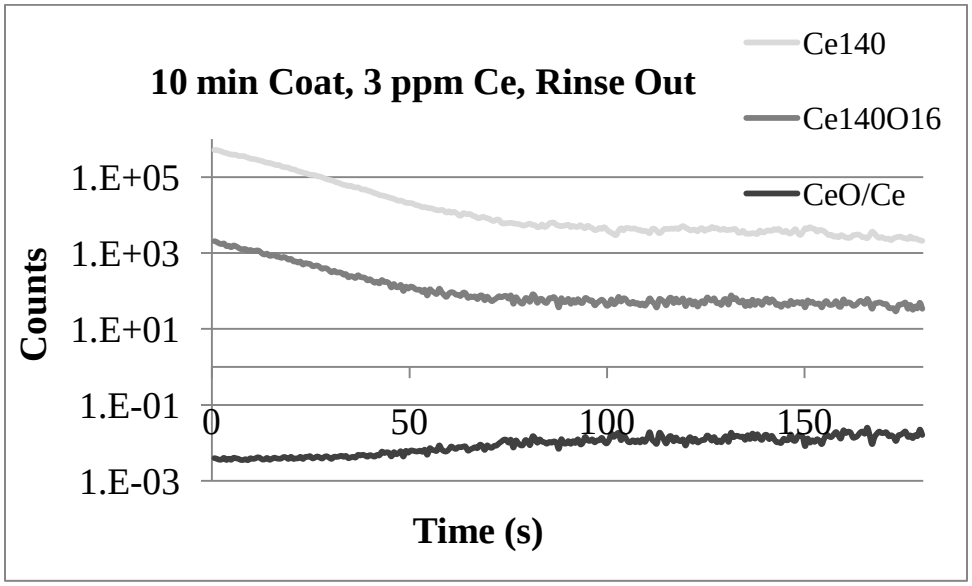

(b)

Figure 6a-b. Run on HP4500 ICP-MS. Note longer run time but lack of memory effect.

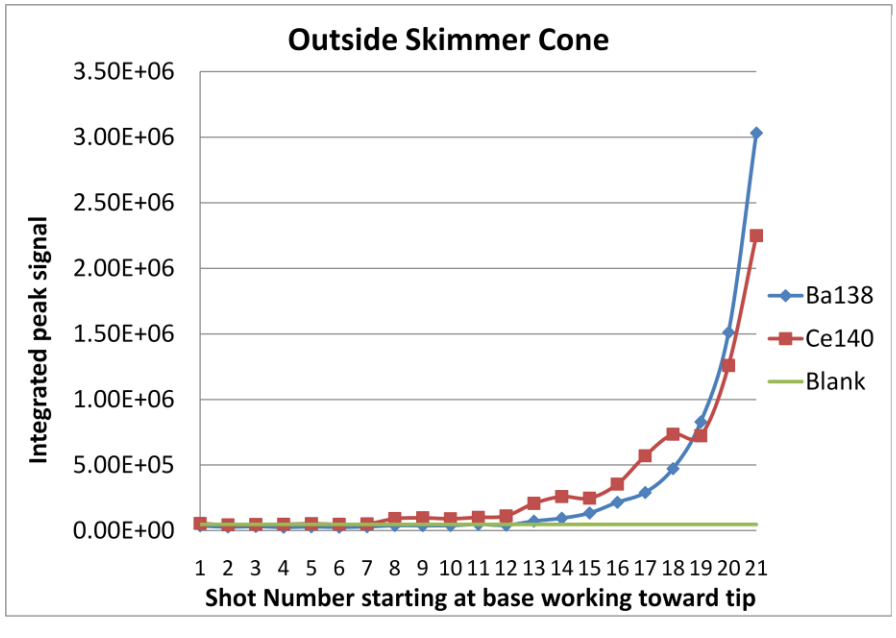

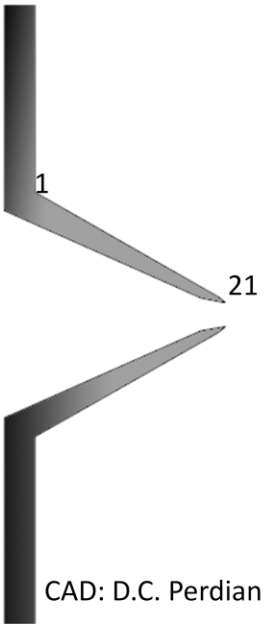

(a)

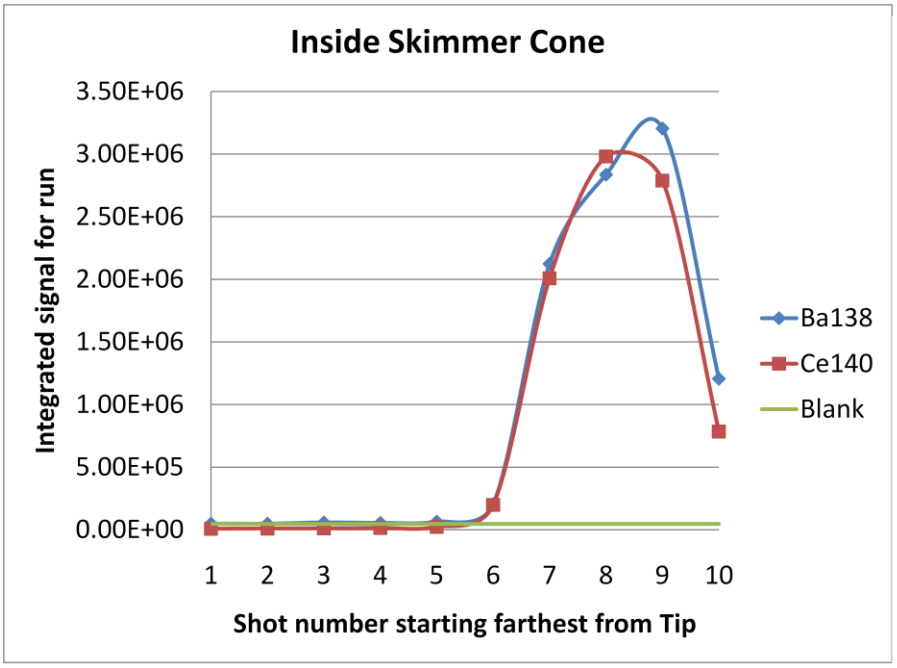

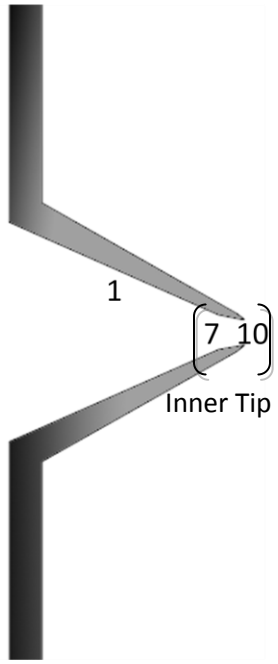

(b)

Figure 7.

Chapter 6. General Conclusions

ICP-MS is the leading trace element analysis technique. One of its weaknesses are polyatomic ions. This dissertation has added to the fundamental understanding of some of these polyatomic ions, their origins and behavior. Although mainly continuing the work of others, certain novel approaches have been introduced here. Chapter 2 includes the first reported efforts to include high temperature corrections to the partition functions of the polyatomic ions in ICP-MS. This and other objections to preceeding papers in this area were addressed. Errors in the measured T_{gas} values were found for given errors in the experimental and spectroscopic values. The ionization energy of the neutral polyatomic ion was included in calculations to prove the validity of ignoring more complicated equilibria. Work was begun on the question of agreement between kinetics of the plasma and interface and the increase and depletion seen in certain polyatomic ions. This dissertation was also the first to report day to day ranges for T_{gas} values and to use a statistical test to compare different operating conditions. This will help guide comparisons of previous and future work.

Chapter 4 was the first attempt to include the excited electronic state $^2\Pi$ in the partition function of ArO^+ as well as the first to address the different dissociation products of the ground and first electronic levels of ArO^+. Chapter 5 reports an interesting source of memory in ICP-MS that could affect mathematical corrections for polyatomic ions.

For future work on these topics I suggest the following experiments and investigations. Clearly not an extensive list, they are instead the first topics curiosity brings to mind!

1. Measurement of T_{gas} values when using the flow injection technique of Appendix B. It was believed that there was a fundamental difference in the plasma when the auto-sampler was used versus a continuous injection. Is this reflected in T_{gas} values?
2. The work of Chapter 3 can be expanded and supplemented with more trials, new cone materials (i.e. copper, stainless steel) and more cone geometries. Some of this equipment is already present in the laboratory, others could be purchased or made.
3. T_{gas} values from Chapter 3 could be correlated with instrument pressures during the experiment. Pressures after the skimmer cone were recorded for many days but have yet to be collated with the measured T_{gas} values.
4. The work in Chapter 5 could be expanded to include more metals. Does the curious correlation between measured T_{gas} and element boiling point persist?
5. Investigate non-linear correlations to T_{gas} values of the MO^+ memory in Chapter 5. Temperatures along the skimmer walls are not a linear gradient. Ring deposits have been observed on the cone and photographs of the interface show light intensities shaping a sort of tailing peak along the outside skimmer wall. Is there a physical property of the metals or metal oxides that would give this peak with the T_{gas} values?
6. Chemical state speciation of the metal deposits on the skimmers of Chapter 5. There may be a more logical correlation between T_{gas} and a physical property of the depositing chemical if all the metals do not deposit in the same form.
7. A collaboration with our computational collegues would be most welcome. Newer calculations for ArO^+ and RuO^+ would be very helpful.

APPENDIX A.

POLYATOMIC IONS IN INDUCTIVELY COUPLED PLASMA – MASS SPECTROMETRY. PART II: ORIGINS OF N_2H^+ AND H_XCO^+ IONS USING EXPERIMENTAL MEASUREMENTS COMBINED WITH CALCULATED ENERGIES AND STRUCTURES

Jill Wisnewski Ferguson, Timothy J. Dudley, Kyle C. Sears, Sally M. McIntyre,

Mark S. Gordon, and R. S. Houk

Ames Laboratory U. S. Department of Energy

Department of Chemistry

Iowa State University, Ames Iowa 50011, USA

A paper published in Spectrochimica Acta Part B, 2009, 64, 690-696.

Abstract

Several polyatomic ions in ICP-MS are studied experimentally and by computational methods. Novel calculations based on spin-restricted open shell second order perturbation theory (ZAPT2) and coupled cluster (CCSD(T)) theory are performed to determine the energies, structures and partition functions of the ions. These values are combined with experimental data to evaluate a dissociation constant and gas kinetic temperature (T_{gas}) value. In our opinion, the resulting T_{gas} value can sometimes be interpreted to deduce the location where the polyatomic ion of interest is generated. The dissociation of N_2H^+ to N_2^+ leads to a calculated T_{gas} of 4550 to 4900 K, depending on the computational data used. The COH^+ to CO^+ system yields a similar temperature, which is not surprising considering the similar energies and structures of COH^+ and N_2H^+. The dissociation of H_2CO^+ to HCO^+ leads to a much lower T_{gas} (<1000 to 2000 K). Finally, the dissociation of H_2COH^+ to $HCOH^+$ generates a T_{gas} value between those from the other H_xCO^+ ions studied here. All of these measured T_{gas} values correspond to formation of extra polyatomic ion in the interface or extraction region. The computations reveal the existence of isomers such as HCO^+ and COH^+, and H_2CO^+ and $HCOH^+$, which have virtually the same *m/z* values and need to be considered in the interpretation of results.

Keywords: polyatomic ions, dissociation reaction, inductively coupled plasma – mass spectrometry, ICP-MS, spectral interferences, N_2H^+, HCO^+, COH^+, H_2CO^+, $HCOH^+$, H_2COH^+.

Abbreviations

ICP-MS: Inductively Coupled Plasma-Mass Spectrometry

ZAPT2: Second order Z-averaged Perturbation Theory

CCSD(T): Coupled Cluster Singles and Doubles with Perturbative Triples

T_{gas}: Gas kinetic temperature

IPA: Isopropanol

Introduction

Inductively coupled plasma-mass spectrometry (ICP-MS) is a highly sensitive technique for the identification and quantification of elements in various samples. One strength of this method is the ability of the ICP to atomize and ionize the sample; the resulting atomic analyte ions are desired for multielement analysis. However, the ICP does not completely atomize everything. Polyatomic ions survive and are observed in the spectra. These ions cause interferences and require correction or attenuation by methods such as high resolution, solvent removal, cool plasma, and collision cells, particularly when analysis is done at the lowest possible analyte concentrations.

A number of papers describe various fundamental aspects of polyatomic ion production in ICP-MS [1-15]. Our group has described ways to evaluate the likely origin of a particular ion from measured ion signal ratios and information about the electronic, vibrational, and rotational energy states of the ions. Perhaps steps could then be taken to reduce the abundance of the polyatomic ion, thus improving the figures of merit of all ICP-MS devices.

Previous work used literature values from experimental measurements of these fundamental properties and was thus restricted to species abundant enough to be studied in detail by other methods, e.g., photoionization MS. The present work reports such results using our own energy level parameters obtained by electronic structure calculations. This greatly extends the range of polyatomic ions that can be evaluated, which is valuable because many species can be seen at low abundance from the ICP. The computations also divulge the presence of isomeric structures that would be difficult to find experimentally [16]. The high sensitivity and resolution of a magnetic sector MS and the ability to assign elemental formulas from accurate m/z measurements are particularly valuable for these measurements. Some of these polyatomic ions may be of interest in their own right in other scientific areas such as interstellar chemistry [17] or the low pressure plasmas used in semiconductor production.

Theory

Previous papers describe the process of studying a polyatomic ion in detail [1-3]. Briefly, the ions AB^+ and A^+ are measured and identified with a MS, in this case a magnetic sector instrument capable of high resolution. A dissociation reaction is written:

$$AB^+ \rightleftharpoons A^+ + B \qquad D_0 (A^+\text{-}B) = \text{dissociation energy} \tag{1}$$

As stated by Houk and Praphairaksit [1,2], this reaction can be written as convenient for analytical measurement, as it does not need to take competing reactions into account. For this generic dissociation reaction, the dissociation constant K_d (Eqn. 2) is evaluated experimentally using the measured signal ratio A^+/AB^+, including correction for mass bias, and an es-

timate of n_B, the number density of the neutral product B (usually Ar atoms or H or O atoms from solvent):

$$K_d = \left(\frac{n_{A^+}}{n_{AB^+}} \right) n_B = f\left(T_{gas}, D_0\right) \qquad (2)$$

$$\log K_d = \frac{3}{2} \log T_{gas} - \frac{5040\, D_0}{T_{gas}} + \frac{3}{2} \log \frac{M_{A^+} M_B}{M_{AB^+}} + \log \frac{Z'_{A^+} Z'_B}{Z'_{AB^+}} + 20.274 \qquad (3)$$

where n is the number density of the indicated species (particles/cm^3), D_0 is the dissociation energy of the ion AB^+ (eV), M is the atomic or molecular weight of the indicated species (g/mol), Z' is the product of the electronic, vibrational, and rotational partition function terms, T_{gas} is the gas kinetic temperature (K), and the logarithms are in base 10. Note that the neutral species density and partition functions are themselves dependent on T_{gas}, and are calculated separately for each T_{gas}. For a single atom species such as H or O, the Z' term is comprised only of the electronic partition function [1].

The experimentally-measured K_d value (Eqn. 2) is used in Eqn. 3 with a Microsoft Excel spreadsheet to determine the T_{gas} value where the two sides are most nearly equal [1]. In the likely range of temperatures seen in these experiments, only one such T_{gas} value results.

We contend that this measured T_{gas} value can be interpreted to identify the likely origin of the AB^+ ion. There are three common scenarios. The first is when the calculated T_{gas} is approximately 5500 to 6500 K, close to the usual value at the sampling position for an ICP operated in "hot" mode. Two other ICP-MS results that support this generic value of T_{gas} ~ 5000 to 6000 K for the usual sampling position are the pressure reduction method [18,19] and the slope of a plot of ion energy vs m/z ratio [20]. Recent work by Farnsworth et al. determined T_{gas} from gas flow velocity from fluorescence measurements behind the sampler

[21]. The results are hard to compare exactly to those in the present work for a variety of reasons. For example, the sampling positions differ (12 mm vs 10 mm); the load coil in the present work is shielded, and the shield probably absorbs some of the forward power. For similar power values (1000 to 1200 W) and aerosol gas flow rates (1.0 to 1.15 L/min), Farnsworth et al. found T_{gas} values of 5500 to 6400 K (see Fig. 3 of ref. 21), again in a similar range as the T_{gas} values cited above as "typical" for common ICP-MS operating conditions. A number of measurement methods for T_{gas} in the conventional ICP (i.e., one that has no sampler cone present) also yield values in this general range: OH rotational temperatures [22,23] Rayleigh scattering [24], and widths and shapes of emission lines [25-27].

In general, these findings suggest that polyatomic ions whose abundance corresponds to T_{gas} values ~ 6000 K are present in the ICP itself. This diagnosis is common for strongly bound MO^+ ions such as CeO^+.

The second outcome occurs when the determined T_{gas} is less than 5500 K. There is more AB^+ in the spectrum than that expected from the ICP itself, which suggests that extra AB^+ is being generated after the ICP. Alternatively, perhaps the ICP does not atomize everything as expected. For example, droplet clouds in the ICP are obviously not in equilibrium with the rest of the plasma [28] and likely account for effects like the abundant $C_xH_yO_z^+$ ions seen from aqueous carbohydrate samples by Longerich et al. [29]. We minimize such effects by using low-flow nebulizers, which minimize solvent load and provide dry or nearly dry particles to the ICP.

The "extra" AB^+ could also be generated via reactions in the supersonic jet or in the extraction process. Such reactions are used in other systems to deliberately make cluster species like Ar_2 and Ar_2^+ [30]. Although the high starting temperature of the ICP is expected

to suppress these species [31], some could still be made this way. A number of ions, including OH^+ and H_2O^+, are consistently observed at abundances that yield a T_{gas} value of ~4000 K, which is close to the T_{gas} value expected at the axial position where Mach number (M)= 1. This is about 0.5 mm behind the upstream tip of the sampling orifice [5,31]. We believe this common T_{gas} value indicates that these ions have a similar origin and are formed in moderate excess by collisions in the early phases of the supersonic expansion [3]. Cooling of the extracted gas due to thermal conduction to the sampler cone may also contribute to T_{gas} values in this range of ~4000 K [32].

Finally, in some cases the measured T_{gas} value is greater than 6000 K; the polyatomic ion AB^+ is less abundant that that expected from the ICP. Some process removes AB^+ relative to A^+, perhaps via collision induced dissociation in the extraction process or supersonic jet. The dissociation of NO^+ to N^+ exhibits these high T_{gas} values [1-3].

The vibrational, rotational, and electronic partition functions are necessary for the ions in question. Through our collaborative efforts, we attain energies calculated via the CCSD(T) and ZAPT2 methods with a high degree of certainty. Articles by Gordon and coworkers explain the general methods used [33]. Specific dissociation energies and structures for the ions in question in this study have been published [16]. The vibrational frequencies and rotational constants derived from these structures and used in the partition function calculations and T_{gas} determinations are reported in various tables below. Agreement between results from different computational methods helps validate the results.

In general, the structures of these ions (e.g., N_2H^+) have been studied previously by either experiment or computation. Our calculated values are consistent with previously published values [17,34-36].

Experimental Section

Groups of ions of similar mass to charge ratio (*m/z*) are measured using a magnetic sector ICP-MS device, capable of resolution of approximately 300, 4000, or 11,000. A single magnet mass setting is used for a particular group of ions to aid in their identification, as the offset between actual *m/z* and measured *m/z* varies with magnetic field setting [3]. In this work, the ions studied generally differ by one H atom, so they can be measured by electrostatic scanning using a single magnet mass setting.

Once spectra are collected in the *m/z* range of interest, the offsets determined between the *m/z* values measured for M^+ ions from elemental standards and their actual *m/z* values are used to determine an accurate *m/z* value for the unknown ions. A line correction equation is derived from the *m/z* values for atomic ions from standard solutions to assist in actual mass estimation. The approximate actual *m/z* of unknown ions from the spectra are then compared to that of various combinations of atoms to help assign an identity. Suggested elemental compositions are guided by the fact that species with many atoms are not likely from the ICP, compared to the plethora of molecules considered in organic mass spectrometry. The elemental formulas are confirmed by the examination of isotope peaks, addition of organic solvent, and/or nebulization of D_2O [3].

Mass bias corrections are determined from the M^+ signals from multielement standard solutions, as described previously [3]. In the present work, the ions in the ratio $n_A+/n_{AB}+$ in Eqn. 2 differ by only one H atom, so mass bias is much less extensive than when ion ratios

involving loss of O or Ar atoms are used. The number density of H atoms is estimated from the solvent load as described [3].

Operating conditions (Table 1) are chosen to provide maximum M^+ signal from multielement standards. These conditions also provide reproducible levels of MO^+ and M^{2+} ions (signal ratios for CeO^+/Ce^+ ~ 1%; Ce^{2+}/Ce^+ ~ 2%). We refer to this condition as "hot" plasma mode, to distinguish it from "cool" mode. The forward power and sampling position are normally kept constant and the aerosol gas flow rate is adjusted to achieve this condition. The optimum value of aerosol gas flow rate differs slightly from day to day, which is common, so a range of values are shown in Table 1. Also, this method of selecting operating conditions is much like that used in common analytical practice. It provides very consistent T_{gas} values from day to day for most species and between three different ICP-MS instruments [1,3].

The sample was 1% aqueous HNO_3 for the smaller ions. For the larger H_xCO^+ ions, 10% isopropanol (IPA) was added to enhance their abundances. This nonvolatile alcohol did not change the optimum aerosol gas flow rate, solvent load, or T_{gas} outcome significantly .

Results

4.1. N_2H^+ and N_2^+

N_2^+ is a common polyatomic ion seen in ICP-MS. The presence of N_2^+ in the mass spectrum is expected since the plasma flows into the air, nitric acid is a common solvent, N_2 is a likely impurity in the argon tanks, and the sample could also contain some dissolved N_2 gas. However, the authors were initially surprised to note that N_2H^+ was more abundant than

N_2^+ (Figs. 1 and 2). Polyatomic ions with more atoms are generally expected to be less abundant at the high temperatures present in the ICP. This anomaly is significant analytically. $^{29}Si^+$ is often chosen to determine Si because of the $^{14}N_2^+$ interference commonly considered to be more severe on the major $^{28}Si^+$ isotope.

Once the true identity of the ions was clear via accurate *m/z* measurements, isotope ratio measurements, and solvent manipulation, we used the following reaction.

$$N_2H^+ \rightleftharpoons N_2^+ + H \qquad K_{d4} = K_d(N_2^+\text{-}H) \qquad (4)$$

Energy level values for N_2H^+ are reported in Table 2.

For a 1% aqueous HNO_3 sample, the experimental N_2^+/N_2H^+ signal ratio of 1.7 yields a T_{gas} value of 4550 K using energies provided by the ZAPT2 calculation; CCSD(T) data produces a T_{gas} value around 4900 K. The difference in temperature is primarily attributed to the variation in calculated dissociation energy between the two methods. The CCSD(T) method is the higher level calculation and thus is thought to be superior. In this case, the two computation methods yield T_{gas} values that differ by only 350 K based on high dissociation energies (6.891 vs 7.449 eV) that differ by a large amount (~0.5 eV). Thus, even a large uncertainty in a large dissociation energy does not affect the basic diagnosis of the likely origin of the ions. Errors in other terms like the partition functions make even less difference [37].

T_{gas} values in this range (4550 or 4900 K) are lower than those seen from ions which are believed to originate in the plasma, such as CeO^+ [1,9,18,31]. This observation suggests that additional N_2H^+ is being produced in the interface or extraction process. The high dissociation energy and larger vibrational and rotational partition functions for N_2H^+ also help ac-

count for its larger abundance compared to N_2^+. In retrospect, a stable Lewis structure can be drawn for N_2H^+ as $:N\equiv N\text{-}H^{]+}$

Interestingly, computational modeling of dissociation of N_2H^+ provides information about the likely mechanism of the reaction [16]. The lowest energy pathway for dissociation is loss of H^+, instead of the H atom as shown in Rxn. 4. Upon dissociation, the more easily ionized product would be expected to carry the positive charge, as expected from the following cycle:

$N_2H^+ \rightleftharpoons N_2 + H^+$	$D_0(N_2\text{-}H^+)$	K_{d5}	(5)
$H^+ + e \rightleftharpoons H$	$\Delta H = -IE\ (H) = -13.598$ eV	$1/K_6$	(6)
$N_2 \rightleftharpoons N_2^+ + e$	$\Delta H = IE\ (N_2) = 14.65$ eV	K_7	(7)
$N_2H^+ \rightleftharpoons N_2^+ + H$	$D_0(N_2^+\text{-}H) = D_0(N_2\text{-}H^+) + 1.05$ eV		(8)

However, whether the calculations are done in one overall step (Eqn. 4) or three steps (Eqns. 5, 6, and 7), the final K_d values should be equivalent:

$$K_{d4} = K_{d5}K_7/K_6 \qquad (9)$$

where K_{d5}, K_6 and K_7 are the "equilibrium" constants defined above for Reactions 5, 6, and 7. The same result for T_{gas} and probable ion origin should result, if the position of Reactions 5, 6, and 7 are described by the same numerical value of temperature. Experimentally, this is fortunate. Direct use of Reaction 5 would require measurement of H^+, which is possible but difficult. Correction for mass bias at *m/z* 1 is harder still.

4.2. HCO^+, COH^+, and CO^+

The computational results (Table 3) agree closely. HCO^+ is a strongly bound ion. The isomer COH^+ is much more easily dissociated than HCO^+.

The computations indicate the probable presence of both HCO^+ and COH^+ isomers at *m/z* 29.0027:

$$HCO^+ \rightleftharpoons COH^+ \rightleftharpoons CO^+ + H \quad (10)$$

The mass spectrometer cannot discriminate between these two species; the signal observed is that for the sum of HCO^+ and COH^+. The question of whether the presence of COH^+ affects the diagnosis of the origin of HCO^+ and COH^+ is addressed as follows. The formalism is much like that used to calculate the abundances of various forms of a polyprotic weak acid in solution.

$$HCO^+ \rightleftharpoons COH^+ \qquad E_r = \text{rearrangement energy} \quad (11)$$

$$K_r = n_{COH^+}/n_{HCO^+} \quad (12)$$

$$HCO^+ \rightleftharpoons CO^+ + H \qquad K_d \quad (13)$$

$$K_d = \left(\frac{n_{CO^+}}{n_{HCO^+}}\right) n_H = \left(\frac{n_{CO^+}}{N_{29.0027}}\right)(K_r + 1)\, n_H \quad (14)$$

where $N_{29.0027}$ is the total signal at m/z 29.0027, i.e., the m/z value for both HCO^+ and COH^+.

The measured signal ratio $CO^+/(HCO^+ + COH^+)$ from 1% aqueous HNO_3 is about 2.5. The T_{gas} values that result from use of various dissociation reactions for these ions are given in Table 4. Some observations from the table are as follows. Use of either CCSD(T) or ZAPT2 results does not affect the measured T_{gas}. Inclusion of the COH^+ isomer also has little effect. The dissociation energy of COH^+ is almost 5 eV lower than that of HCO^+, so COH^+ does not appear to be very important in this system. However, incorrect assignment of the lowest energy isomer to COH^+ would lead to a much lower T_{gas} value and thus cause a large difference in the diagnosis of the origin of these ions.

For the HCO^+, COH^+/CO^+ system, the measured T_{gas} value is similar to that found for N_2H^+/N_2^+. On one hand, this similarity of T_{gas} values is expected based on the similar disso-

ciation energies and partition functions for these groups of ions. On the other hand, the measured signal ratio for N_2H^+/N_2^+ is 1.7, substantially higher than that for $(HCO^+ + COH^+)/CO^+$ (0.4, Figs. 1 and 2).

4.3. H_2CO^+ and $HCOH^+$

The H_2CO^+ system presents an additional challenge. For most species, ZAPT2 and CCSD(T) produce structural results that are very similar. However, for the H_2CO^+ system, the two calculation methods identify different isomers to have the lowest energy: $HCOH^+$ by ZAPT2 , and H_2CO^+ by CCSD(T) (Table 5). Furthermore, the product ion also has two isomers: HCO^+ and COH^+. Both computational methods yield very low dissociation energies, so neither $HCOH^+$ nor H_2CO^+ are expected to be very abundant. Indeed, the measured signal ratio for $(H_2CO^+ + HCOH^+) / (HCO^+ + COH^+)$ is only ~ $5x10^{-4}$, a small value.

T_{gas} is evaluated in the following way.

$H_2CO^+ \rightleftharpoons HCOH^+$	$E_r\ (H_2CO^+)$	(15)
	$K_r\ (H_2CO^+)$	(16)
$H_2CO^+ \rightleftharpoons HCO^+ + H$	$D_0(H_2CO^+)$	(17)
$HCO^+ \rightleftharpoons COH^+$	$E_r\ (HCO^+)$	(18)
	$K_r\ (HCO^+)$	(19)

If only the isomers of H_2CO^+ are considered, the equation for K_d is:

$$K_d = \left(\frac{n_{HCO^+}}{N_{30.0106}} \right) \left[K_r\left(H_2CO^+\right) + 1 \right] n_H \qquad (20)$$

where $N_{30.0106}$ is the total signal at the m/z value for both H_2CO^+ and $HCOH^+$. Including the isomers of HCO^+ in the numerator gives:

$$K_d = \left(\frac{N_{29.0027}}{N_{30.0106}} \right) \left[\frac{K_r\left(H_2CO^+\right)+1}{K_r\left(HCO^+\right)+1} \right] n_H \qquad (21)$$

Table 6 lists T_{gas} values from the same measured signals derived from these various possibilities. Here the sample is 1% aqueous HNO_3 + 10% IPA; the latter additive enhances the abundance of the larger H_xCO^+ ions. The entries are grouped according to the various isomers used. Basically, all the measured T_{gas} values derived from ZAPT2 data are ~1500 K. All the values from CCSD(T) data are ~ 2200 to 2300 K.

The modest difference between T_{gas} values derived from ZAPT2 data vs. CCSD(T) data is not considered important. What does matter is that all these temperatures are lower than those found above for N_2H^+/N_2^+, $(HCO^+ + COH^+)/CO^+$, and a number of other polyatomic ions [3]. One explanation for this discrepancy is that excess $HCOH^+$ and/or H_2CO^+ ions continues to be made further aft in the supersonic expansion, where the T_{gas} is expected to be cooler, than is the case for the other species. Perhaps there is a shock wave there [5,38,39]. Another possibility is that there is a kinetically favorable route to make H_2CO^+ during ion extraction, more so than HCO^+ or COH^+. The measured T_{gas} values are still well above those of ~150 K estimated for a clean supersonic expansion at the skimmer orifice [31].

4.4. H_2COH^+

The two computational methods yield almost the same energies and a single structure for H_2COH^+ (Table 7). However, the lowest energy dissociation product is either $HCOH^+$ (according to ZAPT2) or H_2CO^+ (from CCSD(T)).

$$H_2COH^+ \rightleftharpoons HCOH^+ + H \quad (22)$$

$$H_2COH^+ \rightleftharpoons H_2CO^+ + H \quad (23)$$

Although the dissociation energies of H_2COH^+ are fairly high, it is the least abundant ion from the H_xCO^+ family in the mass spectrum.

To observe H_2COH^+, a 10% IPA:1% HNO_3 in water solution was nebulized. Using the values in Table 7, measured T_{gas} values are 3650 K (ZAPT2) and 3610 K (CCSD(T)). These two values are similar to those measured for N_2H^+ and the HCO^+/COH^+ systems. The ICP was not obviously different with this dose of isopropanol. The IPA would be expected to cool the plasma, if it had much effect.

The different product ions predicted by the two computational methods make little difference in the diagnosis of the origin of H_2COH^+. Inclusion of isomers in the product $H_2CO^+/HCOH^+$ also makes only a 100 K difference in the resulting T_{gas} (data not shown).

4.5. Effect of T_{gas} regime on importance of isomers

Inclusion of isomers does not make much difference in the interpretation of the experimental T_{gas} measurements in the above examples. This is largely because the ions studied are observed at abundances well above those expected from the ICP alone, i.e., the T_{gas} values that result from the measurements are lower than that expected from the ICP. More energetic isomers are less populated at low temperatures. However, such isomers would be more important if the ions came from a region where T_{gas} was larger. To illustrate this effect, the fundamental data (ZAPT2 or CCSD(T)) are used to generate hypothetical ion signal ratios characteristic of two hotter regimes: T_{gas} = 4500 K (often seen for H_xO^+ ions from water) and 5800 K (characteristic of MO^+ ions) [1,3]. These hypothetical signal ratios are then

used in different spreadsheets that include the isomers. The resulting change in T_{gas} indicates whether the isomers matter.

First, the simple reaction

$$HCOH^+ \rightleftharpoons HCO^+ + H \qquad T_{gas} = 4500 \text{ K or } 5800 \text{ K assumed}$$

was examined using ZAPT2 fundamental data. This system is chosen because the isomers have similar energies. The apparent temperature changed, first from 4500 K to 5300 K, then from 5800 K to 7330 K, when the same signal ratios were used with all the likely isomers included:

$$HCOH^+ \rightleftharpoons H_2CO^+ \rightleftharpoons HCO^+ \rightleftharpoons COH^+ \quad (24)$$
$$+ H$$

The related reaction was also studied using CCSD(T) data:

$$H_2CO^+ \rightleftharpoons HCO^+ + H \qquad T_{gas} = 4500 \text{ K or } 5800 \text{ K assumed}$$

Again, the apparent temperatures changed; 4500 became 5260 K, and 5800 K became 7250 K, when the more complicated reaction was used:

$$H_2CO^+ \rightleftharpoons HCOH^+ \rightleftharpoons HCO^+ \rightleftharpoons COH^+ \quad (25)$$
$$+ H$$

T_{gas} values ~5800 K vs. ~7300 K would lead to quite different diagnoses as to the origin of the ions. So the presence of isomers can make a difference in temperature regimes close to those of the ICP, although this is not an issue for the polyatomic ions studied here.

Acknowledgements

This research was supported by the National Science Foundation (Award No. CHE-0309381) through the Institute for Physical Research and Technology at ISU. JWF was also

supported by the Velmer A. and Mary K. Fassel Fellowship, and SMM is supported by the Conoco Phillips Fellowship. The nebulizers used were provided by Elemental Scientific Inc. The ICP-MS device was obtained with funds provided by the U. S. Department of Energy, Office of Nuclear Nonproliferation (NA-22) and the Office of Basic Energy Sciences. Ames Laboratory is operated for the U.S. Department of Energy by Iowa State University under Contract No. W-7405-Eng-82.

References

1. R. S. Houk, N. Praphairaksit, Dissociation of polyatomic ions in the inductively coupled plasma, Spectrochim. Acta Part B 56 (2001) 1069-1096.

2. R. S. Houk, Erratum to "Dissociation of polyatomic ions in inductively coupled plasma – mass spectrometry," Spectrochim. Acta Part B 61 (2006) 235-236

3. J. W. Ferguson, R. S. Houk, High resolution studies of the origins of polyatomic ions in inductively coupled plasma – mass spectrometry part I: identification methods and effects of neutral density assumptions, extraction voltage, and cone material, Spectrochim. Acta Part B, 61 (2006) 905-915.

4. H. Niu, R. S. Houk, Fundamental aspects of ion extraction in inductively coupled plasma mass spectrometry, Spectrochim. Acta Part B 51 (1996) 779-815.

5. A. L Gray, Visual observation of shock waves in an ICP-MS expansion stage, J. Anal. At. Spectrom. 4 (1989) 371-373.

6. N. Nonose, M. Kubota, Non-spectral and spectral interferences in inductively coupled plasma high resolution mass spectrometry Part I: optical characteristics, J. Anal. At. Spectrom. 16 (2001) 551-559.

7. N. Nonose, M. Kubota, Non-spectral and spectral interferences in inductively coupled plasma high resolution mass spectrometry Part II:comparison of interferences in quadrupole and high resolution, J. Anal. At. Spectrom. 16 (2001) 560-566.

8. N. Nonose, Formation of interfering polyatomic ion species in ICP-MS, J. Mass Spectrom. Soc. Jpn. 45 (1997) 77-89.

9. S.D. Tanner, Plasma temperature from ion kinetic energies and implications for the source of diatomic oxide ions in inductively coupled plasma-mass spectrometry, J. Anal. At. Spectrom. 8 (1993) 891-897.

10. J.S. Becker, H.-J. Dietze, Investigations on cluster and molecular ion formation by plasma mass spectrometry, Fresenius' J. Anal. Chem. 359 (1997) 338-345.

11. E. H. Evans, L. Ebdon, L. Rowley, Comparative study of the determination of equilibrium dissociation temperature in inductively coupled plasma-mass spectrometry, Spectrochim. Acta Part B 57 (2002) 741-754.

12. M.M. Fraser, D. Beauchemin, Effect of concomitant elements on the distribution of ions in inductively coupled plasma-mass spectrometry—Part 2: polyatomic ions, Spectrochim. Acta Part B 57 (2001) 2479-2495.

13. A.E. Holliday, D. Beauchemin, Spatial profiling of ion distributions in a nitrogen-argon plasma in inductively coupled plasma-mass spectrometry, J. Anal. At. Spectrom. 18 (2003) 289-295.

14. N.F. Zahran, A.I. Helal, M.A. Amr, A. Abdel-Hafiez, H.T. Mohsen, Formation of polyatomic ions from the skimmer cone in ICP-MS, Int. J. Mass Spectrom. 226 (2003) 271-278.

15. S. Liu, D. Beauchemin, The effect of pre-evaporation on ion distribution in inductively coupled plasma mass spectrometry, Spectrochim. Acta Part B 61 (2006) 157-163.

16. K. C. Sears, J. W. Ferguson, T. J. Dudley, R. S. Houk, M. S. Gordon, Theoretical investigation of small polyatomic ions observed in inductively coupled plasma mass spectrometry: H_xCO^+ and $H_xN_2^+$ (x=1, 2, 3), J. Phys. Chem. A 112 (2008) 2610-2617.

17. J. Crovisier, Constants for molecules of astrophysical interest in the gas phase: photodissociation, microwave and infrared spectra. Version 4.2 (May 2002), http://wwwusr.obspm.fr/~crovisie/basemole/.

18. S. D. Tanner, Plasma temperature from ion kinetic energies and implications for the source of diatomic oxide ions in ICP-MS, J. Anal. At. Spectrom. 8 (1993) 891-897.

19. D. J. Douglas, Some current perspectives on ICP-MS, Canad. J. Spectrosc. 34 (1989) 38-49.

20. J. E. Fulford and D. J. Douglas, Ion kinetic energies in ICP-MS, Appl. Spectrosc. 1986 (40) 971-974.

21. J. B. Olsen, J. H. Macedone and P. B. Farnsworth, Source gas kinetic temperatures in an ICP-MS determined by measurements of the gas velocities in the first vacuum stage, J. Anal. Atomic Spectrom. 21 (2006) 856-860.

22. T. Hasegawa, M. Umemoto, H. Haraguchi, C. Hsieh and A. Montaser, Fundamental properties of ICPs, in A. Montaser and D. W. Golightly, Eds., ICPs in analytical atomic spectrometry, 2nd ed., VCH, New York, Sect. 8.2.3, p. 386 (1992).

23. I. Ishii and A. Montaser, A tutorial discussion on measurement of rotational temperatures in an ICP, Spectrochim. Acta Part B 46 (1991) 1197-1206.

24. S. A. Lehn, K. A. Warner, M. Huang and G. M. Hieftje, Effect of an ICP-MS sampling interface on electron temperature, electron number density, gas-kinetic temperature and analyte emission intensity upstream in the plasma, Spectrochim. Acta Part B 57 (2002) 1739-1751.

25. H. G. C. Human and R. H. Scott, The shapes of spectral lines emitted by an ICP, Spectrochim. Acta part B 31 (1976) 459-473.

26. P. W. J. M Boumans and J. J. A. M. Vrakking, The widths and shapes of about 350 prominent lines of 65 elements emitted by an ICP, Spectrochim. Acta Part B 41 (1986) 1235-1275.

27. L. M. Faires, B. A. Palmer and J. W. Brault, Line widths and line shape analysis in the ICP by high resolution Fourier transform spectrometry, Spectrochim. Acta Part B 40 (1985) 135-143.

28. J. W. Olesik, Investigating the fate of individual sample droplets in ICPs, Appl. Spectrosc. 51 (1997) 158A-175A.

29. V.F. Taylor, R.E. March, H.P. Longerich, C.J. Stadey, A mass spectrometric study of glucose, sucrose, and fructose using an inductively coupled plasma and electrospray ionization, Int. J. Mass Spectrom. 243 (2005) 71-84.

30. H. C. Beijerinck, R. J. F. van Gerwen, E. R. T. Kerstel, J. F. M. Martens, E. J. W. Van Vliembergen, M. R. Th. Smits and G. H Kaashoek, Campargue-type supersonic beam sources: absolute intensities, skimmer transmission and scaling laws for mono-atomic gases He, Ne and Ar, Chem. Phys. 96 (1985) 153-173.

31. D. J. Douglas, J. B. French, Gas dynamics of the inductively coupled plasma mass spectrometry interface, J. Anal. Atom. Spectrom. 3 (1988) 743-747.

32. R. L. Spencer, J. Krogel, J. Palmer, A. Payne, A. Sampson and C. N. Woods, Modeling the gas flow upstream and in the sampling nozzle of the inductively coupled plasma mass spectrometer via the direct simulation Monte Carlo algorithm, Spectrochim. Acta Part B 2009 in press.

33. M. W. Schmidt, K. K. Baldridge, J. A. Boatz, S. T. Elbert, M. S. Gordon, J. H. Jensen, S. Koseki, N. Matsunaga, K. A. Nguyen, S. Su, T. L. Windus, M. Dupuis, J. A. Montgomery,

Jr., General atomic and molecular electronic structure system, J. Comp. Chem. 14 (1993) 1347-1363; M.S. Gordon, M.W. Schmidt, "Advances in Electronic Structure Theory: GAMESS a Decade Later", Theory and Applications of Computational Chemistry, Ch.. 41, C. E. Dykstra, G. Frenking, K.S. Kim, G.E. Scuseria, Eds., Elsevier, 2005.

34. NIST Chemistry Webbook, Vibrational and/or electronic energy levels. http://webbook.nist.gov

35. J. Liu, B. Uselman, B. Van Devener, S. L. Anderson, Vibrational mode effects as a probe of inter-channel coupling in the reactions of formaldehyde cation with ammonia and water, J. Phys. Chem. A 108 (2004) 9945-9956.

36. P. Blowers, R. I. Masel, Calculated vibrational spectra for CH_nOH_m species, J. Phys. Chem A 104 (2000) 34-44.

37. S. M. McIntyre, Ph.D. dissertation, Iowa State University, 2010.

38. H. Niu and R. S. Houk, Langmuir probe measurements of the ion extraction process in ICP-MS. I. Spatially resolved measurements of electron density and electron temperature, Spectrochim. Acta Part B 49 (1994) 1283-1303.

39. T. N. Olney, W. Chen and D. J. Douglas, Gas dynamics of the ICP-MS interface: impact pressure probe measurements of gas flow profiles, J. Anal. At. Spectrom. 14 (1999) 9-17.

Tables

Table 1. Experimental conditions

Resolution	Medium (m/Δm ≈ 4000), except where otherwise stated
Nebulizer	Elemental Scientific Inc. PFA 100 µL/min
	or 20 µL/min as needed
Spray Chamber	Teflon Scott type double pass
Cones	Nickel sampler (1.0 mm hole diam.)
	and skimmer ("H" geometry, 0.8 mm diam.)
	Sampler skimmer spacing 9.2 mm
Power	1200 W
Gas flow rates (L/min):	
Outer gas	15
Auxiliary gas	1.0
Aerosol gas	1.0 to 1.1
	Optimized daily to maximize M^+ signal
Solutions	Standards in 1% nitric acid. Other solutions used as indicated.
Torch	Fassel type, 20 mm OD
	Shielded with shield grounded
Sampling	12 mm downstream from load coil
Position	On center

Table 2. Calculated properties of N_2H^+ by ZAPT2 and CCSD(T) theory.

	ZAPT2	CCSD(T)
Dissociation Energy (eV) to $N_2^+ + H$	6.891	7.449
Vibrational Frequencies (cm^{-1})	731.87	732.58
	731.87	732.58
	2151.1	2283.9
	3418.2	3434.9
Rotational Constant (cm^{-1})	1.536	1.557

Table 3. Calculated properties of HCO^+, COH^+, and CO^+.

ZAPT2

	HCO^+	COH^+	CO^+
Dissociation Energy to CO^+ (eV)	6.929	2.03	
Vibrational	859.76	321.80	2115.1
Frequencies (cm^{-1})	859.76	321.80	
	2150.4	1761.9	
	3251.4	3349.4	
Rotational Constant (cm^{-1})	1.536	1.487	1.960

CCSD(T)

	HCO^+	COH^+	CO^+
Dissociation Energy to CO^+ (eV)	6.925	1.75	
Vibrational	861.84	149.43	2203.1
Frequencies (cm^{-1})	861.84	149.43	
	2212.3	1942.6	
	3327.1	3482.8	
Rotational Constant (cm^{-1})	1.487	1.487	1.939

Table 4. T_{gas} results for HCO^+ COH^+ CO^+ system, 1% aqueous HNO_3 + 10% IPA.

Reaction	Comp. Method	T_{gas} (K)
$HCO^+ \rightleftharpoons CO^+ + H$	ZAPT2	4710
$HCO^+ \rightleftharpoons CO^+ + H$	CCSD(T)	4710
$HCO^+ \rightleftharpoons COH^+ \rightleftharpoons CO^+ + H$	ZAPT2	4710
	CCSD(T)	4710
$COH^+ \rightleftharpoons CO^+ + H$	ZAPT2	1590
$COH^+ \rightleftharpoons CO^+ + H$	CCSD(T)	1510

Table 5. Calculated properties of $HCOH^+$ and H_2CO^+ .

ZAPT2		$HCOH^+$	H_2CO^+
Dissociation Energy to HCO^+ (eV)	0.845		0.13
Vibrational		971.65	856.28
Frequencies (cm^{-1})		1001.5	1114.1
		1248.9	1321.9
		1727.8	1633.3
		3122.0	2898.2
		3497.4	3045.6
Rotational Constant x (cm^{-1})	13.74		8.861
Rotational Constant y (cm^{-1})	1.271		1.348
Rotational Constant z (cm^{-1})	1.167		1.174

CCSD(T)		H_2CO^+	$HCOH^+$
Dissociation Energy to HCO^+ (eV)		1.378	0.23
Vibrational		855.58	969.57
Frequencies (cm^{-1})		1071.0	1000.8
		1272.6	1254.5
		1663.2	1691.7
		2811.4	3076.9
		2920.5	3515.4
Rotational Constant x (cm^{-1})		8.917	13.68
Rotational Constant y (cm^{-1})		1.327	1.264
Rotational Constant z (cm^{-1})		1.160	1.160

Table 6. Measured T_{gas} values for $HCOH^+$ H_2CO^+ HCO^+ system, 1% HNO_3 + 10% IPA

Reaction	Comp. Method	T_{gas} (K)
$HCOH^+ \rightleftharpoons HCO^+ + H$	ZAPT2	1500
$H_2CO^+ \rightleftharpoons HCO^+ + H$	CCSD(T)	2180
$HCOH^+ \rightleftharpoons HCO^+ + H$ $HCO^+ \rightleftharpoons COH^+$	ZAPT2	1500
$HCOH^+ \rightleftharpoons HCO^+ + H$ $HCOH^+ \rightleftharpoons H_2CO^+$ $HCO^+ \rightleftharpoons COH^+$	ZAPT2	1540
$HCOH^+ \rightleftharpoons HCO^+ + H$ $HCOH^+ \rightleftharpoons H_2CO^+$	ZAPT2	1540
$H_2CO^+ \rightleftharpoons HCO^+ + H$ $H_2CO^+ \rightleftharpoons HCOH^+$ $HCO^+ \rightleftharpoons COH^+$	CCSD(T)	2280
$H_2CO^+ \rightleftharpoons HCO^+ + H$ $H_2CO^+ \rightleftharpoons HCOH^+$	CCSD(T)	2280

Table 6 continued

Reaction	Comp. Method	T_{gas} (K)
$H_2CO^+ \rightleftharpoons HCO^+ + H$	CCSD(T)	2180
$HCO^+ \rightleftharpoons COH^+$		

Table 7. Calculated properties of H_2COH^+ by ZAPT2 and CCSD(T) methods

	ZAPT2	CCSD(T)
Dissociation Energy (eV)	5.341 (to $HCOH^+$)	5.17 (to H_2CO^+)
Vibrational frequencies (cm^{-1})	1054.3	1038.3
	1123.8	1121.0
	1266.3	1246.8
	1396.3	1400.4
	1510.3	1488.7
	1688.9	1663.2
	3150.5	3109.5
	3301.4	3255.5
	3610.0	3620.4
Rotational Constant x (cm^{-1})	6.658	6.637
Rotational Constant y (cm^{-1})	1.153	1.146
Rotational Constant z (cm^{-1})	0.9869	0.9800

Figures

Captions

Figure 1: Medium resolution spectrum of CO^+ (left or low mass peak) and N_2^+ (right or high mass peak) from 1% nitric acid.

Figure 2: Medium resolution spectrum of HCO^+ (left or low mass peak) and N_2H^+ (right or high mass peak) from 1% nitric acid.

Figure 1

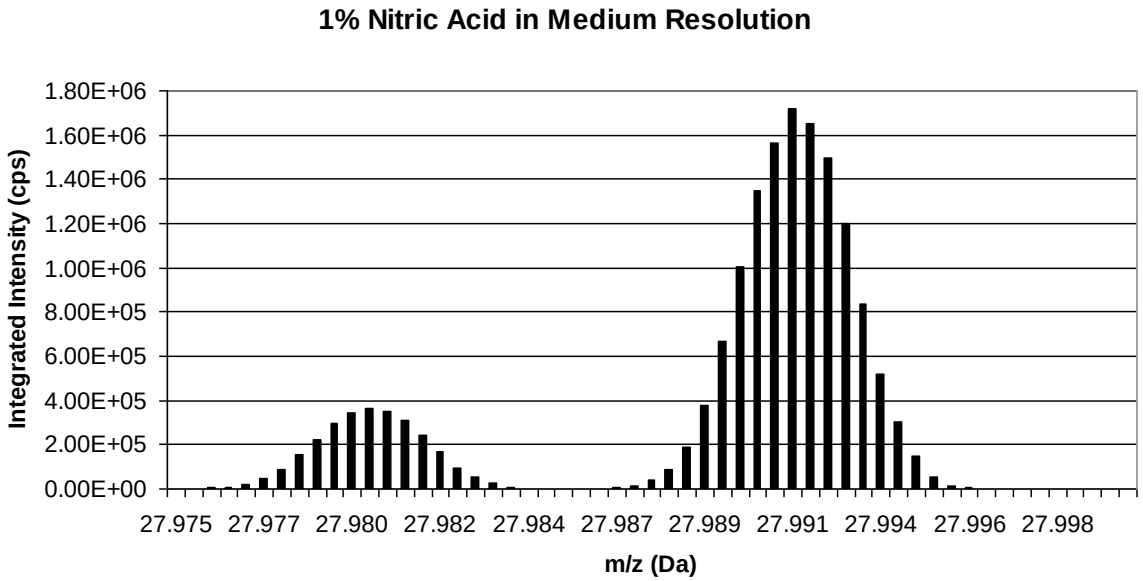

Figure 1: Medium resolution spectrum of CO^+ (left or low mass peak) and N_2^+ (right or high mass peak) from 1% nitric acid.

Figure 2

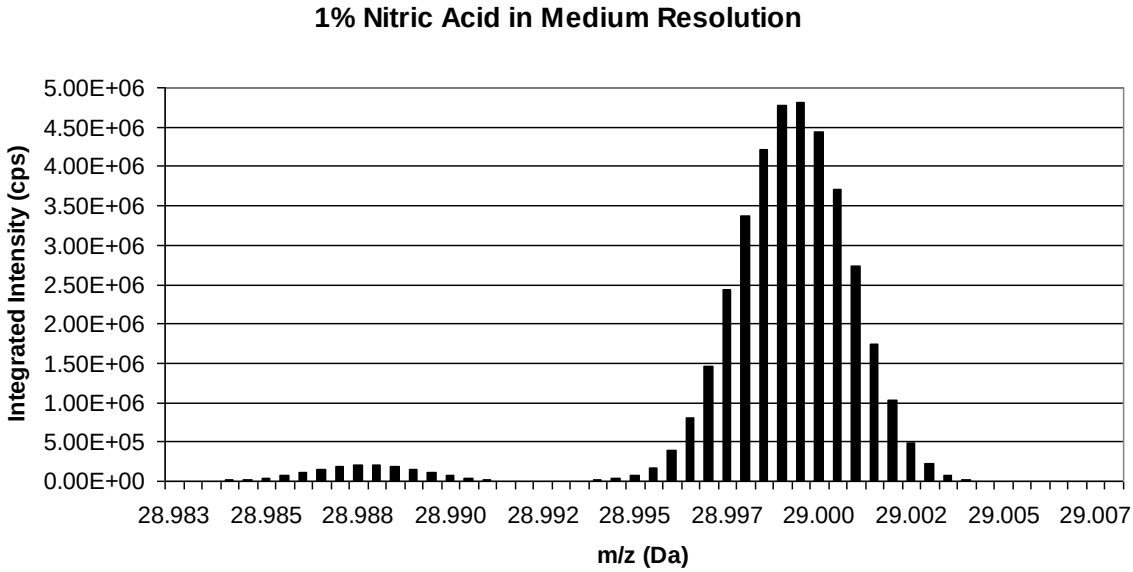

Figure 2: Medium resolution spectrum of HCO^+ (left or low mass peak) and N_2H^+ (right or high mass peak) from 1% nitric acid.

Appendix B.

Reduction of Matrix Effects in Inductively Coupled Plasma Mass Spectrometry by Flow Injection with an Unshielded Torch

Cory T. Gross, Sally M. McIntyre and R.S. Houk

Ames Laboratory U. S. Department of Energy

Department of Chemistry

Iowa State University, Ames, Iowa 50011 USA

A paper published in Analytical Chemistry, 2009, 81, 4898-4905.

Abstract

Solution samples with matrix concentrations above ~0.1% generally present difficulties for analysis by inductively coupled plasma mass spectrometry (ICP-MS) due to cone clogging and matrix effects. Flow injection (FI) is coupled to ICP-MS to reduce deposition from samples such as 1% sodium salts (as NaCl) and seawater (~3% dissolved salts). Surprisingly, matrix effects are also less severe during flow injection, at least for some matrix elements on the particular instrument used. Sodium chloride at 1% Na and undiluted seawater cause only 2 to 29 % losses of signal for typical analyte elements. A heavy matrix element (Bi) at 0.1% also induces only ~14% loss of analyte signal. However, barium causes a much worse matrix effect, i. e., ~90% signal loss at 5000 ppm Na. Also, matrix effects during FI are much more severe when a grounded metal shield is inserted between the load coil and torch, which is the most common mode of operation for the particular ICP-MS device used.

Introduction

ICP-MS is a sensitive and accurate means to determine the trace element content of solutions. Unfortunately, the analyte signal depends not only on analyte concentration but also on the concentration and identity of matrix elements. Many previous studies show that matrix elements usually suppress analyte sensitivity.[1-10] Such signal losses are usually blamed mainly on space charge effects as the ions leave the skimmer.[1,11-13.] However, signal enhancements caused by matrix elements are occasionally seen.[14] Solid materials from the

sample matrix also coat onto the sampler and/or skimmer cone, which is one cause of signal drift.

Internal standardization is commonly used to correct for these problems. In general, the quality of the internal standardization correction is best if the extent of change of analyte signal with matrix concentration is less severe. Since the magnitude of the matrix effect varies with the atomic weight of the analyte ion,[4,15] several different internal standard elements that span the m/z range are usually added to correct for matrix effects in multielement analysis.

For these reasons, the total solute content of the sample is usually restricted to no more than 0.1% in ICP-MS. Chemical separations for matrix removal and/or analyte preconcentration are one option for analyzing samples with higher matrix levels.[16-21] Analyzing the sample directly is preferable because it is simpler, faster and better suited to the determination of more elements. Alternative procedures that attenuate matrix effects and cone clogging could allow more routine measurements at lower dilution factors, which would have various scientific benefits.

Introduction of only a discrete plug of sample solution by FI attenuates cone clogging.[22,23] Indeed, the matrix effect experiments in the first ICP-MS paper required FI because the pinhole sampler (60 μm diam.) clogged easily.[24] Memory effects are also reduced by FI, and sample rinse-out times are shortened. Field et al.[25] have recently demonstrated the use of a new, commercial FI system with a magnetic sector instrument for fast analysis of seawater, a difficult matrix. They dilute the sample tenfold to attenuate matrix effects and salt deposition on the cones; addition of glucose also helps reduce deposition. The sector instrument still provides sufficient sensitivity for the intended application, the quantification of

diagnostic elements to trace exhaust of ballast by ocean-going ships. The present work describes recent experiments that indicate that the matrix effect can also be attenuated by FI, at least for one type of instrument and certain sample matrices.

Experimental Section

ICP-MS Instrumentation. These experiments were performed on a quadrupole ICP-MS (HP 4500, now Agilent, Santa Clara, CA). The operating parameters (Table 1) were selected in the following fashion. First, lens voltages, power, sample gas flow rate, sampling position, and other parameters were selected to maximize signal for $^{7}Li^{+}$, $^{89}Y^{+}$ and $^{205}Tl^{+}$. The sample gas flow rate was then adjusted slightly to give tolerable levels of CeO^{+} (~2%) and Ce^{2+} (~1%, relative to Ce^{+}) from clean, multielement standards. Under these conditions, this instrument typically gives about the same count rates for $^{89}Y^{+}$ and $^{205}Tl^{+}$ from the 10 ppb tuning solution. Sensitivity for Ce^{+} is often about 50% higher than that for Y^{+} and Tl^{+}, for reasons that are unclear. The optimum lens voltages found in this fashion were almost the same from day to day throughout the course of these experiments and were typical of those that provide maximum signal for other users of this type of instrument.

The standard, reversed load coil[26] supplied with the instrument was used. The torch was not shielded (i.e., the shield was not present) in all except the last result reported below.

FI and Sample Introduction. The Babington nebulizer originally supplied with the instrument was replaced with a microconcentric nebulizer (PFA-100, Elemental Scientific Inc., Omaha, NE, nominal uptake rate ~ 100 μL/min). The glass spray chamber was the standard double pass type,[27] internal volume ~ 70 mL, cooled to 2°C.

FI was performed with an autosampler equipped with a programmable sample valve and loops (Model FAST SC-2, Elemental Scientific Inc., Omaha, NE).[25] This device featured an onboard vacuum pump to fill the 100 μL sample loop. Small segments of the loop were then injected for 1, 5 or 10 seconds via a computer controlled injection valve. Thus, the volumes injected were 1.7, 8.3 or 17 μL; these volumes are smaller than those common with this FI system. The sample plug emerging from the loop is unsegmented and is driven by the carrier (1% aqueous HNO_3) behind it. To minimize dispersion, the loop and valve were mounted as close to the nebulizer as possible; the dead volume in the liquid between loop and nebulizer was only ~20 μL.

Sample Preparation and Standard Solutions. One set of samples was prepared by dissolving weighed amounts of solid NaCl (certified A.C.S. grade, Fisher Scientific, Fair Lawn, NJ) into a multielement standard solution (Spex Certiprep, Metuchen NJ) containing 10 ppb of various analytes, including Li, Sc, Y, Ce, and Tl. These elements were chosen to span most of the elemental mass range. Final matrix concentrations were 1000, 2000, 5000, and 10,000 ppm Na.

The second group of solutions was prepared using a coastal seawater reference material (CASS-1, ~3.2% total salts, acidified to pH 1.6 with nitric acid by the supplier, Marine Analytical Chemistry Standards Program, Division of Chemistry, National Research Council of Canada (NRCC), Ottawa, ON, Canada). The expected concentrations of the major cations were approximately 10,000 ppm Na, 1000 ppm Mg, 500 ppm Ca and 340 ppm K.[28] This sample was diluted to varying degrees: 10x, 5x, or 2x. One portion of seawater was left undiluted. Each of these solutions were also spiked with 10 ppb of the same multielement standard described in the previous paragraph. The seawater sample was spiked to minimize

possible contributions from polyatomic ions in subsequent measurements of matrix effects. Again, signals from the seawater samples were compared to those from the 10 ppb clean multielement standard. These seawater samples all contained 1% aqueous HNO_3.

The Ba matrix samples were prepared by dissolving weighed amounts of solid $BaCl_2$ (certified A.C.S grade, Fisher Scientific, Fair Lawn, NJ) into the same multielement standard described in the NaCl preparation. Final Ba matrix concentrations were 1000 ppm, 5000 ppm, and 10,000 ppm. Bismuth matrix samples were prepared using a 1000 ppm Bi elemental standard solution (PlasmaChem, Bradley Beach, NJ). The 1000 ppm Bi and a 500 ppm dilution were spiked with 5 ppb of Li, Sc, Y, Ce, and Tl.

Matrix blanks containing only NaCl, $BaCl_2$, or the Bi matrix were also prepared and analyzed; none of these matrix blanks contained appreciable analyte compared to the 10 ppb spikes. The unspiked seawater sample was analyzed and found to contain negligible amounts of the analyte elements except Li, which is typically present at ~0.15 ppm in seawater.[29] Thus, the effect of dilution factor on Li sensitivity was not measured in seawater.

All dilutions were performed with distilled deionized water (18 MΩ, Nanopure-II, Barnstead Co., Newton, MA). All solutions were acidified to 1% HNO_3 (A.C.S. reagent grade plus, Fisher, Fair Lawn, NJ).

Data Acquisition. Samples were loaded into the sample rack of the autosampler, which was programmed to fill the sample loop and open the injection valve for the appropriate length of time. When the sample was not being injected a 100 μl/min carrier flow of 1% HNO_3 was continuously nebulized to keep solvent load on the nebulizer and plasma constant.

Data were collected during each injection for the five analyte elements (Li, Sc, Y, Ce, and Tl at m/z = 7, 45, 89, 140, and 205 respectively) and presented in time resolved mode.

The integration period for each m/z value was 10 ms, which was fast enough to cover the FI peak for the shortest (1 s) injections tested. After the injection of a sample the sample probe was double rinsed in 1% HNO_3, and the process was repeated. The matrix effect is measured by comparing the steady state signal for each element with matrix present to that from clean standard solutions. Peak areas were used for the 1 s injections because the signals did not reach the steady state level. Similar experiments were done while measuring only one analyte element at a time to verify that the number of elements measured did not affect the matrix interference results.

Results and Discussion

Matrix Effects from NaCl. For reference, results obtained during continuous sample introduction are shown first (Figure 1a), using Tl as the analyte element. Here the FI system was removed and the sample was aspirated by natural uptake at ~ 100 µl/min, the same flow rate used subsequently. Signal is observed between ~35 and 60 s after the sample is changed. The solutions were analyzed in order of increasing matrix concentration; the cones were not cleaned between measurements. At 2000 ppm Na, Tl^+ signal is suppressed by ~32%. At 10,000 ppm Na, the suppression is worse, and either cone clogging or poor nebulizer performance causes the signal to fall soon after injection. Signals from other, lighter elements are suppressed even more extensively (Table 2).

The general magnitude of signal losses due to the NaCl matrices for continuous injection (Figure 1a and Table 2) are more or less the norm in ICP-MS. The extent of the signal suppression is a bit less dependent on the atomic weight of the analyte than that seen by many workers.[4,15]

Analogous results from FI experiments are described next (Figure 1b). The sample gets to the nebulizer and plasma faster in FI mode because of the shorter connecting tubing from the valve to the nebulizer. For the 1 s injections (Figure 1b), Na at 5000 ppm causes only ~ 15% loss of Tl^+ signal. Similar suppression curves were obtained for 1000 and 2000 ppm Na; the data are not plotted for clarity. The 10,000 ppm Na solution suppresses Tl^+ signal more extensively, but still only by ~ 30%.

Injections for 5 and 10 s (Figures 2a and 2b) are long enough for the Tl^+ signal to reach the steady state briefly. The suppressions observed for a given matrix concentration at these longer injections are similar to each other. The rinse-in profiles (i.e., the curve between the initial signal rise and the plateau or steady-state) for these longer injections are almost the same as for continuous nebulization and are characteristic of the time required to replace the blank droplets in the spray chamber with those from the newly-injected sample.[27,31]

In some cases the actual signal levels for a given element differ among the various plots, here and below. These experiments were done over a period of several months to verify their reproducibility. Factors like detector gain, cone condition, and small variations in selection of operating conditions affect the signal seen on a given day. Figures 1b and 2 were obtained in the same experiment, so their signals can be compared. The maximum count rates for the clean Tl^+ standard for the 1 s injection (Figure 1b) are about half of those for the 5 or 10 s injections (Figure 2). Thus, the dispersion coefficient[30] for the 1 s injections is ~0.5.

Note also that analyte signals from the matrix blanks are negligible in Figures 1 and 2, so the apparent tolerance to matrix effects is not merely caused by impurities in the matrix compounds.

Matrix effects from NaCl for continuous introduction and FI (5 s injections) are summarized for the five analyte elements in Table 2. Here signal recovery is expressed as the following ratio: (analyte signal from matrix solution/analyte signal from clean solution) x 100%. In Table 2, the general magnitude of the matrix effect is about as expected for the control experiments done with continuous flow; the variation of matrix effect with analyte atomic weight will be discussed separately below. When the sample is introduced by FI, the matrix effects for each analyte are still present, but they are much less pronounced.

If the matrix effect is less extensive, perhaps the quality of corrections derived from internal standardization is also improved. Table 3 illustrates this to be the case; a single internal standard element (Y^+) does a much better job of correction for the FI results, especially at higher Na concentrations. In some cases, the quality of the internal standard corrections approaches the inherent limit of the measurement precision, typically no better than ~ 2%. Thus, there is less need for multiple internal standard elements with FI.

Matrix Effects in Seawater Samples. Seawater is generally diluted extensively before analysis by ICP-MS; some analyte elements then require chemical matrix removal and/or preconcentration. Compared to the results presented above for a synthetic NaCl matrix (Figures 1 and 2; Tables 2 and 3), similar improvements in signal recovery are seen with seawater samples during FI. Representative results are shown for Tl^+ and Sc^+ in Figure 3. Even for undiluted seawater (~3% total solutes), the Ce^+ signal is suppressed by only ~26%. The signal recoveries for all analyte elements in seawater are summarized in Table 4.

Results for Li in seawater are not shown because the sample had substantial Li originally. Also, the nebulizer performed poorly if straight seawater was nebulized continuously, so matrix effects during continuous nebulization were not evaluated for seawater. Undiluted

seawater could be injected repeatedly by FI for 10 s intervals without appreciable signal loss due to cone clogging (data not shown), in general agreement with other observations that FI greatly reduces deposition on the cones.[22-24]

Variation of Matrix Effects with Atomic Weight of Analyte. For a given matrix, many workers find that recoveries for heavier analyte elements (e.g., Tl^+) are closer to unity than recoveries for lighter analytes (e.g., Li^+).[4,15] This is why the analyte elements were chosen to span most of the m/z range. However, this common trend is not prominent in Tables 2 and 4. For example, consider the continuous flow results in Table 2. Only at the highest matrix concentrations is the Li recovery greatly lower than that for Sc, Y and Ce. All the analyte elements, including Li, have recoveries of 60 to 70% at 1000 ppm Na; Li and Tl are suppressed about the same, and more than the other analytes, at 10,000 ppm Na. The recoveries for Sc are consistently as good as, or even better than, those for Tl, for either NaCl (Table 2) or seawater matrices (Table 4). The expectation is that recovery for Sc would be lower than that for Tl.[4,15]

Effects of Other Matrix Elements. The matrix effect is usually more extensive the greater the atomic weight of the matrix element.[4,15] Traditionally, this variation is considered to be an attribute of space charge effects.[12,13,15] Scandium signals from Bi solutions up to 1000 ppm are shown in Figure 4a. The Sc^+ signal recovery in 1000 ppm Bi is ~80%, worse than with the Na matrix, but still reasonable.

A similar experiment with Ba matrix (Figure 4b) shows quite a different result. Originally, we thought Ba would simply act as a matrix element with an intermediate atomic weight between that of Na and Bi. Thus, only small matrix effects were expected during FI. However, Figure 4b shows that the matrix effect from Ba is substantial, more like those nor-

mally observed. Barium caused similar large matrix effects on the other analyte elements (data not shown).

Why should Ba be different from the other matrix elements studied? It forms substantial numbers of doubly charged ions, and the main ionization form (Ba^+) has accessible electronic states with excitation energies in the visible. The most abundant matrix element (i.e., the Na in NaCl or seawater) in the other samples studied lacks these characteristics. For that matter, matrix effects in ICP emission spectrometry caused by alkali metal matrices (e.g., Na and K) differ from those induced by alkaline earth matrices (e.g., Ca).[32]

Matrix Effects with a Shielded Torch. Modern versions of this particular ICP-MS instrument usually use a grounded metal shield inserted between the load coil and torch. This shield reduces capacitive coupling between the load coil and plasma, thus the plasma potential is lower with the shield.[1,26,33] A lower plasma potential yields ions with a narrower spread of kinetic energy, which can improve sensitivity and is particularly valuable when a collision cell is used to reduce polyatomic ion interferences by kinetic energy discrimination.[34]

To look for possible reasons for the low matrix effects reported above, a few experiments were done with a shielded torch. The effect of NaCl matrix on Sc^+ signal with a grounded shield present during FI is shown in Figure 5. Here the same forward power and sampling position are used as in the previous results, but the sample gas flow rate is reduced by ~ 0.15 L/min to re-maximize Ce^+, and keep the CeO^+/Ce^+ and Ce^{2+}/Ce^+ signal ratios about the same as before, ~2% and ~1%, respectively. The need for lower sample gas flow is consistent with the expectation that the actual power reaching the plasma is slightly lower with the shield, as the power that gets to the plasma by capacitive coupling is now dissipated into

the shield. In our experience, this method of adjusting ICP operating parameters to yield certain values of MO^+/M^+ and M^{2+}/M^+ is an effective way to sample a comparable region of the plasma when some external parameter is altered. Using this optimization criterion, the tip of the sampler cone is typically just 1 or 2 mm downstream from the end of the initial radiation zone seen when a high concentration of an oxide-forming element like yttrium is introduced, even when large changes to the plasma are made, such as use of the shield.

First, comparison of Figures 4b and 5 shows that the shield improves the Sc^+ signal for the clean standard by ~ 3X, in agreement with other observations with this make of instrument.[33] Note also that the matrix effect in Figure 5 is more like that seen in conventional ICP-MS experiments, i.e., 40% signal loss at 1000 ppm Na, 90% signal loss at 10,000 ppm Na. Thus, whether the torch is shielded plays a key role in the extent of matrix interferences, which is not expected. One report by Appelblad et al.[35] does indicate an analogous result concerning the effect of a torch shield on matrix effects with a magnetic sector instrument; in Appelblad's work, the M^+ sensitivity is much higher with the shield present.

Conclusion

These observations indicate that some samples can be analyzed with less extensive dilution, fewer internal standard elements, and/or better internal standard corrections using FI, at least on one particular instrument. The compromise is a three fold loss of sensitivity with an unshielded torch.

These experiments also raise questions about the basic mechanism(s) responsible for matrix effects. Indeed, it is hard to see why the duration of the sample injection pulse should

have any influence on the matrix effect if the latter occurs mainly by space charge effects inside the vacuum system. The ions pass through the sampler, skimmer and ion lens in only a few μs,[1,36,37] much faster than even the shortest FI injections (~4 s).

The observations that a) the matrix effect from Ba is much worse than that from the other elements tested in FI mode, and b) the shield makes matrix effects worse, argue that matrix effects in ICP-MS can be more significant outside the sampler, in the ICP itself, than usually thought, at least on some instruments. Some indications along these lines have surfaced occasionally over the years.[35,38,39] Most previous studies of matrix effects were done with continuous sample introduction and steady-state signals. Perhaps a) conditions in the ICP take a certain time to reach steady state after the matrix element is first added, and b) properties of the matrix element other than ionization efficiency and atomic weight matter more than previously thought. Conditions in the axial channel upstream inside the load coil could be influenced by the nature and concentration of the matrix and the presence or absence of the shield. This region of the ICP has not been studied extensively; indeed, it is hard to observe it optically due to the bright emission from the surrounding induction region. For example, Blades and Hieftje[40] propose that radiative processes transfer energy from the induction region into the upstream reaches of the axial channel, and such processes are known to be influenced by matrix elements in some DC plasmas.[41] Other effects of the matrix like a) spatial changes in the positions of atomization and ionization,[42] and b) deposition and conditioning of the cones due to deposited material, could also play a role. The general subject of the basic reason(s) for the moderate matrix effects reported in this paper merits further study.

Acknowledgements

The authors thank Agilent for donating the ICP-MS instrument as well as ESI for donating the autosampling unit used in this research. Funding was provided by the Chemical and Biological Sciences Program, Office of Basic Energy Sciences, Ames Laboratory U. S. Department of Energy under Contract No. DE-AC02-07CH11358.

References

1. Niu; H.; Houk, R.S. *Spectrochim. Acta, Part B,* **1996**, *51*, 779- 815.
2. Olivares, J.A.; Houk, R.S. *Anal. Chem.*, **1988**, *58*, 20-25
3. Crain, J.S.; Houk, R.S.; Smith, F.G. *Spectrochim. Acta, Part B*, **1989**, *44*, 1355-1364.
4. Tan, S.; Horlick, G. *J. Anal. Atomic Spectrom.*, **1987**, *2*, 745-763.
5. Evans, E.H.; Giglio, J.J. *J. Anal. Atomic Spectrom.*, **1993**, *8*, 1-18.
6. Gregoire, D.C. *Spectrochim. Acta Part B* **1987**, *42B*, 895-907.
7. Vanhoe, H.; Dams, R.; Vandecasteele, C.; Versieck, J. *Anal. Chim. Acta*, **1993**, *281*, 401-411.
8. Kawaguchi, H.; Tanaka, T.; Nakamura, T.; Morishita, M.; Mizuike, A. *Anal. Sci.*, **1987**, *3*, 305-308.
9. Hobbs, S.E.; Olesik, J. *Appl. Spectrosc.*, **1991**, *45*, 1395-1407.
10. Lazar, A.C.; Farnsworth, P.B. *Appl. Spectrosc.*, **1999**, *53*, 465-470
11. Gillson, G.R.; Douglas, D.J.; Fulford, J.E.; Halligan, K.W.; Tanner, S.D. *Anal. Chem.*, **1988**, *60*, 1472-1474.
12. Tanner, S.D. *Spectrochim. Acta, Part B*, **1992**, *47*, 809-823.

13. Praphairaksit, N; Houk, R. S. *Anal. Chem*. **2000**, *72*, 2351-2356; 2356-2361; 435-4440.

14. Liu, S.; Beauchemin, D. *Spectrochim. Acta, Part B*, **2006**, *61*, 319-325.

15. Montaser, A., Inductively Coupled Plasma Mass Spectrometry, Wiley-VCH, NY, **1998,** Chap. 7.

16. Keil, O.; Dahmen, J.; Volmer, D. *Fresenius J. Anal. Chem.*, **1999**, *364*, 694-699.

17. Alves, L.C.; Allen, L.A.; Houk, R.S. *Anal. Chem.*, **1993**, *65*, 2468-2471.

18. Plantz, M.R.; Fritz, J.S.; Smith, F.G.; Houk, R.S. *Anal. Chem.*, **1989**, *61*, 149-153.

19. Beauchemin, D.; McLaren, J.W.; Mykytiuk, A.P.; Berman S.S. *J. Anal. Atomic Spectrom.*, **1988**, *3*, 305-308.

20. Beauchemin, D.; Berman, S.S *Anal. Chem.*, **1989**, *61*, 1857-1862.

21. Huang, Z.Y.; Chen, F.R.; Zhuang, X.R.; Lee, F.S.C. *Anal. Chim. Acta.*, **2004**, *508*, 239-245.

22. Thompson, J.J.; Houk, R.S. *American Mineralogist*, **1982**, *67*, 238-243.

23. McClenathan, D.M.; Ray, S.J.; Hieftje, G.M. *J. Anal. Aomic. Spectrom.*, **2001**, *16*, 987-990.

24. Houk, R. S., Fassel, V. A.; Flesch, G. D.; Svec, H. J.; Gray, A. L.; Taylor, C. E. *Anal. Chem.* **1980**, *52*, 2283-2289.

25. Field, M. P.; La Vigne, M.; Murphy, K. R.; Ruiz, G. M.; Sherrell, R. M. *J. Anal Atomic Spectrom.*, **2007**, *22*, 1145-1151.

26. Gray, A. L. *J. Anal. Atomic Spectrom.*, **1986**, *1*, 247-249.

27. Scott, R. H.; Fassel, V. A.; Kniseley, R. N.; Nixon, D. E. *Anal. Chem.* **1974**, *46*, 75-80.

28. Willie, S. N. The Preparation of National Research Council Certified Reference Materials, in Reference Materials for Environmental Analysis, Clement, R. E.; Keith, L. E.; Siu, K. W. M.; Eds.; CRC, Boca Raton FL, 1996.

29. Okamoto, H.; Okamoto, Y.; Hirokawa, T.; Timerbaev, A. R. *Analyst* **2003**, *128*, 1439-1442.

30. Skoog, D. A.; Holler, F. J.; Nieman, T. A. Principles of Instrumental Analysis, 5th ed., Brooks/Cole/Thomson Learning, p. 836.

31. Sharp, B. L. *J. Anal. Atomic Spectrom.* **1988**, *3*, 939-963.

32. Chan, G. C.-Y.; Hieftje, G. M. *Spectrochim. Acta Part B* **2008**, *63B*, 355-366.

33. Sakata, K.; Kawabata, K. *Spectrochim. Acta Part B* **1994**, *49*, 1027-1038; Sakata, K. personal communication, 1994.

34. Yamada, N.; Takahashi, J.; Sakata, K. *J. Anal. Atomic Spectrom.*, **2002**, *17*, 1213-1222.

35. Appelblad, P.K.; Rodushkin, I.; Baxter, D.C. *J. Anal. Atomic Spectrom.*, **2000**, *15*, 359-364.

36. Douglas, D.; French, J. B. *J. Anal. Atomic Spectrom.*, **1988**, *3*, 743-747.

37. Spencer, R. L.; Krogel, J.; Palmer, J.; Payne, A.; Sampson, A.; Woods, C. N. *Spectrochim. Acta Part B* **2009**, submitted.

38. Olesik, J.; Thaxton, K.; Olesik, S. *J. Anal. Atomic Spectrom.*, **1997**, *12*, 507-515.

39. Duersch, B. S.; Farnsworth, P. B. *Spectrochim. Acta Part B* **1999**, *54*, 545-555, esp. Fig. 9.

40. Blades, M. W.; Hieftje, G. M. *Spectrochim. Acta Part B* **1982**, *37B*, 191-197.

41. Miller, M. H.; Eastwood, D.; Hendrick, M. S. *Spectrochim. Acta Part B* **1984**, *39B*, 13-56.

42. Fraser, M. M.; Beauchemin, D. *Spectrochim. Acta Part B* **2000**, *55B*, 1705-1731.

Tables

Table 1. ICP-MS Operating Conditions

Forward power	1200 W
Argon gas flow rates (L/min):	
Outer	14
Auxiliary	1.5
Sample	0.95
Sampling position	8 mm from load coil
	On center
Sampler cone	Nickel, 1.1 mm diam.
Skimmer cone	Nickel, 0.4 mm diam.
Ion lens voltages	
Extract 1	-227 V
Extract 2	-65 V
Einzel 1, 3	-123 V
Einzel 2	14.5 V

Table 2. Signal Recoveries (%) for 10 ppb Analyte Solutions with NaCl Matrix.

		RECOVERIES (%) AT INDICATED Na CONCENTRATIONS (ppm)						Count Rates (c/s)*
		Continuous Flow			FI, 5 s Injections			for FI, 5 s,
	m/z	1000	5000	10,000 ppm	1000	5000	10,000 ppm	10 ppb Std.,No Matrix
Li	7	63	55	36	97	80	71	5,000
Sc	45	67	61	45	94	89	82	10,000
Y	89	69	65	57	97	91	84	8,000
Ce	140	60	50	45	87	85	80	15,000
Tl	205	68	56	38	96	91	81	8,500

*Original count rates for matrix-free analyte solution are given here.

Table 3. Signal Recovery Ratios (%) Using Y^+ as Internal Standard for NaCl Matrix at Indicated Na Concentrations (ppm)

		RECOVERY RATIOS (M^+/Y^+) (%) AT INDICATED Na CONCENTRATIONS (ppm)					
		Continuous Flow			FI, 5 s Injections		
Analyte	m/z	1000	5000	10,000 ppm	1000	5000	10,000 ppm Na
Li	7	91	85	63	100	88	84
Sc	45	97	94	79	97	98	98
Ce	140	87	77	79	90	93	95
Tl	205	98	86	67	99	100	96

Table 4. Signal Recoveries (%) for Analyte Elements Spiked at 10 ppb into CASS-1 Seawater Matrix at Various Dilution Factors

		RECOVERIES (%) AT INDICATED DILUTION FACTORS FI, 5 s Injections				COUNT RATES (c/s)* FI, 5 s Injections,
	m/z	10x dil.	5x	2x	Undiluted	10 ppb Standards, No Matrix
Sc	45	92	86	80	76	6,000
Y	89	97	95	91	86	4,500
Ce	140	90	89	85	74	9,000
Tl	205	92	86	81	76	5,000

*Original count rates for matrix-free analyte solution are given here.

Figures

CAPTIONS

Figure 1. Matrix effects on Tl^+ signal from NaCl at indicated Na concentrations: a) continuous introduction, b) FI with 1 s injections. In b) the curves for 1000 ppm and 2000 ppm Na fall between those for Tl alone and 5000 ppm Na; these curves at intermediate Na concentrations are not plotted for clarity.

Figure 2. Matrix effects on Tl^+ signal from NaCl at indicated Na concentrations: a) FI with 5 s injection, b) FI with 10 s injections. Again, the curves for 1000 ppm and 2000 ppm Na fall between those for Tl alone and 5000 ppm Na. Note the different time scales in the two plots.

Figure 3. Matrix effects on Tl and Sc at 5 ppb in clean 1% HNO_3 standard vs. 5 ppb spiked into CASS-1 seawater at various dilutions during FI, 10 s injections.

Figure 4. Matrix effects on Sc, 5 s injections: a) effect of Bi matrix on 5 ppb Sc; b) effect of Ba matrix on 10 ppb Sc. Barium causes a much more severe matrix effect than the other elements studied.

Figure 5. Matrix effects on Sc at 10 ppb, 5 s injections, for NaCl matrix at indicated Na concentrations, with grounded shield in torch. With the unshielded torch and 5 s injections, recoveries for Sc were 94%, 89% and 82% at 1000, 5000 and 10,000 ppm Na, respectively (Table 2).

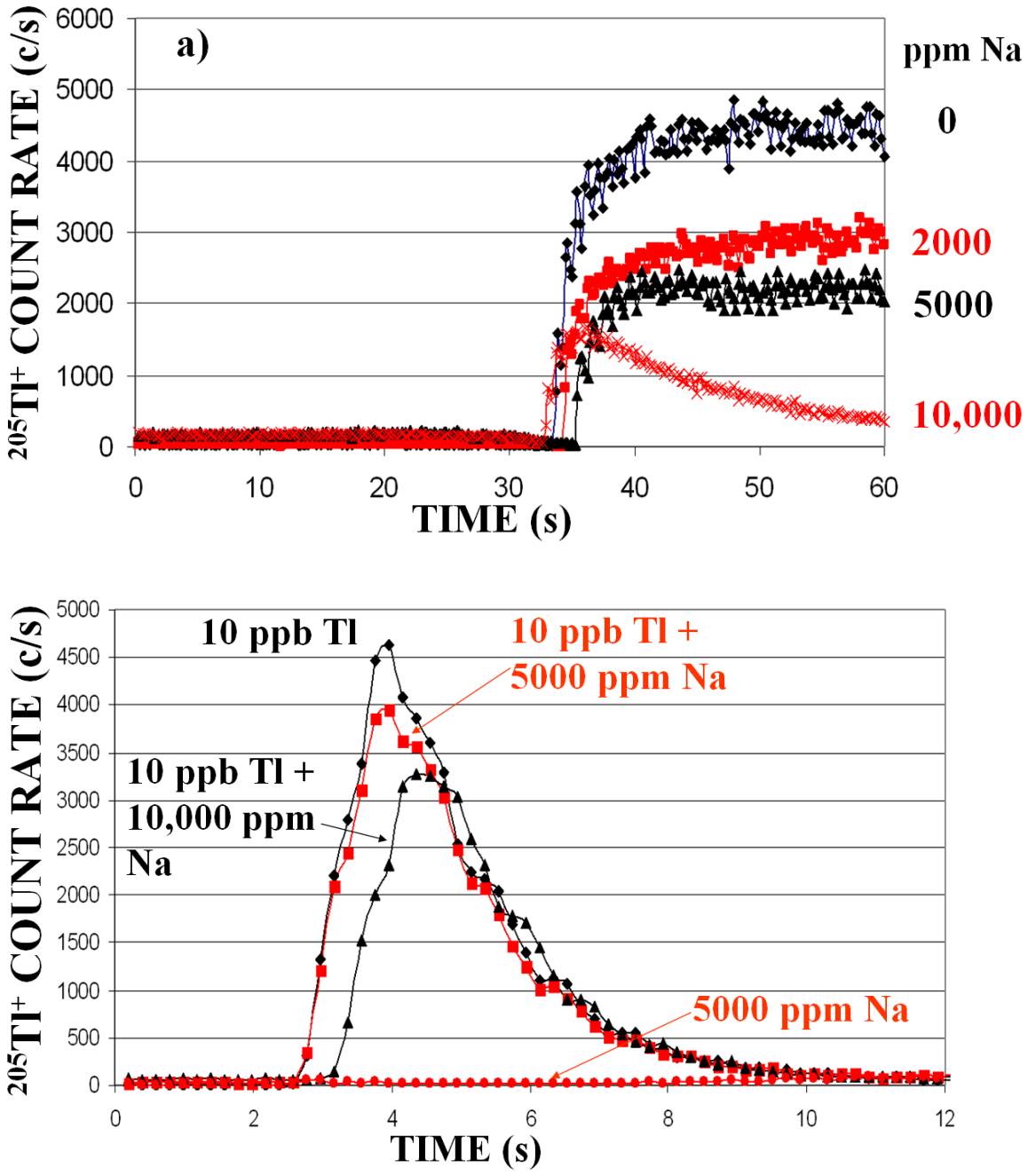

Figure 1. Matrix effects on Tl^+ signal from NaCl at indicated Na concentrations: a) continuous introduction, b) FI with 1 s injections. In b) the curves for 1000 ppm and 2000 ppm Na fall between those for Tl alone and 5000 ppm Na; these curves at intermediate Na concentrations are not plotted for clarity.

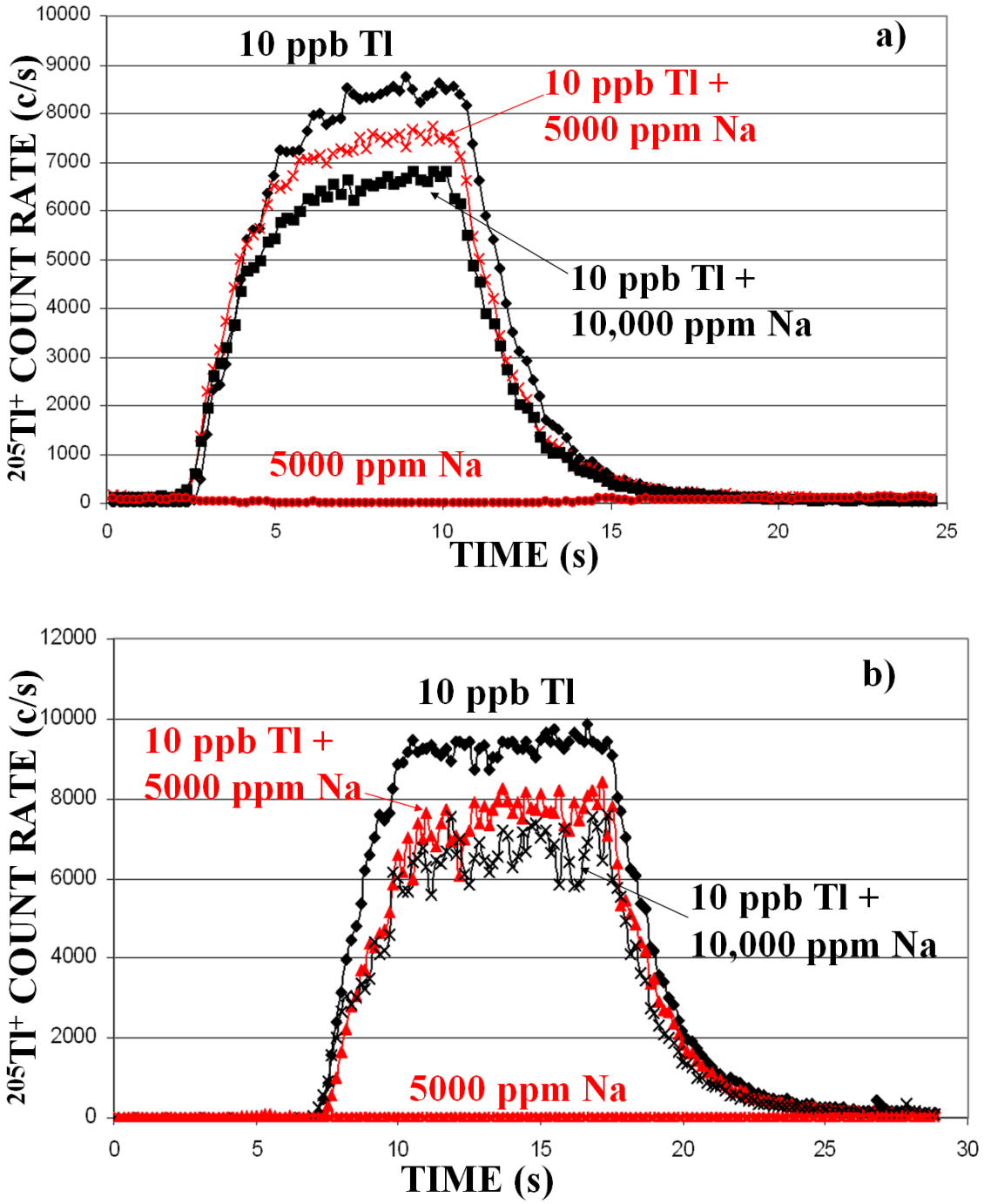

Figure 2. Matrix effects on Tl^+ signal from NaCl at indicated Na concentrations: a) FI with 5 s injection, b) FI with 10 s injections. Again, the curves for 1000 ppm and 2000 ppm Na fall between those for Tl alone and 5000 ppm Na. Note the different time scales in the two plots.

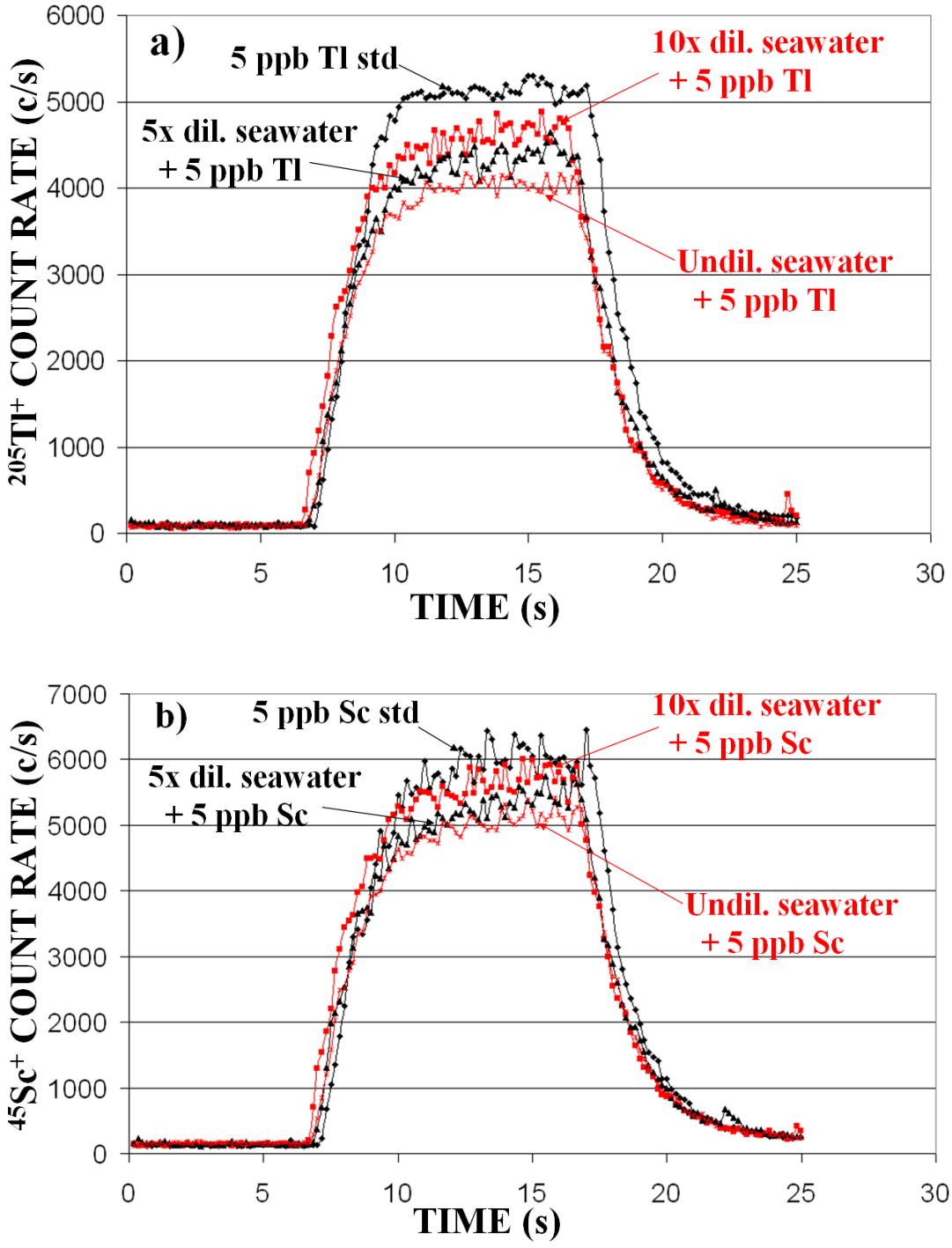

Figure 3. Matrix effects on Tl and Sc at 5 ppb in clean 1% HNO_3 standard vs. 5 ppb spiked into CASS-1 seawater at various dilutions during FI, 10 s injections.

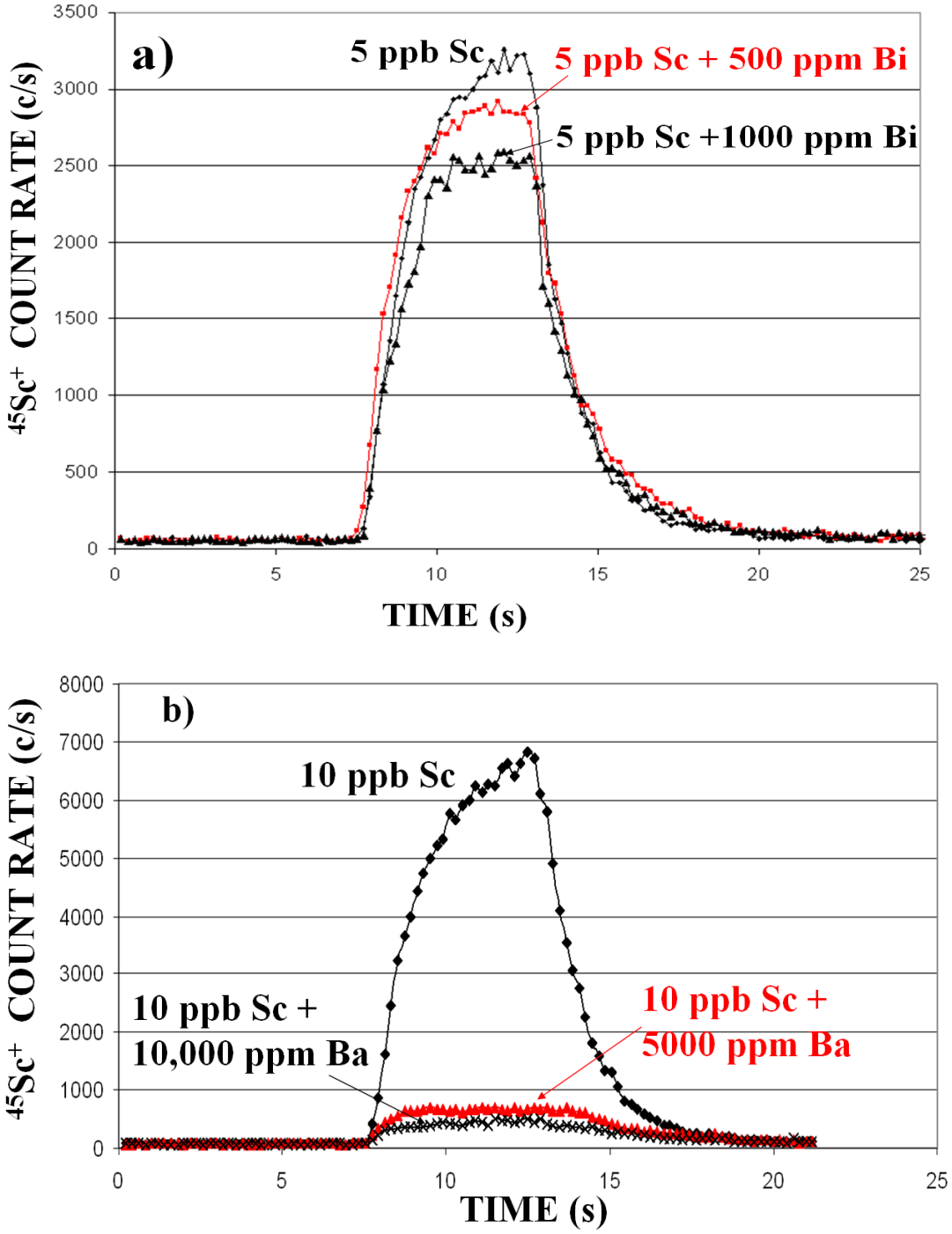

Figure 4. Matrix effects on Sc, 5 s injections: a) effect of Bi matrix on 5 ppb Sc; b) effect of Ba matrix on 10 ppb Sc. Barium causes a much more severe matrix effect than the other elements studied.

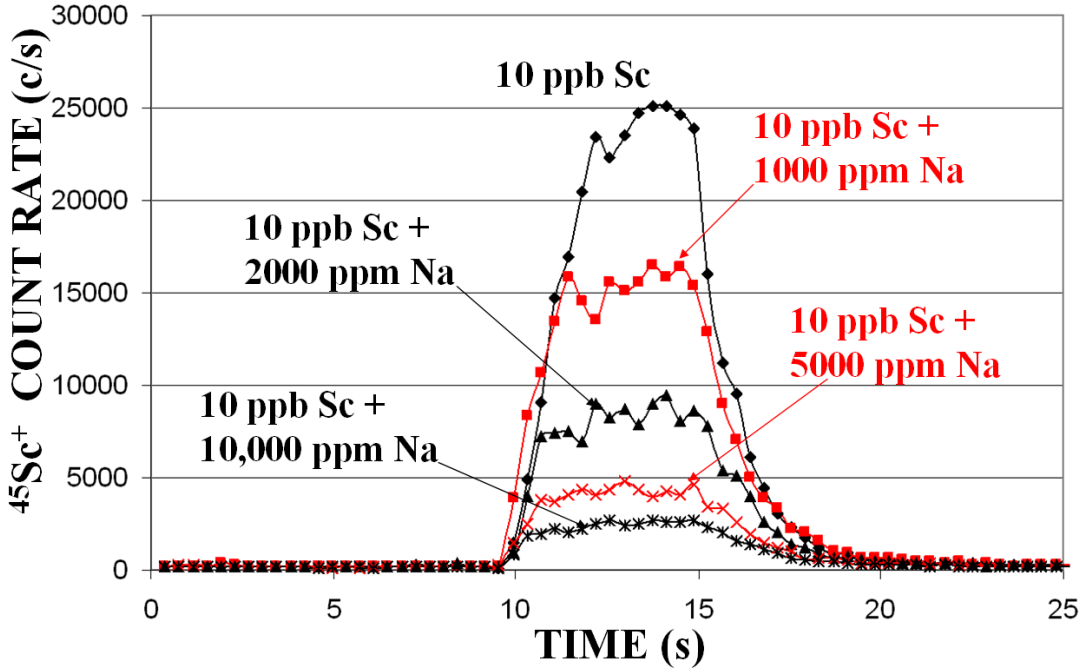

Figure 5. Matrix effects on Sc at 10 ppb, 5 s injections, for NaCl matrix at indicated Na concentrations, with grounded shield in torch. With the unshielded torch and 5 s injections, recoveries for Sc were 94%, 89% and 82% at 1000, 5000 and 10,000 ppm Na, respectively (Table 2).